Nora H. Stray

Planetary waves in the northern MLT: Vertical coupling and effects

Trondheim, January 2015

Norwegian University of Science and Technology
Faculty of Natural Sciences and Technology
Department of Physics

NTNU

Abstract

One of the major difficulties climate models face is the lack of data on the way in which the atmosphere couples energy, dynamics and composition vertically in the Earth's climate system. This PhD thesis focuses on planetary wave activity in the mesosphere-lower thermosphere (MLT): How the observed planetary wave activity is coupled to the underlying atmosphere and how it affects its surroundings. A method has been developed to observe planetary wave activity in the northern hemisphere (50-66°N) MLT using neutral atmosphere winds derived from meteor trail drifts observed by a longitudinal chain of Super Dual Auroral Radar Network (SuperDARN) radars as a "ground-based" satellite. Using these observations, the PhD thesis investigates the intra and inter-annual variability of planetary wave activity in the MLT, its effect on the atmosphere and coupling to the underlying atmosphere. To investigate the coupling to the underlying atmosphere, reanalysis and model results have been used.

The seasonal climatology of nine years (2000-2008) of planetary wave activity in the MLT shows an enhancement of wave activity during winter, mid-summer and autumn. The autumn enhancement has been shown to occur simultaneously with a minimum in gravity wave forcing in the MLT and a poleward perturbation of the meridional circulation, suggesting a temporary forcing through westward momentum deposition by planetary waves. The enhancement in summer results from a year-to-year consistent quasi-stationary planetary wave S_1 structure. Investigations of the source of this structure rule out direct propagation and modulation of gravity wave filtering by planetary waves at the tropopause. Finally the winter enhancement has been shown to be triggered by stratospheric sudden warmings and their modification of the underlying wind field.

List of Papers

Paper I

Kleinknecht[1], N. H., P. J. Espy, and R. E. Hibbins (2014), The climatology of zonal wave numbers 1 and 2 planetary wave structure in the MLT using a chain of Northern Hemisphere SuperDARN radars, J. Geophys. Res. Atmos., 119, 1292-1307, doi:10.1002/2013JD019850.

This paper shows that the meteor winds from a chain of northern hemispheric (∼60°N) SuperDARN radars can be used to observe planetary waves with zonal wave number 1 and 2 in the mesosphere-lower thermosphere and presents the climatology of these planetary wave components in this region.

NHK developed and performed the data analysis and wrote the paper. PJE and REH took part in discussions, and provided guidance and help in finalizing the paper. SuperDARN data were obtained from the SuperDARN community and REH used the standard SuperDARN analysis to obtain meteor winds. SuperDARN is a collection of radars funded by the national scientific funding agencies of Australia, Canada, China, France, Japan, South Africa, United Kingdom, and United States of America. Wind data from the UK Meteorological Office assimilated data set were used to validate the analysis. These data were made available by the British Atmospheric Data Centre.

[1]Please note that the author changed her surname from Kleinknecht to Stray in Juli 2014

Paper II

Stray, N. H., R. J. de Wit, P. J. Espy, and R. E. Hibbins (2014), Observational evidence for temporary planetary-wave forcing of the MLT during fall equinox, Geophys. Res. Lett., 41, 17, 6281-6288, doi: 10.1002/2014GL061119.

This paper presents evidence for temporary planetary-wave forcing of the MLT during fall equinox using planetary wave observation extracted from meteor winds derived from a chain of northern hemispheric SuperDARN radars.

NHS did most of the analysis and wrote the paper. RJW provided the gravity wave forcing from the meteor radar in Trondheim. PJE, REH and RJW took part in discussions and helped finalizing the paper. PJE and REH provided guidance during the work on the paper. SuperDARN data were obtained from the SuperDARN community and REH used the standard SuperDARN analysis to obtain meteor winds. SuperDARN is a collection of radars funded by the national scientific funding agencies of Australia, Canada, China, France, Japan, South Africa, United Kingdom, and United States of America. Zonal wind data from the UK Meteorological Office assimilated data set were used to monitor the stratosphere. These data were made available by the British Atmospheric Data Centre.

Paper III

Stray, N. H., P. J. Espy, V. Limpasuvan, and R. E. Hibbins (2014), Characterisation of quasi-stationary planetary waves in the Northern MLT during summer, J. Atmos. Solar-Terr. Phys., doi: 10.1016/j.jastp.2014.12.003.

This paper documents observations of quasi-stationary climatologically stable longitudinal variations in the meridional wind in the summer mesosphere-lower thermosphere using meteor winds from a SuperDARN network. This structure of the variation in the meridional wind corresponds to a wave number one quasi-stationary planetary wave and results in enhanced summer conditions above Greenland. The paper further investigates mechanisms which in theory have the potential to generate such a variation in the meridional wind. For this investigation NASA's Modern-Era Retrospective Analysis for Research and Applications (MERRA) reanalysis data are used.

NHS did the analysis of the data and wrote the paper. VL provided the MERRA data and contributed with helpful comments. PJE and REH took part in discussions, provided guidance and helped finalizing the paper. SuperDARN data were obtained from the SuperDARN community and REH used the standard SuperDARN analysis to obtain meteor winds. SuperDARN is a collection of radars funded by the national scientific funding agencies of Australia, Canada, China, France, Japan, South Africa, United Kingdom, and United States of America.

Paper IV

Stray, N. H., Y. J. Orsolini, P. J. Espy, V. Limpasuvan, and R. E. Hibbins (2015), Observations of PW activity in the MLT during SSW events using a chain of SuperDARN radars and SD-WACCM, Atmospheric Chemistry and Physics Discussions, 15(1), 393-413, doi: 10.5194/acpd-15-393-2015.

This paper documents observations of enhanced planetary wave activity in the mesosphere-lower thermosphere after reversals of the stratospheric polar cap zonal-mean zonal wind that are related to stratospheric sudden warming events. The observations are supported by modelling using the Special Dynamics Whole Atmospheric Community Climate Model. The study provides observational evidence *confirming and extending previous modelling studies. The planetary wave observations in the MLT have been extracted from meteor winds derived from a chain of northern hemispheric SuperDARN radars.*

NHS did the analysis of the observational data and wrote the paper. YJO and VL provided the model data, analyzed SD-WACCM and contributed with helpful comments. PJE and REH took part in discussions, provided guidance and helped finalizing the paper. SuperDARN data were obtained from the SuperDARN community and REH used the standard SuperDARN analysis to obtain meteor winds. SuperDARN is a collection of radars funded by the national scientific funding agencies of Australia, Canada, China, France, Japan, South Africa, United Kingdom, and United States of America.

Papers not included in the thesis

Paper V

Demissie, T. D., **N. H. Kleinknecht**, R. E. Hibbins, P. J. Espy and C. Straub (2013), Quasi-16-day period oscillations observed in middle atmospheric ozone and temperature in Antarctica, Ann. Geophys., 31, 1279-1284, doi:10.5194/angeo-31-1279-2013.

This paper observes the 16-day planetary wave in the middle atmosphere over Antarctica using ozone and temperature measurements as a tracer.

TDD did most of the analysis and wrote the paper. The hydroxyl temperatures and raw ozone spectra were provided by the British Antarctic Survey. NHK transformed the raw ozone spectra into ozone mixing ratios and contributed to the analysis. REH and PJE took part in the discussion and provided valuable comments. CS took part in the final discussion.

Paper VI

Demissie, T. D., K. Hosokawab, **N. H. Kleinknecht**, P. J. Espy and R. E. Hibbins (2013) Planetary wave oscillations observed in ozone and PMSE data from Antarctica, J. Atmos. Sol.-Terr. Phys., 105-106, 207-213, doi:10.1016 /j.jastp.2013.10.008

This paper investigates planetary wave activity in the middle atmosphere above Antarctica during summer using measurements of ozone and Polar Mesospheric Summer Echoes (PMSE) as a tracer.

TDD did most of the analysis and wrote the paper. KH extracted the PMSE data from SuperDARN radar measurements at Sanae. The raw ozone spectra were provided by the British Antarctic Survey. NHK transformed the raw ozone spectra into ozone mixing ratios and contributed to the analysis. REH and PJE took part in the discussions, provided valuable comments and helped finalizing the paper.

Paper VII

Demissie, T. D., P. J. Espy, **N. H. Kleinknecht**, M. Hatlen, N. Kaifler and G. Baumgarten (2014), Characteristics and sources of gravity waves observed in noctilucent cloud over Norway, Atmos. Chem. Phys., 14, 12133-12142, doi:10.5194/acp-14-12133-2014.

This paper studies the source and characteristics of gravity waves. The gravity waves have been observed from noctilucent cloud images above Norway and GROGRAT has been used for ray-tracing.

TDD wrote the paper. He also did the image analysis, extracted the wave parameters and performed ray-tracing. The automated digital camera was installed by the Leibniz-Institut für Atmosphärenphysik, Germany and is maintained by the Norwegian University of Science and Technology (NTNU). TDD helped with the camera maintenance. NHK helped develop the analysis to extract GW parameters from the images. All co-authors took part in discussions, supported TDD during the data analysis and helped finalizing the paper.

Contents

1. Introduction

Vertical coupling in the atmosphere is primarily due to waves. Waves generated in the lower atmosphere can propagate upwards through the atmosphere. When they break they dissipate energy and deposit momentum in the atmosphere. This leads for example to the planetary wave (PW) driven Brewer-Dobson circulation in the upper troposphere-lower stratosphere or the gravity-wave driven mesospheric meridional circulation. The strength of this meridional circulation determines the strength of the vertical flow in the Polar Regions and hence determines how far long-lived species are transported in the atmosphere. [e.g. *Lindzen*, 1981; *Brasseur and Solomon*, 2005]

Changes in wave activity in the mesosphere-lower thermosphere (MLT) have the ability to create variations in the strength of this meridional circulation. Thus any change in the wave activity will lead to variations of the vertical flow and the chemical transport between the stratosphere and the mesosphere.

The existence of the meridional circulation in the mesosphere has been shown to be controlled mainly through momentum deposition of gravity waves (GWs). This has been investigated in many model [e.g. *Holton*, 1983; *Garcia and Solomon*, 1985] and observational studies [e.g. *Fritts et al.*, 2012; *de Wit et al.*, 2014b]. However some model studies indicate that PW activity is also present in the MLT region [e.g. *Liu and Roble*, 2002; *Limpasuvan et al.*, 2012; *Chandran et al.*, 2013a, b]. Observations focusing on PW activity in the MLT are, however, less common. Furthermore, the effect of PWs on the MLT is relatively undocumented, and their main generation mechanisms, as well as how they are coupled to conditions in the underlying atmosphere, are still open questions. This thesis seeks to answer these questions through long-term, multi-station observations of PW activity in the MLT and by investigating both the effect of variability in the underlying atmosphere on PW activity in the MLT as well as the effect of the PW activity observed in the MLT on the circulation and temperature of this region.

For the observation and characterization of PW activity in the MLT, simultaneous measurements of meteor winds from a chain of northern hemispheric SuperDARN radars have been used to document the inter and intra- annual variability of PW activity with zonal wave numbers 1 and 2. The SuperDARN community has provided high quality meteor wind data over several decades for various northern hemispheric stations. This, and the number and spatial distribution of SuperDARN stations in the northern hemisphere, makes it possible to extract zonal wave number one and two PWs over several years. For this thesis, PW activity in the MLT has been retrieved over nine years (2000-2008). Furthermore the PW observations have been combined with model and re-analysis data to study how variations of the atmospheric background conditions in the middle atmosphere affect PW activity in the MLT, and to what degree PW activity in the MLT can affect the atmosphere.

The way in which the PWs in the MLT are viewed varies. Some view PWs in the MLT as images of PWs in the lower atmosphere that are projected into the MLT through GW filtering by the PWs in the lower atmosphere [e.g *Smith*, 2003]. Others see them as non-interacting individual waves, each with their own period [*Mitchell et al.*, 1999; *Taylor et al.*, 2001; *Day et al.*, 2012] rather than the superposition of waves, interacting with the background wind, but maintaining their zonal character. In this work PWs are observed along a longitude band and characterised by their zonal wave number. This view shows the temporal variation of the superposition of all PWs with the same zonal wave number in the background atmosphere, but maintains the possibility to extract single temporal components.

This thesis is a collection of journal articles, meaning that the main results are summarized and discussed in the main part of the thesis (Chapter 2-5) while the full details on the studies can be found in the papers I-IV in Appendix A.

2. How does PW activity in the MLT vary?

To answer this question, PW activity has been observed through simultaneous observation of hourly meteor winds from a chain of northern hemispheric SuperDARN radars [*Greenwald et al.*, 1985, 1995] along a latitude band ($\sim$ 60°N) in the MLT (approximately 95 km, [*Hall et al.*, 1997]). The simultaneous use of several similar and continuously running observation sites that are located close in latitude and widely spread in longitude allows for a global view at this latitude. This global view is similar to what can be achieved by satellites. However, in contrast to a satellite, no aliasing problems arise since all the observations occur simultaneously at ground-based positions and hence do not move relative to the earth. Due to these qualities, the network has been called a "ground-based satellite" in this thesis. The "ground-based satellite" and how it is used to observe PW activity with wave numbers 1 and 2 in the MLT is presented and validated in Paper I [*Kleinknecht et al.*, 2014] and explained briefly below.

2.1. The "ground-based satellite"

The advantage of a satellite compared to a single ground based station is its ability to collect measurements at many different locations on earth and give a global picture. However the satellite's continuous change of position with time leads to these different spatial locations being observed at different times, aliasing the frequency of phenomena that vary both spatially and temporally [*Wu et al.*, 1995]. Satellites in non-sun synchronous modes, as for example the satellite of the

Thermosphere Ionosphere Mesosphere Energetics and Dynamics (TIMED) mission (`http://www.timed.jhuapl.edu/WWW/index.php`), needs 60 days to scan through all solar local times at a given location. This will strongly smooth temporal variations of the atmosphere that occur on time scales shorter than this, including those of PWs. Other satellites in sun-synchronous modes, as for example Aura (`http://aura.gsfc.nasa.gov/about.html`), measure each individual location at the same solar local time. One therefore has to assume that conditions do not change in the time it takes the satellite to arrive at each new measurement location or between measurements at the same location. That is, one must assume that the amplitude and phase of the atmospheric tides remain constant over the course of the satellite measurements.

This assumption is, however, not valid in general. *Mitchell et al.* [2002] have for example shown that both the amplitude and the phase of the semidiurnal tide in the high northern latidudes is highly variable. The assumption that the measurements take place during a single tidal phase will therefore lead to wrong conclusions. To illustrate that point Figure 2.1 shows the daily mean meridional wind derived from the SuperDARN radar at Stokkseyri (64.7°N, -26.9°E) in comparison with the meridional wind at Stokkseyri measured at noon (12 SLT). It can be seen that the variations of the tidal amplitude of the wind with time will give a totally different picture of the state of the atmosphere and its variation than the daily-mean wind.

As an alternative to satellites, global networks of ground-based stations can be used to get a global view of our atmosphere. A global network of approximately identical ground-based stations that continuously measure atmospheric quantities, for example the wind velocity, could give a global picture of the atmosphere similar to that covered by a satellite. However, unlike a satellite, tidal effects can be removed if the ground-based measurements at each location were performed frequently throughout a day (e.g. hourly measurement). Such geographically distributed stations measuring simultaneously are able to remove the spatial-temporal aliasing present in satellite observations, and therefore are referred to as a *ground-based satellite* in this thesis.

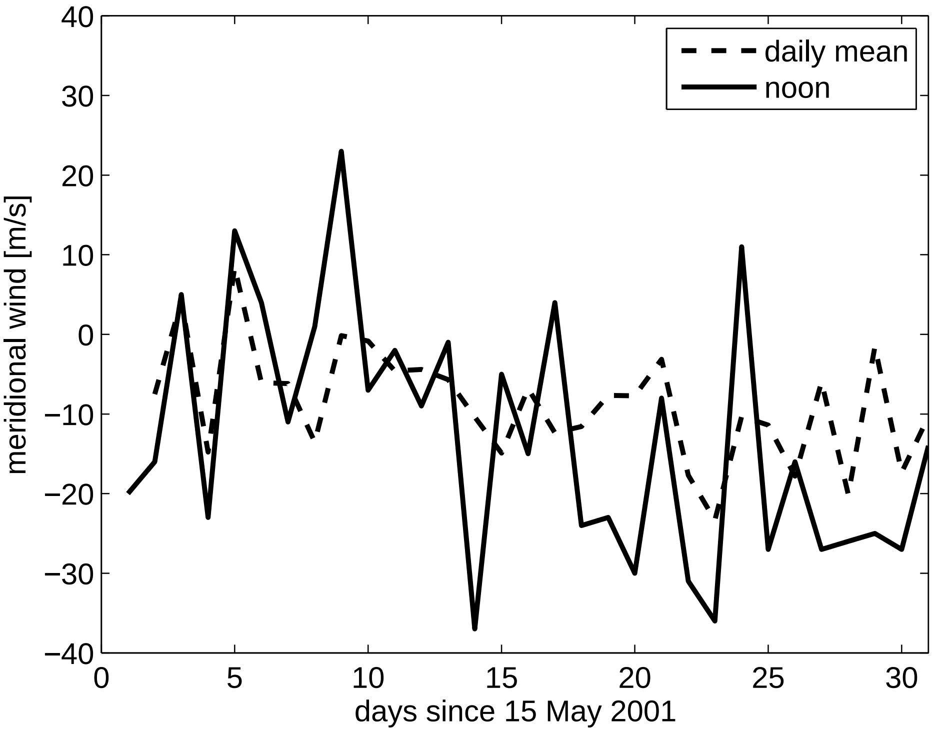

Figure 2.1.: Daily-mean meridional meteor wind (dashed line) and the meridional meteor wind at noon (solid) from the SuperDARN station at Stokkseyri. The snapshot of the atmosphere at noon gives a different picture than the daily mean due to the presence of atmospheric tides with variable amplitude and phase.

2.2. The SuperDARN network

The Super Dual Auroral Radar Network [*Greenwald et al.*, 1985, 1995], known as SuperDARN, is a global network of over 30 high-frequency radars built to sense backscatter from ionospheric irregularities in the E-region (Kennelly-Heaviside layer; 90-150 km) and F-region (Appleton-Barnett layer; 150-800 km) of the atmosphere.

The focus area of the network has been the Arctic and Antarctic regions and most of the radars are therefore placed at high-latitudes. However, stations at mid-latitudes have also been established in recent years. Figure 2.2 gives an overview of the expanded network as of year 2014.

The first radar at Goose Bay, Newfoundland (gbr) started its operation in 1983 and is still in operation today. The newest SuperDARN radar stations started operation in 2013 and are placed at South Pole Station, Antarctica (sps) and Dome-C, Antarctica (dce).

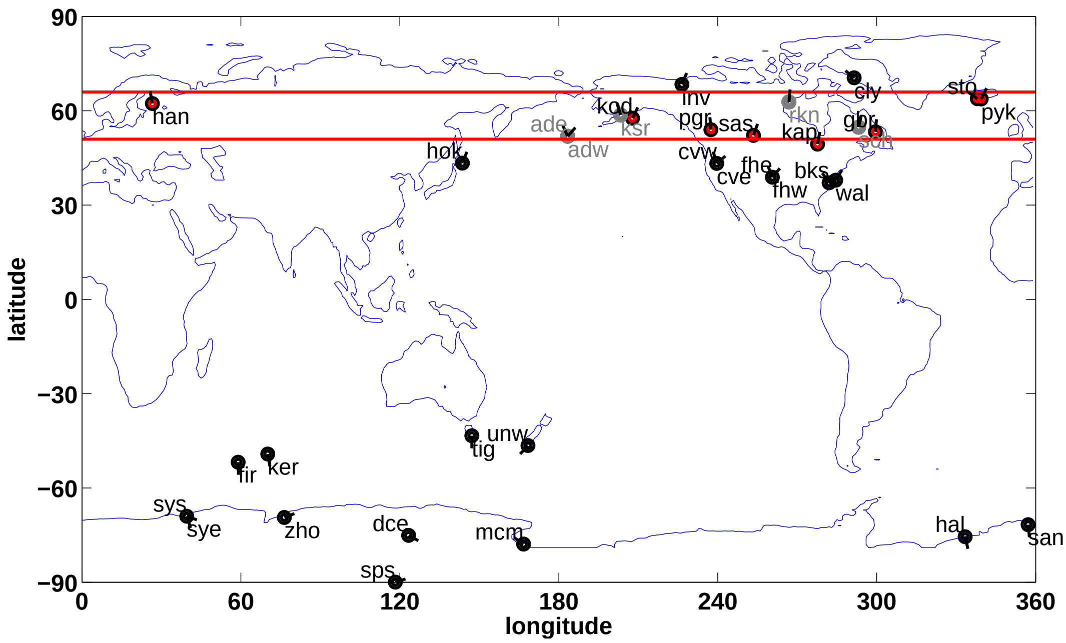

Figure 2.2.: The expanded SuperDARN radar network in 2014. The circles display the geographical location of the radar sites. The direction of the arrows shows the boresite (viewing direction) of the radar stations and the end point of the arrow approximately indicates the centroid location of the beam for meteor echoes. The radar stations marked grey did not have sufficient data coverage between 2000 and 2008. The radar stations marked red have been used as a ground-based satellite for the latitude band between 51 and 66°N (red lines). The stations are referred to by their 3-letter abbreviations listed in Appendix C.

The continuous operation of the radars over an extended time, as well as the large number of instruments distributed around the earth, make the SuperDARN network an important tool to study the upper atmosphere. A list of all current radar stations and their abbreviations can be found in Appendix C.

2.2.1. Meteor winds from SuperDARN

SuperDARN radars were originally built to study large-scale dynamical processes in the magnetosphere-ionosphere system through backscatter from ionospheric irregularities. However it was shown later [*Hall et al.*, 1997; *Jarvis et al.*, 1999; *Hussey et al.*, 2000; *Yukimatu and Tsutsumi*, 2002] that they can also be used to measure the neutral wind in the region of the upper-mesosphere lower-thermosphere (MLT) since the sporadic echoes received in the first few range gates are mainly due to scatter from the ionization trails left by meteors ablating in the MLT. These trails travel with the neutral wind, which makes it possible to deduce the line of sight wind over the meteor ablation altitudes (80-100 km) [*Hocking et al.*, 2001]. Meteors observed in the lowest range gates of the multiple beams of the SuperDARN radars can then be combined in order to determine the vector neutral wind at the centroid location of the beams. Standard SuperDARN radars have no altitude discrimination within the lowest range gates used for meteor-trail detection, but the mean altitude of the wind derived from meteor echoes has been estimated to be 94 ($\pm$ 3) km by comparing the derived wind with that observed by a co-located MF radar [*Hall et al.*, 1997]. This result has been verified by comparing winds from an imaging Doppler interferometer (IDI) radar at Halley (75°S, 26°W) and a co-located SuperDARN radar [*Hibbins and Jarvis*, 2008]. Recently, *Chisham and Freeman* [2013] developed a new method for calibrating SuperDARN interferometric data to estimate the meteor altitudes directly, finding a broad distribution between 75 and 125 km with a peak near 102-103 km. Although the peak of this meteor distribution is higher than the altitude of the wind that has been inferred through comparisons with other radars, *Chisham and Freeman* [2013] have suggested that this difference is likely due to the averaging over the vertical structure of the wind.

For the studies performed during this thesis, hourly averaged neutral meteor winds obtained by the SuperDARN community, as processed by the standard SuperDARN analysis, have been used (`http://psddb.nerc-bas.ac.uk/data/access/`).

2.3. SuperDARN as a ground-based satellite

The first part of the work for this thesis was to develop and validate a technique to extract the zonal character of PWs using the meteor wind measurements from a longitudinal chain of SuperDARN radars as a ground-based satellite, presented in Paper I [*Kleinknecht et al.*, 2014] - see Appendix A. A series of operations has to be performed on the radar wind data to extract the PWs with zonal wave numbers 1 and 2. Since most of the stations have a view direction close to the north, the meridional wind is more accurately resolved than the zonal wind. Therefore the meridional wind was used for the extraction of the PWs. The stations used are marked with red dots in Figure 2.2 and the geo-locations of their centroid position are listed in Table 1 of Paper I. These stations are all located between 51 and 66°N and have sufficient data coverage in the years 2000-2008. The chain of SuperDARN radars used spans longitudes between 150°W and 25°E.

First the hourly mean winds with mean locations different from the geometric centroid of the beam, magnitudes above 100 m/s or with standard deviations of zero were excluded to assure data quality. These values were removed since they either indicate a nonstandard operation mode of the radar or unrealistic solutions of the wind fitting algorithm [*Hibbins and Jarvis*, 2008]. Figure 2.3 shows the quality-checked hourly meridional meteor winds from the SuperDARN radar at Hankasalmi (64.4°N, 25.2°E) as an example. The data coverage is similar at all SuperDARN stations in the chain.

To remove the effects of tides and the quasi 2-day wave, daily-mean winds were produced by fitting a bias (which constitutes the mean wind), the tidal components (8, 12 and 24 h) and a 2-day-wave component to a four day sliding window that was moved by one-day intervals. An example of such a fit to a four day window is shown in Figure 2.4.

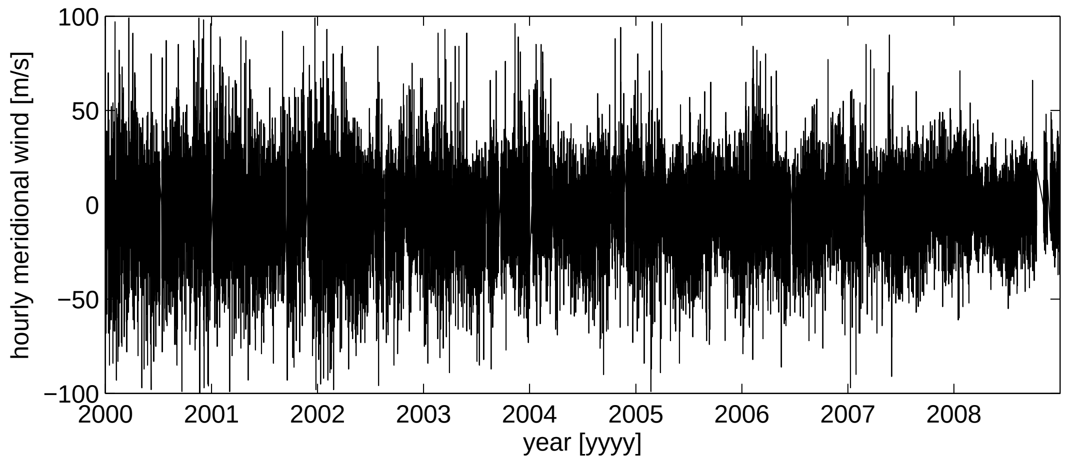

Figure 2.3.: Quality-checked hourly meridional wind measurements at Hankasalmi.

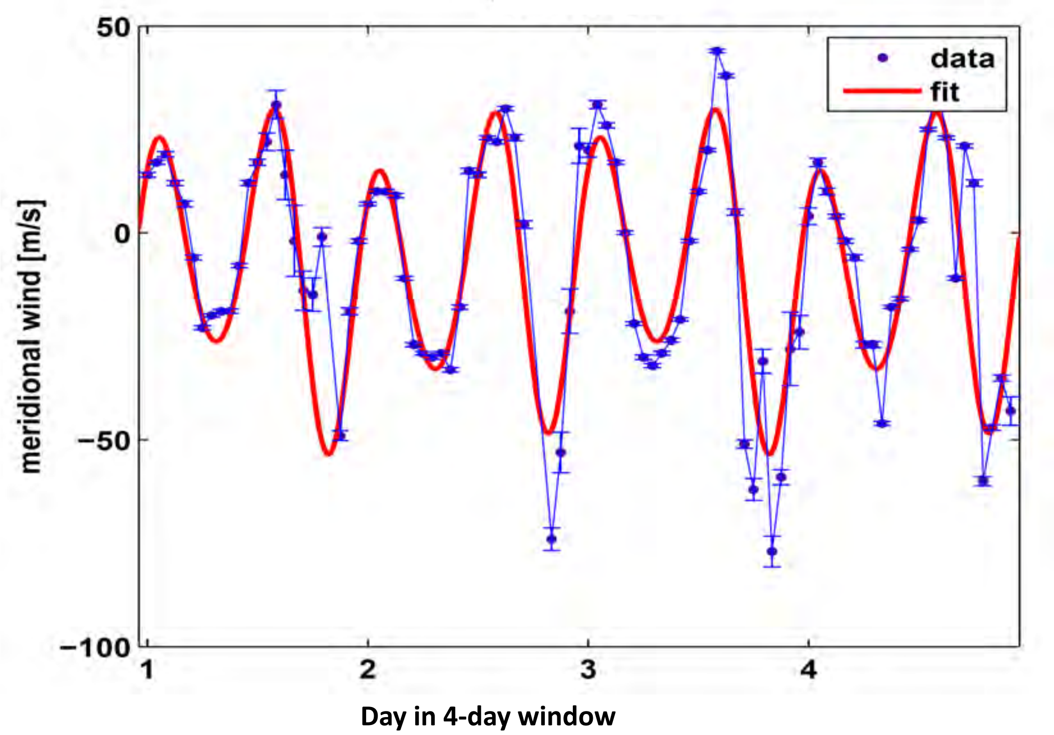

Figure 2.4.: Example of a tidal and two-day-wave fit (red) to a four day window of meridional wind at Hankasalmi. Hourly meridional winds (purple dots) were weighted with the number of meteors by the fitting algorithm.

Since the precision of the radar winds improves as the number of meteor echoes used in their determination increases, the hourly mean meridional winds were weighted by the number of meteors in the fitting process. Only windows that had sufficient data coverage (see Paper I) to ensure an unbiased fit were transformed into daily-mean winds. This analysis was performed at all of the eight SuperDARN stations independently. Figure 2.5 shows the retrieved daily-mean wind at the eight stations during the years 2000-2008.

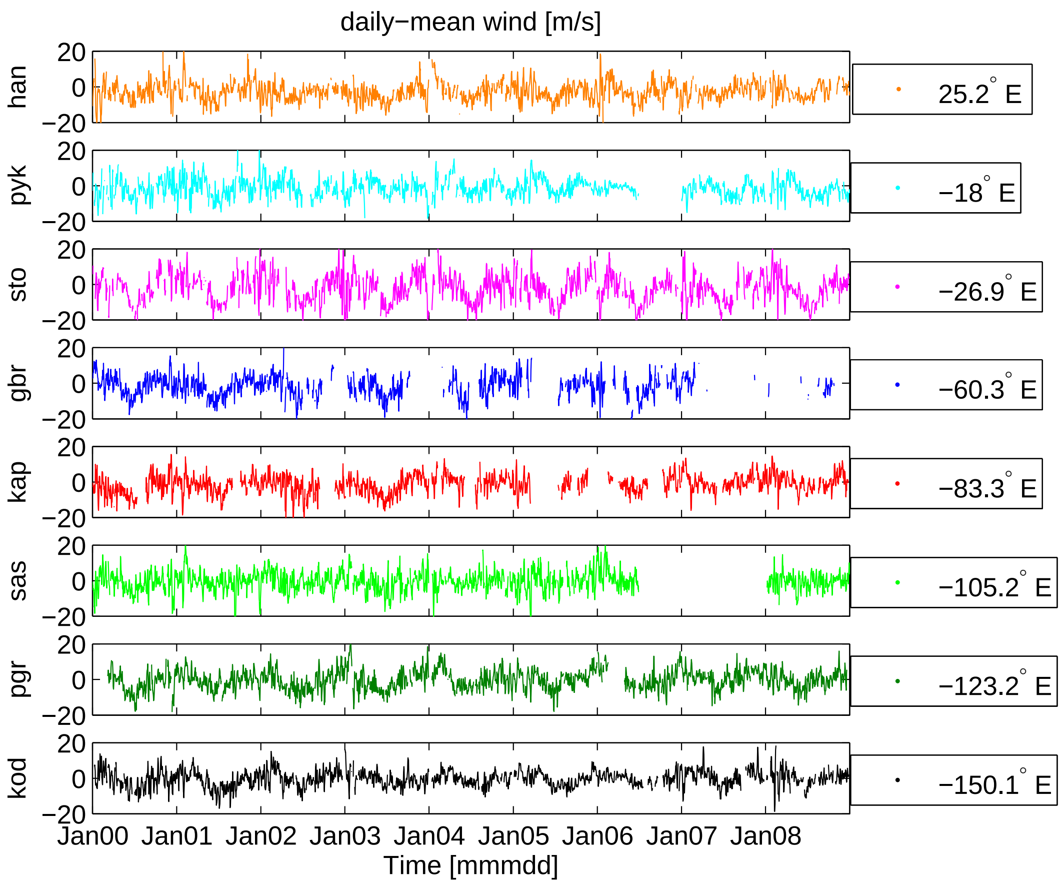

Figure 2.5.: Daily-mean meridional wind at all eight SuperDARN stations during year 2000-2008. The stations are referred to by their 3-letter abbreviations - see Appendix C

The meridional circulation (Section 3.1.2) is clearly visible with negative (i.e. southward/equatorward) winds during summer and positive (i.e. northward/ poleward) winds during winter.

In addition to the daily-mean wind, the daily-mean wind anomaly has been calculated by differencing the mean wind for a particular day from its climatological value. Figure 2.6 shows the daily-mean anomaly for 2000-2008 for all 8 stations. Since both types of waves are of interest, planetary zonal wave structures have been extracted for the daily-mean wind and the daily-mean wind anomaly datasets.

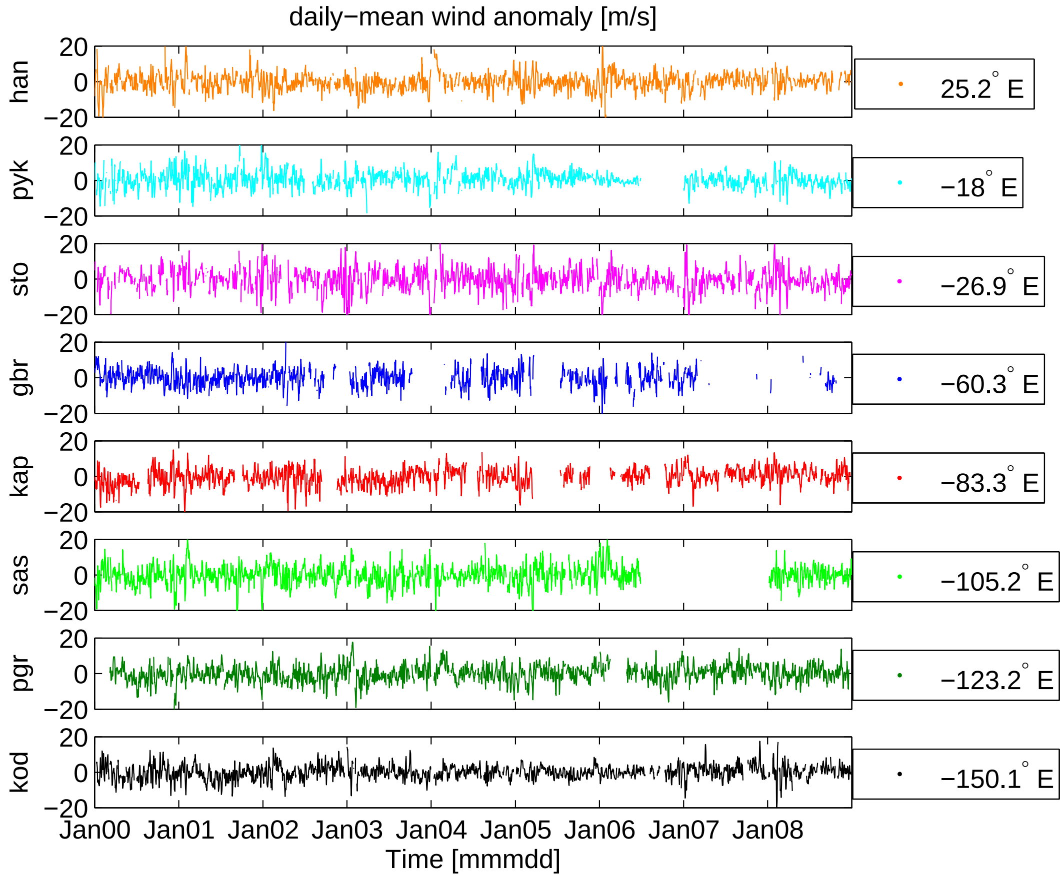

Figure 2.6.: As Figure 2.5, but for the daily-mean meridional wind anomaly.

The zonal characteristics of PWs have then be extracted day by day. For each day, the meridional wind (or wind anomaly) was fitted as a function of station longitude using a constant bias as well as 360° and 180° sinusoidal functions, as shown in Figure 2.7. These components represent the S_0, S_1 and S_2 zonal wave numbers, respectively. The fit was performed for all days where data from at least 6 of the 8 stations, including the most eastward and most westward located radars, were available. No PW activity could be retrieved before year 2000 because the most eastward radar station (Kodiak) only started operation that year. Before that, the longitudinal coverage of the SuperDARN chain was not sufficient to extract the zonal PW components.

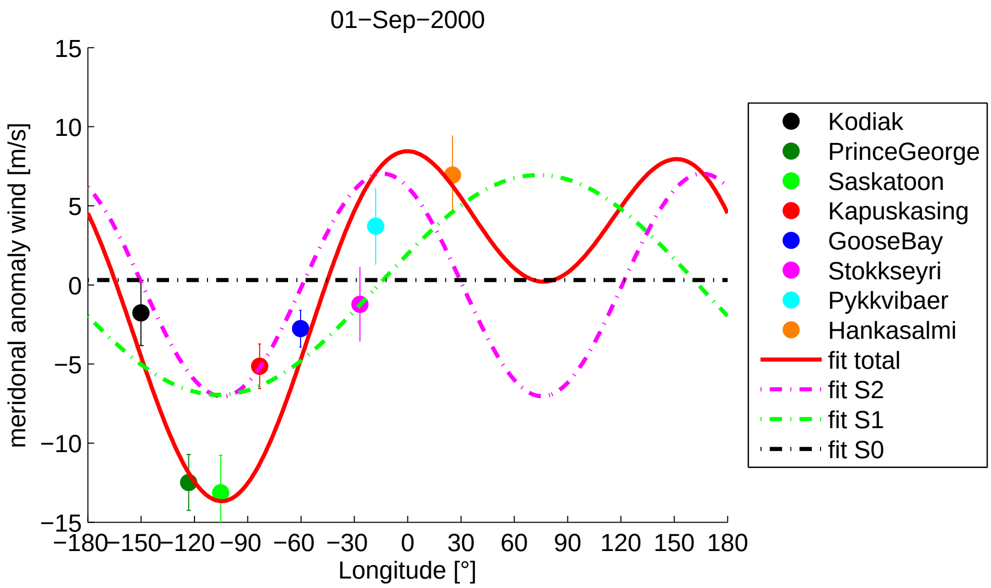

Figure 2.7.: Example of a PW zonal wave number fit. The colored dots mark the longitudinal position (x-axis) and the daily-mean wind anomaly (y-axis) recorded at the stations on the 1 September 2000. The bias is displayed as a black line, the fitted S_1 component is shown in green and the S_2 component is colored magenta. The total fit is shown in red.

A plot of each day's independent fit of the zonal wave number as a function of longitude and time results in a so-called Hovmöller diagram shown in Figure 2.8 for the year 2000. Red and blue colors signify northward (poleward) and southward (equatorward) wind perturbations, respectively.

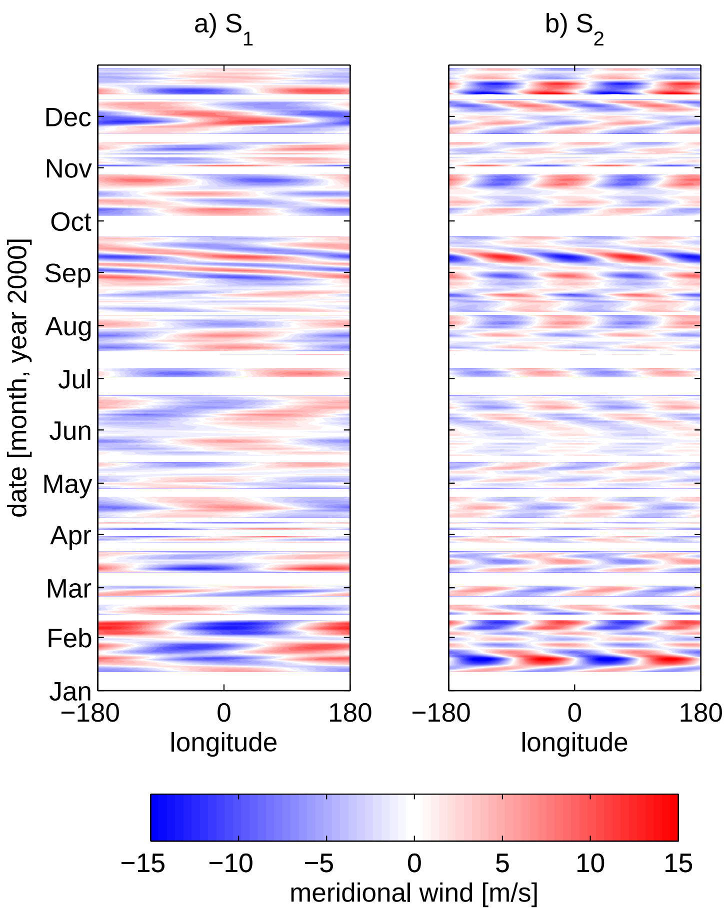

Figure 2.8.: Hovmöller diagram of zonal wave number one (a) and two (b) of the meridional wind anomaly for the year 2000. Red and blue colors signify northward (poleward) and southward (equatorward) wind perturbations, respectively.

A Hovmöller diagram makes it easy to identify each wave component's propagation direction and amplitude variation throughout the year. One should keep in mind that each zonal wave component is the superposition of all waves with the same zonal structure, i.e. a superposition of many different wave periods. The different wave periods can be extracted from the wave components through spectral analysis at a single longitude using a fast Fourier transformation, a wavelet analysis [*Torrence and Compo*, 1998] or in the case of unevenly spaced data, the Lomb-Scargle method [*Press and Teukolsky*, 1988]. An example of an extraction of a specific wave period can be found in Paper I, Figure 4.

2.4. PW activity in the MLT

The intra-annual variation of PW activity in the MLT, visible in the Hovmöller diagram shown in Figure 2.8 for the year 2000 and in Figure 5 and 6 in Paper I for all years between 2000 and 2008, can be examined as a time series and seasonal climatology of the observed PW amplitudes. This has been done for both the PW amplitudes derived from the meridional wind as well as from the meridional wind anomaly (the derivation of the meridional wind from its climatological mean). Figures 2.9 (a) and (b) show the seasonal climatology of PW amplitudes (sum of zonal wave numbers one and two) for (a) the meridional wind and (b) the meridional wind anomaly, respectively. In addition Figures 8 and 9 in Paper I [*Kleinknecht et al.*, 2014] show the PW amplitudes for zonal wave number one and two separately.

The climatology of both datasets shows an enhancement of the PW amplitudes during autumn and late winter. In addition, a very strong enhancement can be seen in the PW amplitudes retrieved from the meridional wind during mid-summer. This observation leads us to the question as to where this activity comes from and if its variability is related to the variability of the underlying atmosphere.

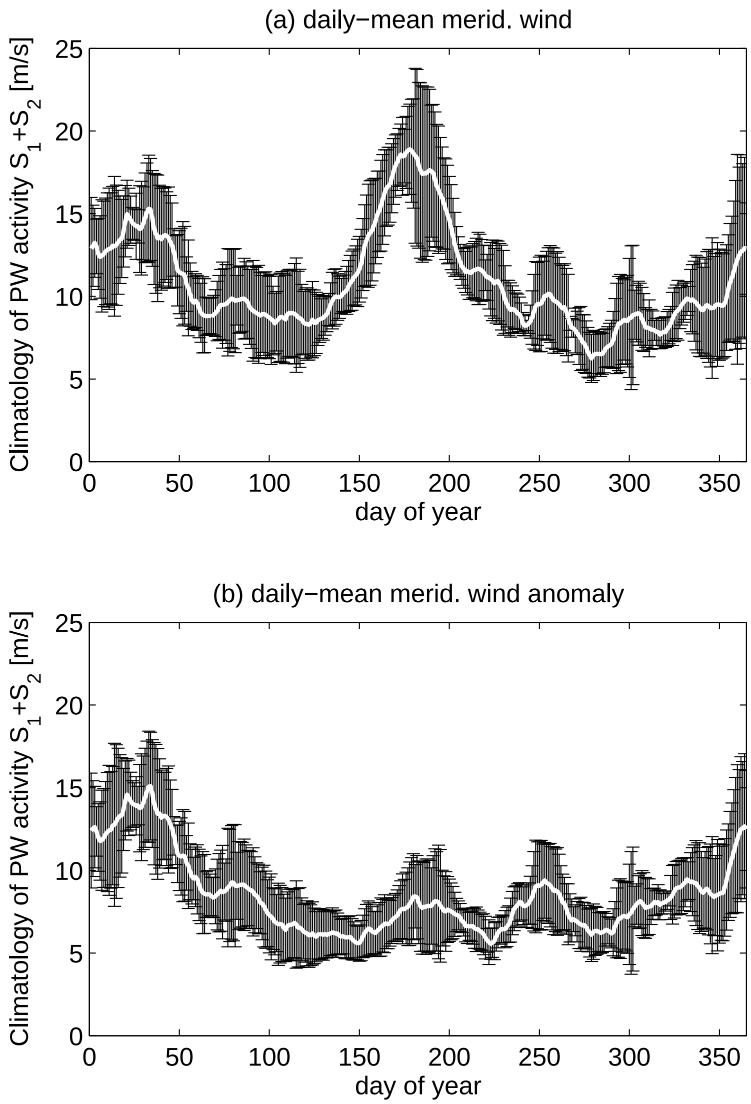

Figure 2.9.: Climatology of MLT PW amplitudes (S_1+S_2) from the SuperDARN chain derived (a) from the daily-mean meridional wind and (b) from the daily-mean meridional wind anomaly. The white line shows the 15 day smoothed climatology. The black error bars depict the year-to-year variability (1-σ standard derivation).

3. How does the variability of the middle atmosphere affect PW activity in the MLT?

To be able to answer the question as to how and if PW activity in the MLT is related to variability in the middle atmosphere we first have to recall how the middle atmosphere varies throughout the year and how PWs are affected by the atmosphere.

3.1. Variability throughout the middle atmosphere

Conventionally the atmosphere is divided in vertical layers according to the sign change of the temperature gradient with height. Figure 3.1 shows (a) the zonal-mean temperature and wind structure of the atmosphere during December solstice and (b) the annual mean temperature distribution as derived from the Whole Atmospheric Community Climate Model (WACCM), which is briefly described in Appendix B. In the lowest layer, the troposphere, the temperature decreases with altitude because the effect of surface heating reduces. It is bounded by the tropopause at around 15 km and followed by the stratosphere, which is bounded by the stratopause at around 50 km. In the stratosphere the temperature rises with altitude due to absorption of solar ultra-violet radiation by ozone, known as ozone heating. The temperature then drops again in the mesosphere due to diminished radiative heating and increased radiative cooling to space by, for example carbon dioxide. The temperature maximum between the stratosphere and the mesosphere is called the stratopause. Both layers together are often referred to as the middle atmosphere and are bound by the mesopause at around 100 km. The region above is called the thermosphere. Here the temperature rises again due to molecular dissociation by very energetic solar radiation.

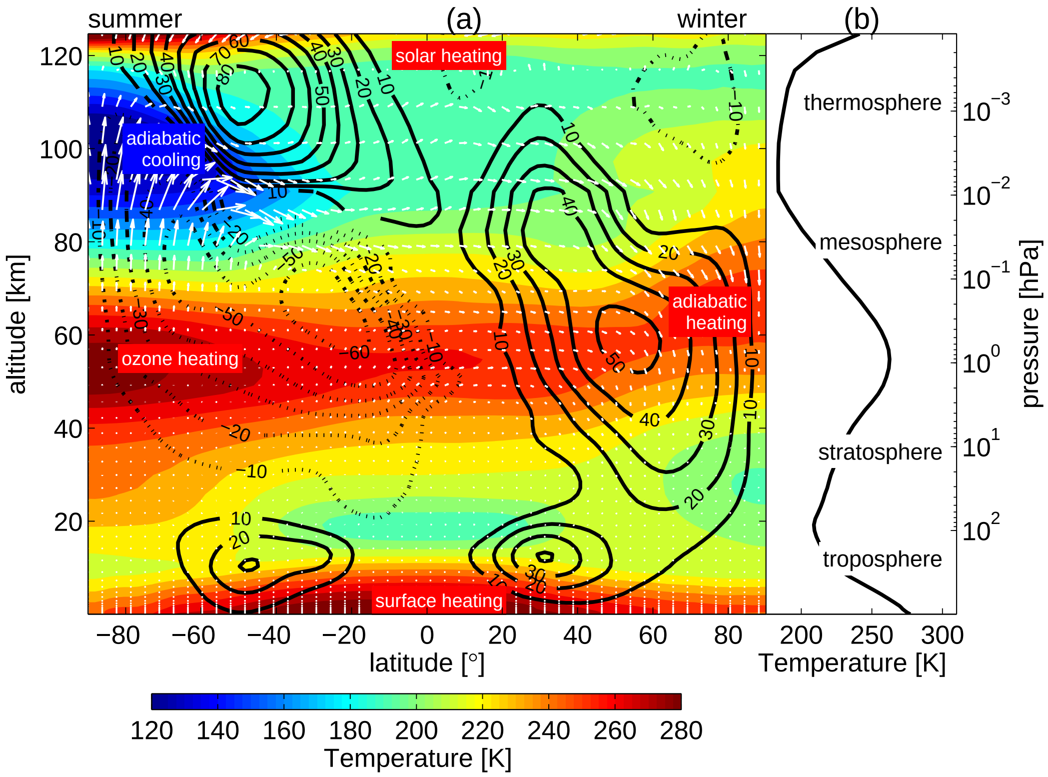

Figure 3.1.: Atmospheric structure derived from WACCM. (a) Solstitial atmospheric conditions of zonal-mean temperature (color plot), zonal-mean zonal wind (black contour lines) and zonal-mean vertical and meridional wind (white arrows). The vertical speed has been enlarged for better visibility. (b) Annual-mean temperature structure.

In addition to the general change of temperature with altitude, strong latitudinal variations between the summer and the winter hemisphere can be observed. These variations are related to differences in solar insolation (i.e. more hours of sunlight during summer) and to the dynamical forcing through waves that results in adiabatic heating and cooling.

3.1.1. Variations in the stratosphere

The 24-hour heating in the polar stratosphere during summer, due to solar absorption by ozone, results in a decreasing temperature gradient towards the equator. This results in a strong, westward, geostrophic, thermal wind in the summer stratosphere. In the winter polar stratosphere, where little or no solar heating takes place, the temperature increases towards the equator leading to strong eastward thermal wind [e.g. *Andrews*, 2010]. This cyclonic circulation (eastward flow around the winter pole) maximizes at mid-latitudes ($\sim 50\,^\circ$ latitude) at an altitude of approximately 1 hPa ($\sim$ 50 km) and is called the polar vortex. This is illustrated in Figure 3.1 which depicts the climatological temperature and wind data from WACCM at December solstice.

This stratospheric zonal wind interacts strongly with GWs (Section 3.1.2) and PWs (Section 3.2). For example, the polar vortex can be weakened and disturbed by PW interaction with the mean flow [*Matsuno*, 1971]. The Arctic polar vortex is less stable than the Antarctic polar vortex since the zonal distribution of water and land masses in the Northern Hemisphere is a source of PWs. The variability of the northern polar vortex leads to strong variations in the stratospheric wind conditions during winter and strong vertical coupling. One extreme example of this is a stratospheric sudden warming (Section 3.1.3), where the polar vortex winds can reverse briefly, reflecting summer time wind conditions.

3.1.2. Variations in the mesosphere

The mesosphere is strongly dynamically driven. The pole-to-pole residual circulation established by wave breaking is strongest around solstice and called the solstitial mesospheric circulation or meridional circulation. It is known to be driven by non-isotropic momentum deposition by GWs in the mesosphere. Density oscillations produced by these waves are coupled to temperature, pressure and wind-velocity variations. Periods of GWs are typically short (i.e. several minutes to 1 day). However, the bulk of the energy and momentum are carried by waves with periods less than 1 hour [*Vincent*, 1984].

GWs can have westward as well as eastward phase speeds. Their propagation depends strongly on the zonal background winds of the atmosphere. GWs that encounter a wind velocity equal or greater than their wave phase velocity will be absorbed by the background flow [*Fritts and Alexander*, 2003]. When this occurs, the waves are said to have reached a critical level.

As shown in Figure 3.1, stratospheric winds reach a maximum near the peak of the ozone heating, and any wave coming from below with a phase velocity less than the maximum wind velocity will reach critical levels below the stratopause. This alters the GW spectrum that can reach the mesosphere, with a predominance of eastward waves in the summer and westward waves in winter. This is illustrated in Figure 3.2.

Since the energy density of a wave is preserved, its amplitude will increase in proportion to the exponential decrease of atmospheric density with height as it moves upward. If the amplitude of the wave gets too large the temperature perturbations related to the wave cause the temperature gradient to exceed the adiabatic lapse rate. This causes the wave to become unstable and break. The momentum carried by the wave will then be transferred to the atmosphere. Waves generally reach amplitudes that lead to breaking in the mesosphere [*Lindzen*, 1981]. Thus the change of the stratospheric wind direction and strength throughout the year (Section 3.1.1) alters the GW momentum deposition in the mesosphere by wave breaking.

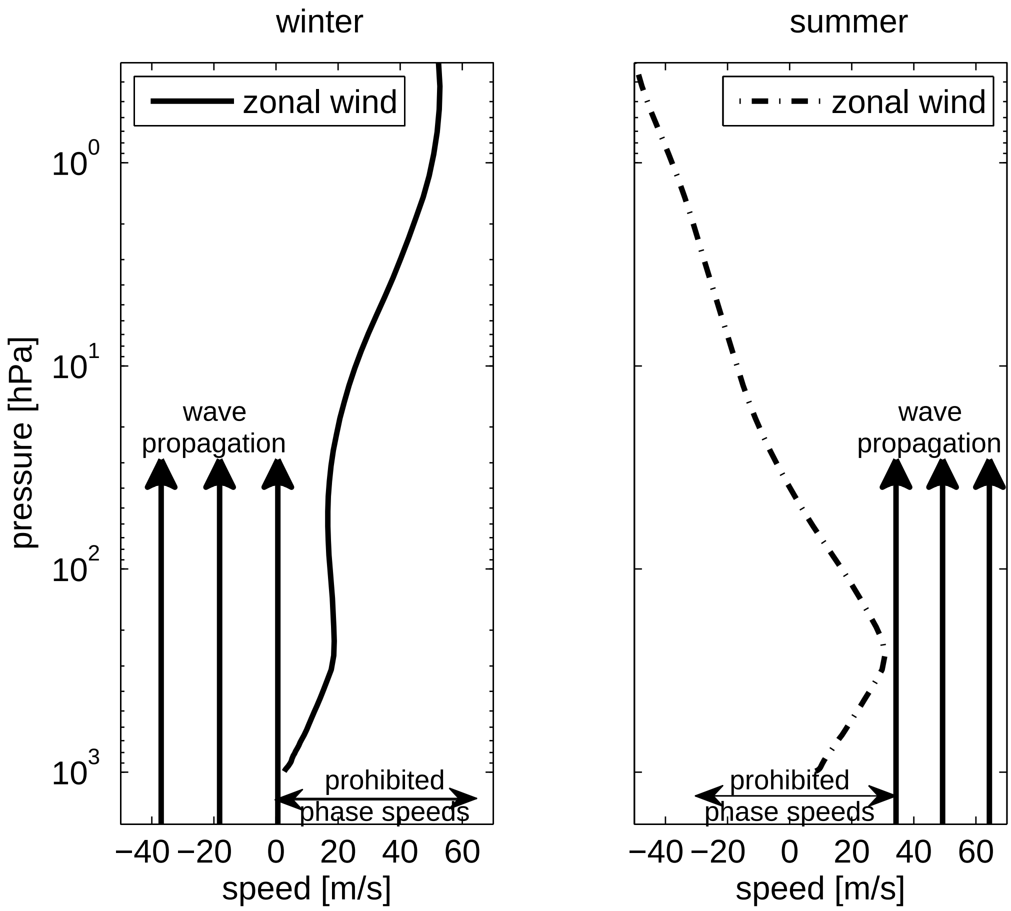

Figure 3.2.: Schematic sketch of a gravity wave filtering by the tropospheric and stratospheric winds. After *Lindzen* [1981]

This seasonal variation of the gravity-wave momentum deposition in the mesosphere, with net-eastward momentum deposited in summer and net-westward momentum in winter, results in a force that pushes the wind to the east in summer and to the west in winter. Since this results in a deceleration of the zonal wind in the mesosphere the force is often referred to as a drag force. However this force does not approach zero when the wind speed approaches zero as is common for a conventional drag force. Rather it continues to turn the zonal wind in the MLT as illustrated in Figure 3.1, where the climatological temperature and wind data from WACCM at December solstice are shown.

The turning of the wind results in an enhanced meridional flow towards the equator in the summer and towards the pole in the winter hemisphere [e.g. *Lindzen*, 1981]. This leads to a residual circulation from the summer to the winter pole. The result of this meridional motion is convergence and downwelling at the mesospheric winter pole and divergence and upwelling at the mesospheric summer pole [e.g. *Brasseur and Solomon*, 2005]. The adiabatic heating and cooling that results from the downwelling and upwelling of air parcels at the poles leads to a warm winter pole and cold summer pole, respectively. This is illustrated in Figure 3.1 with climatological temperature and wind data from WACCM at December solstice.

Additional interaction of PWs with this meridional circulation might alter the strength of the flow and hence result in a modulation of the vertical coupling. The effect of PWs on the mesospheric meridional circulation has been investigated in this thesis and is presented in Section 4.1.2 and 4.1.1 as well as in Papers II and III.

3.1.3. Stratospheric sudden warmings

As mentioned in Section 3.1.1, the polar vortex can be disturbed through interactions with PWs. These disturbances range from local perturbations to total breakdowns of the polar vortex and can lead to effects that are observable all the way from the troposphere into the thermosphere and ionosphere [e.g. *Limpasuvan et al.*, 2004; *Goncharenko et al.*, 2010; *Pancheva and Mukhtarov*, 2011; *Yuan et al.*, 2012]. These strong disturbances are referred to as stratospheric sudden warmings (SSWs) because they were first observed through the sudden heating in the polar stratosphere. SSW events are divided into major and minor events by the World Meteorological Organization (WMO). Major events are defined as a positive poleward temperature gradient between 60° latitude and the pole and a zonal mean wind reversal at 10 hPa and 60° latitude. Minor events are defined as those which show only a significant temperature increase at stratospheric altitudes [*Chandran et al.*, 2013a].

Recent studies of SSW events favour the use of polar cap temperatures or winds to define the existence and strength of an SSW event [*Tweedy et al.*, 2013; *Chandran et al.*, 2014]. For the investigations in this PhD work SSW events have been defined as those characterized by a wind reversal of the zonal-mean zonal polar cap (70-90 $^\circ$ latitude) at an altitude of 0.7 hPa ($\sim$ 50 km), after *Tweedy et al.* [2013]. Figure 3.3 shows SD-WACCM results for the general behaviour of the polar cap zonal-mean temperature (a) and the zonal-mean zonal (b), meridional (c) and vertical (d) winds during a polar cap wind reversal in December 2001. Early in the event (days -30 to -10) there are general wintertime conditions. The temperature (Figure 3.3 a) increases with altitude up to $\sim$ 60 km, whereupon it decreases up to the mesopause, with the maximum temperature, the stratopause, occuring near 60 km. The model zonal wind (Figure 3.3 b) is eastward in the stratosphere and westward in the mesosphere. The meridional (Figure 3.3 c) and vertical (Figure 3.3 d) winds are respectively slightly poleward and downward in the lower mesosphere. During an SSW event strong stratospheric PWs interact with the eastward polar vortex. They deposit westward momentum and decelerate and reverse the zonal wind. Day zero (black vertical line) is set to the onset of the reversal of the stratospheric polar cap zonal-mean zonal wind at 50 km. The deceleration of the wind leads to a heating and decent of the stratopause. The deceleration of the polar vortex also reduces the filtering effect on eastward waves, and during the reversal, produces stronger filtering of westward propagating waves. This leads to a change in the momentum deposition in the mesosphere, resulting in a reversal of the mesospheric winds from westward to eastward and a corresponding change of the meridional circulation [*Limpasuvan et al.*, 2012], as can be seen in Figure 3.3. The resulting equatorward and upwelling flow in the polar mesosphere temporarily produces summertime conditions. Wave interaction with the background atmosphere results finally in a re-establishment of pre-SSW wintertime conditions.

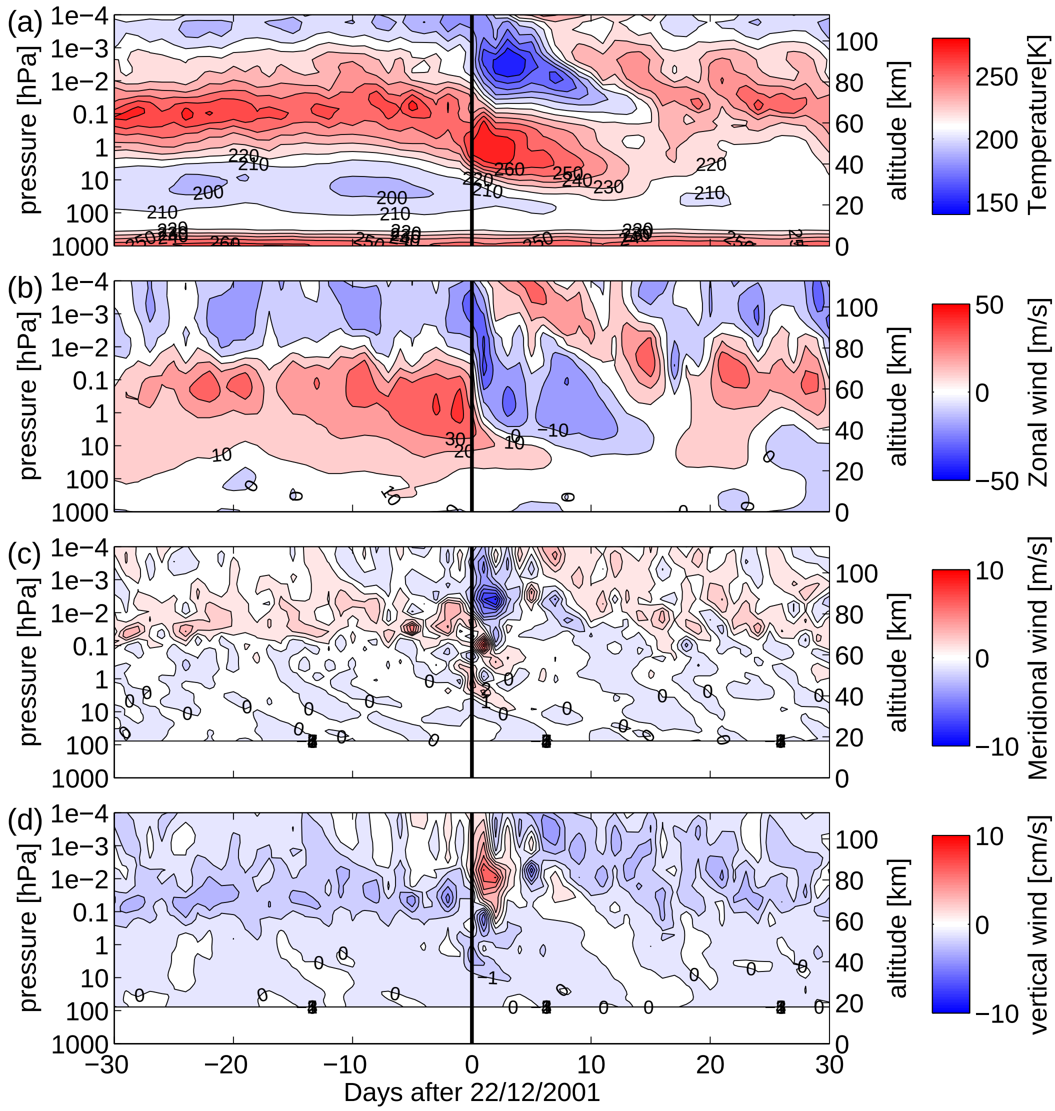

Figure 3.3.: Typical polar cap (70-90°N) zonal-mean temperature (a), zonal-mean zonal (b), meridional (c) and vertical (d) wind variations during a sudden stratospheric warming (here: 22.12.2001) extracted from SD-WACCM.

Some SSWs are followed by a nearly isothermal vertical temperature profile in the upper stratosphere and lower mesosphere, after which the temperature maximum (stratopause) forms again through convergence at altitudes around 75-80 km [*Chandran et al.*, 2014, and references therein]. Such an event is known as an elevated stratopause (ES) event since the altitude of the stratopause is elevated from its climatological wintertime location ($\sim$60 km). This elevated stratopause will propagate downward to its pre-SSW altitude after the warming when the zonal and vertical gradients return to general wintertime conditions. All SSWs have the same general development as the SSW described above, but they vary widely in strength, duration, extent and onset date. The effects of SSWs lead to enhanced vertical coupling which can be seen throughout the whole atmosphere. Their effect on PW activity in the MLT has been investigated in this thesis and is presented in Section 4.2.1 and Paper IV [*Stray et al.*, 2015].

3.2. Planetary waves

Here we briefly recall the concept of PWs and how their propagation can be affected by winds. PWs are large-scale motions of the atmosphere. They have horizontal scales of thousands of kilometres, a vertical size of several kilometres and periods on the order of days. Also known as rotational waves or Rossby waves, they are important for the understanding of many large-scale atmospheric phenomena. The latitudinal gradient of the planetary vorticity caused by the rotation of the earth provides the restoring force for PWs. Briefly, atmospheric motion is controlled by conservation of absolute vorticity (=relative vorticity of an air parcel + planetary vorticity) under non-divergent conditions.

The displacement of an air parcel towards the north will reduce the planetary vorticity and make the parcel spin up in a clockwise sense to conserve absolute vorticity. This creates northward air motion to the west of the parcel and southward air motion to the east of the parcel. This moves parcels west of the initial perturbation northward, where they too spin up in a clockwise sense. On the other hand, the parcels to the east of the initial disturbance are moved southward, slowing their clockwise rotation and ultimately taking an anticlockwise rotation as they pass south of their equilibrium position. Hence the initial northward displacement will move towards the west and can be described by a westward propagating wave motion, as shown in Figure 3.4.

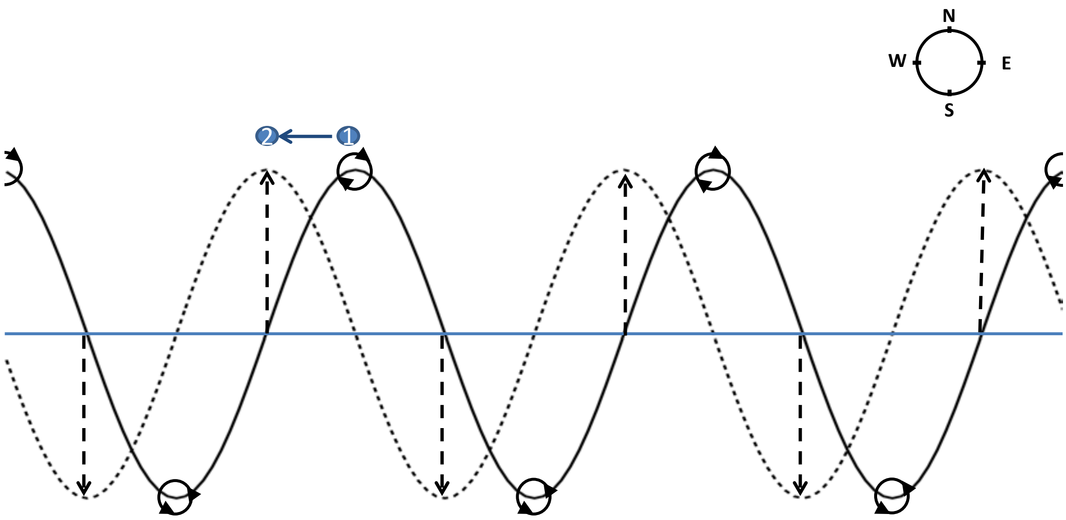

Figure 3.4.: Schematic sketch of a planetary wave. The blue line indicates the equilibrium latitude of the parcel before the displacement. The sine curves symbolize the propagation of the wave to the west, with the dashed line following the solid line in time.

3.2.1. PW interaction with the atmosphere

The propagation of PWs depends strongly on the zonal background wind and the zonal phase speed of the wave: *Charney and Drazin* [1961] used a simplified analytical solvable system to derive that stationary PWs can only propagate into regions of eastward wind that is not too strong. More generally speaking *Volland*

[1988] states that planetary waves can only exist when the zonal mean wind ($\bar{u}$) is both smaller (more westward) than the Rossby critical velocity (U_c),

$$\bar{u} < U_c \tag{3.1}$$

and larger (more eastward) than the zonal phase velocity (c_p) of the wave,

$$\bar{u} > c_p. \tag{3.2}$$

The phase velocity,

$$c_p = -\frac{a\Omega\cos(\phi)}{s\tau},$$

depends on the period, τ, and the zonal wave number of the wave, s, in addition to the Earth's radius, a, the angular velocity, Ω and the latitude of the disturbance, ϕ [*Forbes*, 1995]. The critical velocity, U_c is defined as follows:

$$U_c = a \cdot \Omega \cdot \cos(\phi) \cdot \left(2 \left[\frac{\kappa H g}{\Omega^2 a^2} \right]^{\frac{1}{4}} - \frac{1}{s\tau} \right),$$

where κ is the ratio of the gas constant to the heat capacity at constant pressure, H is the scale height and g is the gravitational acceleration.

The intrinsic frequency of a PW entering an area where the wind is westward with respect to its zonal velocity ($\bar{u} < c_p$) will vanish. That is, the wave energy will be absorbed by the background flow. Borders to such an area are called critical lines or zero wind lines in the specific case of stationary waves (c_p=0). PWs entering areas where the eastward winds are too strong ($\bar{u} > U_c$) will be reflected on so-called turning lines.

Typically PWs are observed with periods between 2 and 20 days with zonal wave numbers between 1 and 3 [*Forbes*, 1995]. The zonal phase velocity of these waves at 50° latitude is around -10 to -60 m/s and their critical velocity is between 10 and 50 m/s, as can be seen in Figure 3.5. Hence their phase speed and critical velocity are on the order of the extratropical middle atmospheric summertime and wintertime zonal wind speeds, respectively. Middle atmospheric winds can therefore strongly alter PW propagation through the atmosphere. In particular the summertime stratospheric westward winds absorb the majority of PWs propagating into the high latitude summer stratosphere. The high latitude middle atmosphere only generates turning lines during winter, and, in contrast to summer, is much more disturbed by PWs.

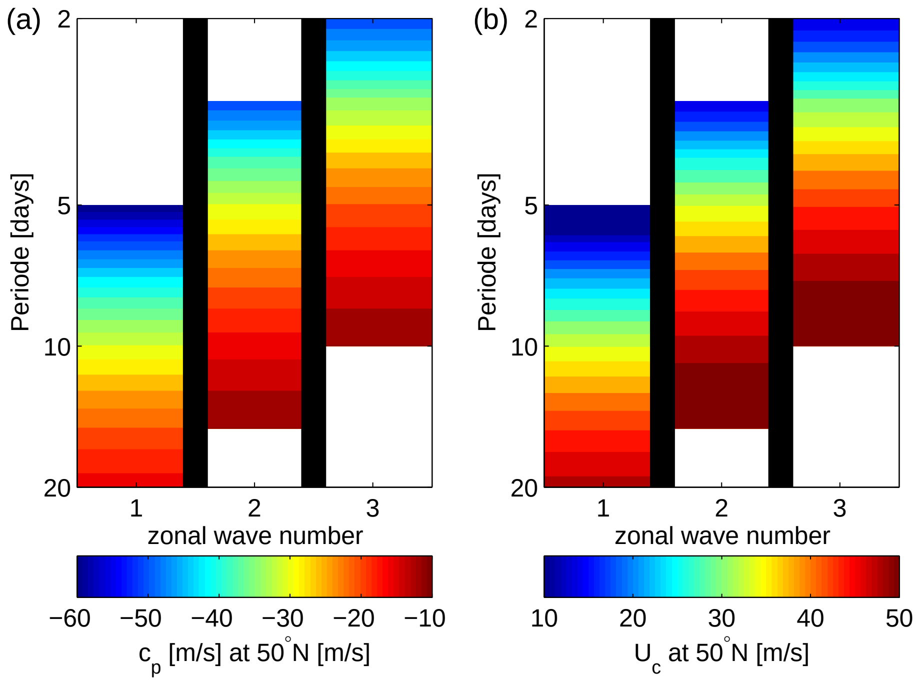

Figure 3.5.: (a) phase speed, c_p, and (b) critical velocity, U_c, at 50°N of PWs typically observed in the middle atmosphere.

In the atmosphere, stationary as well as propagating and travelling normal mode waves with a variety of temporal periods can exist. However the atmosphere responds not to a single mode, but to the superposition of all temporal modes. The superposition of these temporal periods for all waves of a given zonal wave number will itself have that same zonal wave number character, but with a temporally varying amplitude and phase (longitude of maximum amplitude).

4. How does PW activity in the MLT affect the atmosphere?

4.1. PW effects on the atmosphere

The specific question to be addressed was whether PWs can affect the MLT, which is commonly known to be strongly driven by the momentum deposition of GWs [Section 3.1.2]. In Section 4.1.1 we show the presence of a strong, climatologically stable wind and temperature structure in the summertime MLT that represents a PW even through the underlying wind field is in the westward (blocking) direction. In addition, evidence for temporary forcing of the meridional circulation by PW momentum deposition during fall is presented in Section 4.1.2. The details of these studies can be found in Paper III [*Stray et al.*, 2014b] and Paper II [*Stray et al.*, 2014a] in Appendix A.

4.1.1. Quasi-stationary planetary waves in the summer MLT

Meridional winds in the MLT have been observed by the chain of 8 SuperDARN radars as described in Section 2.2. The observed wind is located in a latitude band at $\sim$60°N and at an altitude of $\sim$95 km. The climatology of the meridional wind has been created for all stations from all available data until 2008. These are presented in Figure 4.1 (a). During mid-summer, the magnitude of the wind is a strong function of the station longitude. Examination of the average summertime wind (from day 170 to 190) at the longitude of each station shows a strong wave-like feature to be present, as can be seen in Figure 4.1 (b).

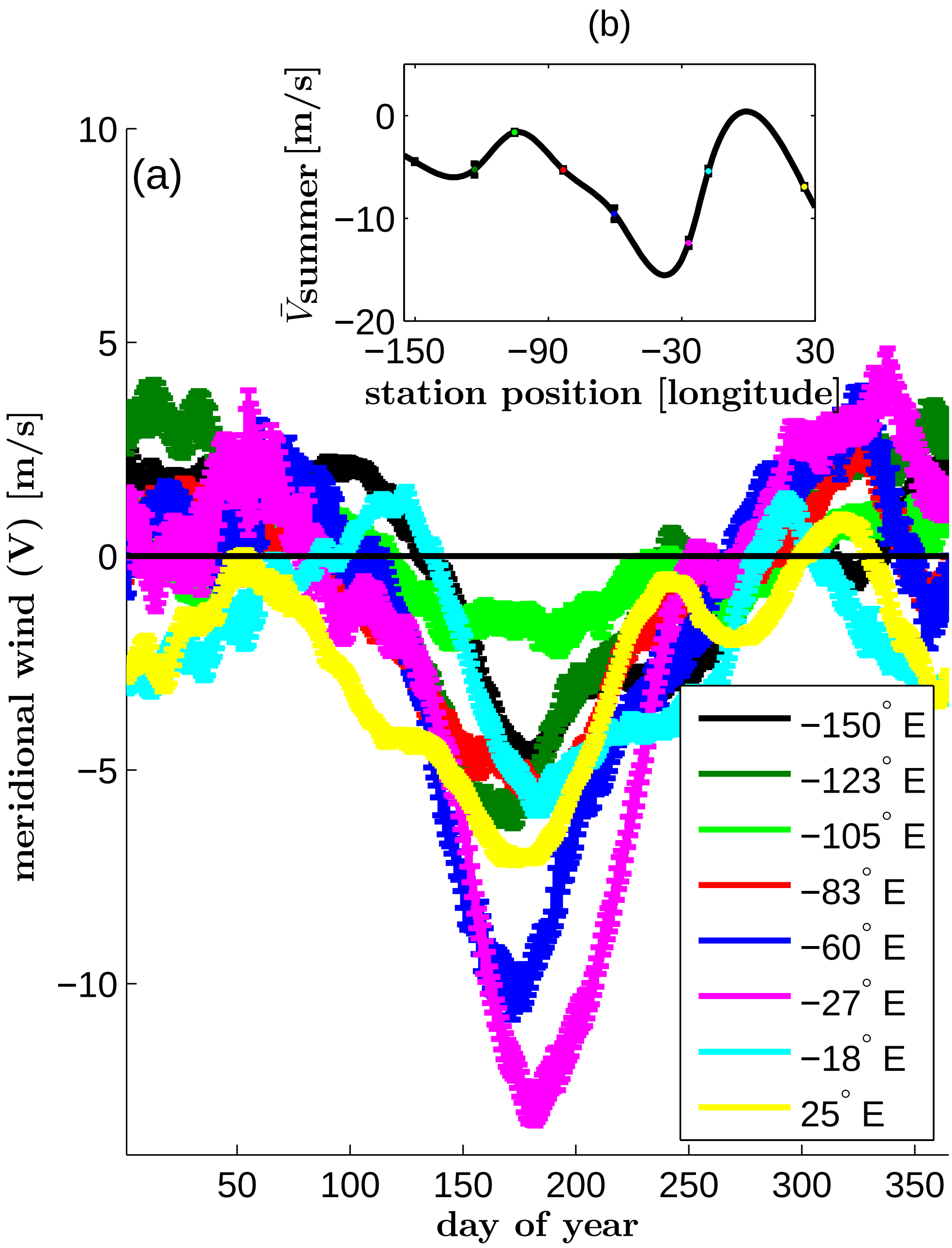

Figure 4.1.: (a) Climatology of daily-mean meridional meteor winds for each of the 8 SuperDARN radar stations. The legend depicts the centroid longitude of the meteor wind measurements for each station. (b) A 20-day average about summer solstice of the daily-mean climatological winds shown in (a) for each of the 8 stations, plotted as a function of the station longitude. From Paper III [*Stray et al.*, 2014b].

This wave-like longitudinal variation can be decomposed into PW zonal wave numbers. The technique described in Section 2.3 has been used to retrieve PW zonal wave numbers 1 and 2 for all days with sufficient data coverage between the years 2000 and 2008. The retrieved PW activity is presented as Hovmöller diagrams for each summer (May-August) and each zonal wave number in Paper III, Figure 3. The Hovmöller diagrams reveal a strong quasi-stationary wave with the zonal wave number one (S_1) component during mid-summer. The amplitude of the retrieved PW is similar each summer as can clearly be seen in the climatology of the PW amplitudes in Figure 2.9 and in Paper I, Figure 9. The longitudinal phase of the zonal wave number 1 PW is not only quasi-stationary throughout each mid-summer (June-August) it also occurs with the same longitudinal phase during all 9 years of observation. This stable phase represents a poleward perturbation of the meridional wind above Russia and an equatorward perturbation of the meridional wind over the Atlantic sector ($\sim$0-60°W).

The existence of such a perturbation of the meridional wind in the MLT suggests a modulation of the meridional circulation in the MLT. The enhanced equatorward winds above the Atlantic sector would suggest stronger upwelling and adiabatic cooling and hence colder temperatures above the Atlantic sector. This could explain the high frequency of occurrence of polar mesospheric clouds (PMC) observed in this sector [*Chandran et al.*, 2010].

The source of the observed longitudinal variation of the meridional wind has been investigated through studies of the wind structure and PW activity in the underlying atmosphere using assimilated winds from the Modern-Era Retrospective analysis for Research and Application (MERRA, Appendix B). The results of this investigation indicate that neither PW modulated filtering of GWs in the lower atmosphere nor direct vertical propagation through the stratosphere represents a significant source. However, longitudinal differences in GW sources and barotropic and baroclinic instabilities, as well as inter-hemispheric coupling, remain as possible explanations for the longitudinal structure in the meridional wind in the MLT.

4.1.2. Temporary forcing of the meridional circulation by planetary waves in the MLT

Here the effect of PWs in the MLT on the meridional circulation during fall is investigated. The results, summarized here and presented in detail in Paper II [*Stray et al.*, 2014a], show evidence for temporary PW forcing of the MLT during the fall equinox. The effect of this temporary forcing by PWs is a concurrent poleward wind perturbation and subsequent temperature enhancement in the MLT around fall equinox. The fall enhancement of PW amplitudes is coincident with a minimum in the magnitude of the stratospheric winds, and consequently a minimum in the stratospheric filtering of GW's [Section 3.1.2] and PW's [Section 3.2] with non-zero phase speed. The GW filtering is reduced since the low zonal wind magnitudes that occur during fall result in fewer GWs encountering critical levels. However, this enhanced momentum deposition does not necessarily result in an enhanced net-forcing. An isotropic source distribution of GWs encountering weak winds with no preferential direction, a situation that occurs during equinox, results in a similar amount of eastward and westward momentum deposition in the MLT [Section 3.1.2]. Thus, there would be little net-forcing. This reduced net-forcing by GWs in fall has been observed with a new generation All-Sky Interferometric (SKiYMET) meteor radar located in Trondheim (63°N,10°E), Norway [*de Wit et al.*, 2014a, b] and is presented in Paper II, Figure 5.

In contrast to GWs, the source spectra of PWs is not isotropic since PWs always have a westward phase speed as discussed in Section 3.2. The weak westward and eastward winds present around equinox will therefore result in few critical ($\bar{u} = c_p$) or turning ($\bar{u} = U_c$) lines, respectively. As a result there is enhanced transmission of PWs into the MLT and an increase of the westward momentum carried to the MLT by PWs. This additional westward momentum temporarily drives the mesospheric meridional circulation towards the pole and leads to increased poleward flow. Such an increased poleward flow in the MLT was observed simultaneously with the enhancement of PW activity in the MLT.

As an example Figure 4.2 shows the climatology of the daily mean meridional wind (blue) in the MLT (∼95 km) measured by the SuperDARN radar at Stokkseyri (64.7°N, 26.9°W) and the 20 day smoothing of this climatology (green). A comparison with the seasonal change of meridional wind due to pure radiative and GW forcing, represented by the annual and semi-annual components of the wind (red line), shows a strong poleward perturbation around fall equinox.

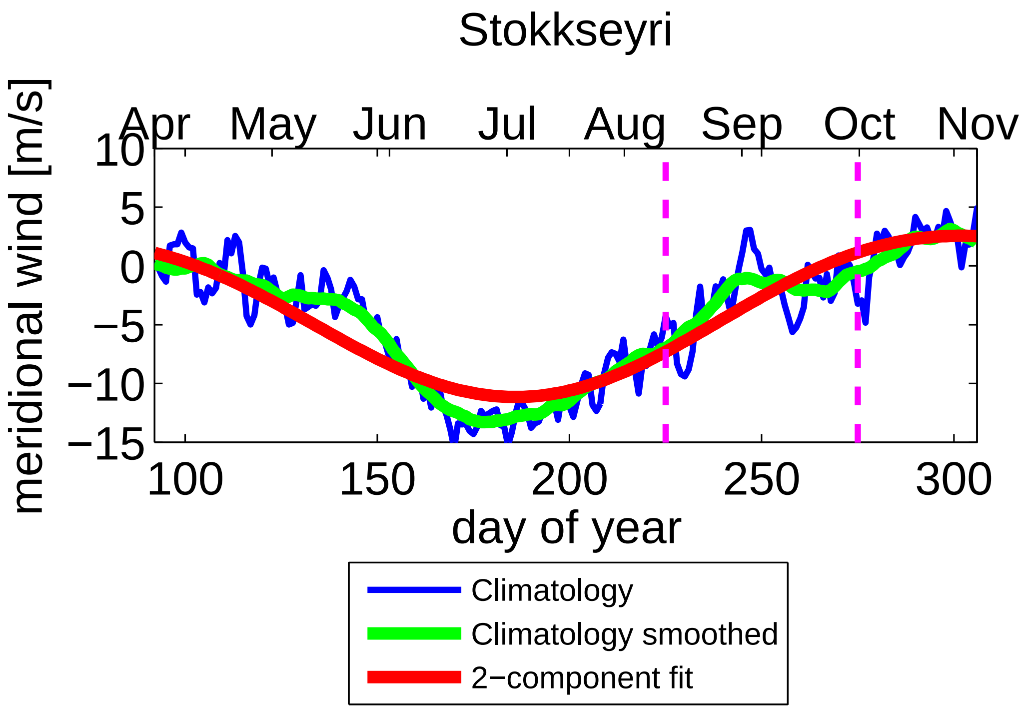

Figure 4.2.: Climatology of the daily mean meridional wind (blue) in the mesosphere (∼95 km) measured by the SuperDARN radar at Stokkseyri and the 20-day smoothing of the climatology (green). The red curve depicts the seasonal effect due to pure radiative and GW forcing. A poleward perturbation away from the standard picture is clearly visible around fall equinox. From Paper II [*Stray et al.*, 2014a].

The increased poleward flow results in stronger convergence and downwelling at the pole than that provided by the GW forcing during this time. This, in turn, leads to a temporary enhancement of the mesospheric temperature. Such a perturbation of the temperature has been observed using LIDAR [*She et al.*, 2000; *Pan and Gardner*, 2003; *Kawahara et al.*, 2004]. These observations show a temperature perturbation that propagates downward from the MLT in time. In addition hydroxyl (OH) rotational temperatures at $\sim$ 87 km show enhanced temperatures following the PW enhancement observed in the MLT [e.g. *Espy and Stegman*, 2002]. An example of such a temperature enhancement can be seen in Figure 4.3 showing a superposed annual epoch of Meinel OH (3,1) rotational temperatures ($\sim$ 87 km) from 1991 to 1998 above Stockholm, Sweden.

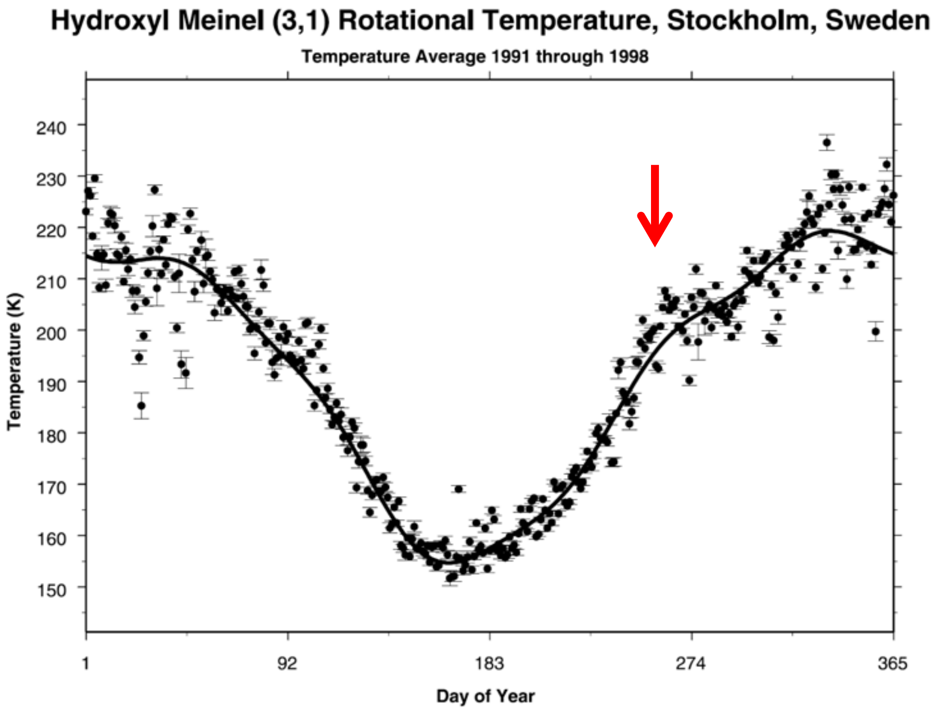

Figure 4.3.: Superposed annual epoch of Meinel OH (3,1) rotational temperatures ($\sim$ 87 km) from 1991 to 1998 (points) from Stockholm, Sweden. The error bars represent the standard error of the mean. The "shoulder" of the enhanced temperature is seen after day 250. From *Espy and Stegman* [2002].

The study shows that at times when the GW forcing is at a minimum, the westward momentum carried by PWs can become the primary driver of the residual meridional circulation in the MLT and results in a perturbation to the smooth seasonal transition.

4.2. The effect of middle atmospheric variability on PW activity in the MLT

The strong PW activity observed during fall equinox showed a strong connection between the stratospheric wind conditions and the occurrence of PWs in the MLT. That is, low stratospheric wind speeds (eastward and westward) throughout the middle atmosphere make the atmosphere transparent to PW propagation. In the following section the correlation between sudden changes of the middle atmospheric wind field and enhanced PW activity in the MLT are presented through investigations of the effect of stratospheric sudden warmings on PW activity in the MLT. Stratospheric sudden warmings have been defined in Section 3.1.3. All details of the study presented below can be found in Paper IV [*Stray et al.*, 2015] in Appendix A.

4.2.1. MLT Planetary wave activity triggered by SSWs

As noted in Section 3.1.1 and 3.1.3 stratospheric sudden warmings (SSWs) often appear in the northern hemisphere and lead to reversals of the polar vortex and strong coupling throughout the atmosphere. This study investigates whether the observation of PW enhancements in the MLT during winter, presented in Section 2.4, could be related to SSWs. Previous model results and a single case study of a strong SSW event have shown the capability of SSWs to trigger enhanced PW activity in the MLT [*Limpasuvan et al.*, 2012; *Chandran et al.*, 2013a, b]. Here observations of MLT PW activity (zonal wave numbers 1 and 2) derived from the SuperDARN network using the technique described in Section 2.3 have been used to investigate whether the MLT PW enhancement is related to strong SSW events only, or if it is in fact a general feature related to any reversal of the stratospheric (~50 km) polar cap (70-90°N) zonal-mean zonal wind that occurs during SSWs, irrespective of the strength of that reversal. The study shows a drastic enhancement of the MLT PW activity after strong SSW events, and this has been confirmed by model results using the Specified Dynamics Whole Atmospheric Community Model (SD-WACCM, Appendix B). These strong events are all followed by elevated stratopause events. In addition, a moderate but significant correlation (correlation coefficient of 0.4) between all reversals of the stratospheric polar cap zonal-mean zonal wind and PW enhancements in the MLT was found. This correlation demonstrates that in general, polar cap stratospheric wind reversals during SSW trigger PW activity in the MLT.

Indications as to the source mechanisms of the observed PW enhancement during stratospheric wind reversals triggered by an SSW can be obtained from the background condition and the PW activity from the ground to ~120 km that has been modelled using SD-WACCM (Appendix B). The modelled PW activity indicates that the PW activity minimizes at altitudes around 80 km before it strengthens again at higher altitudes in the MLT. This minimum suggests that the PW activity in the MLT after the onset of the wind reversal might be locally generated and is not a continuation of the enhanced stratospheric PW activity. Furthermore, the modelled temperatures and winds in the middle atmosphere reveal strong vertical wind and temperature gradients during SSWs. The existence of such strong gradients in wind and temperature favour the development of baroclinic and barotropic instabilities [e.g. *Matsuno*, 1971; *Pedlosky*, 1979; *Nielsen et al.*, 2010] which have the ability to generate secondary PWs in the MLT [e.g. *Chandran et al.*, 2013b]. However, secondary PWs in the MLT can also be generated in-situ by zonal asymmetric GW drag as a result of asymmetric wind conditions during SSWs [e.g. *Liu and Roble*, 2002]. This asymmetric drag results from the filtering of GWs by the zonally asymmetric stratospheric winds.

Further modelling and altitude-resolved observational studies would be required to determine the actual source of the enhanced PW activity. This study however demonstrates not only that the variations in the middle atmosphere conditions can control the PW activity in the MLT, but also that the strong influence of SSWs on PW activity in the MLT is independent of the strength of the stratospheric wind reversal during the events, demonstrating the strong dependence of PW activity in the MLT on variations of middle atmospheric conditions.

5. Conclusions

The importance of gravity waves (GWs) in affecting the mesosphere lower thermosphere (MLT) and creating the meridional circulation has been widely recognized. The existence of planetary waves (PWs) in the MLT and their additional effect on that region is, however, less well documented and studied. This thesis shows how PWs can affect the MLT region, especially the meridional circulation, and how strongly the PW activity in the MLT depends on the variations of the underlying atmosphere.

In this thesis it has been shown that during times when the GW forcing is low, PW momentum deposition directly influences the strength of the meridional circulation. Consequently, this influences the vertical transport in this region, changing the temperature and composition not only in the MLT but also in adjacent regions. At other times it has been shown that PWs modulate the longitudinal structure of the meridional wind and temperature around the pole which, for example, can modulate the longitude where polar mesospheric clouds preferentially form and occur.

The strong correlation to conditions in the underlying atmosphere shows the MLT region is strongly influenced by variations in the middle atmosphere. However these variations occur not only in predictable annual cycles, but also show interannual variability, even occurring suddenly during SSW events that influence the entire atmosphere. This highlights the need to be able to predict the variations in the middle atmosphere. In addition this shows the importance of understanding how middle atmospheric variations couple into the MLT and modulate this region through PW activity.

This thesis developed a "ground-based satellite" using SuperDARN meteor wind measurements to observe PW activity with zonal wave numbers one and two in the MLT. This allowed the question as to when PW activity is present in the MLT to be answered [Paper I, *Kleinknecht et al.*, 2014], and it was shown that strong PW enhancements occur during mid-summer, late winter and fall equinox. It was shown that this enhanced PW activity during fall temporarily drives the global meridional circulation [Paper II, *Stray et al.*, 2014a], and that the strong stationary PWs during summer have the ability to modulate the longitudinal temperature structure and composition of the MLT and the underlying region [Paper III, *Stray et al.*, 2014b]. In addition, this thesis has shown how the observed PW activity is coupled to variations in atmospheric conditions in the underlying atmosphere, demonstrating how polar cap wind reversals during SSWs [Paper IV, *Stray et al.*, 2015] and low stratospheric wind magnitudes during fall equinox [Paper II, *Stray et al.*, 2014a] change the PW activity in the MLT. In addition, possible source mechanisms for the PW activity that has been observed have been investigated using re-analysis data and simulations with coupled chemical-dynamical assimilation models.

As a body, this work shows that PW activity in the MLT has a significant effect on this region and adjacent areas, and that it is strongly related to variations of atmospheric conditions in the underlying middle atmosphere.

The observations of PW activity in the MLT obtained in this work form a starting point for examination how these variations of the neutral atmosphere drive the variations in the ionosphere that have been the subject of recent attention [e.g. *Immel et al.*, 2006; *Pedatella and Forbes*, 2010] and form the basis for the Ionospheric Connection Explorer (ICON), a NASA mission scheduled for 2017 to understand the physics that lies beneath the unpredictability of our space environment. Thus, this work opens the opportunity to utilize the SuperDARN radar system to understand how and when planetary wave activity in the MLT can couple into the ionosphere, how strong this coupling is and how it affects the ionosphere.

References

Andrews, D. G., *An Introduction to Atmospheric Physics*, Cambridge University Press, Cambridge, U.K., 2nd Edition, 2010.

Brasseur, G. P., and S. Solomon, *Aeronomy of the Middle Atmosphere*, Chemistry and Physics of the Stratosphere and Mesosphere Series, Springer, 2005.

Chandran, A., D. W. Rusch, A. W. Merkel, G. E. Thomas, M. J. Taylor, S. M. Bailey, and J. M. Russell III, Polar mesospheric cloud structures observed from the cloud imaging and particle size experiment on the Aeronomy of Ice in the Mesosphere spacecraft: Atmospheric gravity waves as drivers for longitudinal variability in polar mesospheric cloud occurrence, *J. Geophys. Res.*, *115*(D13102), doi: 10.1029/2009JD013185, 2010.

Chandran, A., R. L. Collins, R. R. Garcia, D. R. Marsh, V. L. Harvey, J. Yue, and L. de la Torre, A climatology of elevated stratopause events in the whole atmosphere community climate model, *J. Geophys. Res.*, *118*, 1234–1246, doi: 10.1002/jgrd.50123, 2013a.

Chandran, A., R. R. Garcia, R. L. Collins, and L. C. Chang, Secondary waves in the middle and upper atmosphere following the stratospheric sudden warming event of January 2012, *Geophys. Res. Lett.*, *40*, 1–7, doi: 10.1002/grl.50373, 2013b.

Chandran, A., R. Collins, and V. Harvey, Stratosphere-mesosphere coupling during stratospheric sudden warming events, *Advances in Space Research*, *53*(9), 1265–1289, doi: 10.1016/j.asr.2014.02.005, 2014.

Charney, J. G., and P. G. Drazin, Propagation of planetary-scale disturbance from lower into upper atmosphere, *Geophys. Res. Lett.*, *66(1)*, 83–109, doi: 10.1029/JZ066i001p00083, 1961.

Chisham, G., and M. P. Freeman, A reassessment of SuperDARN meteor echoes from the upper mesosphere and lower thermosphere, *J. Atmos. Solar-Terr. Phys.*, *102*, 207–221, doi: http://dx.doi.org/10.1016/j.jastp.2013.05.018, 2013.

Day, K. A., M. J. Taylor, and N. J. Mitchell, Mean winds, temperatures and the 16-and 5-day planetary waves in the mesosphere and lower thermosphere over Bear Lake Observatory (42° N, 111° W), *12*(3), 1571–1585, doi: 10.5194/acp-12-1571-2012, 2012.

de Wit, R. J., R. E. Hibbins, and P. J. Espy, The seasonal cycle of gravity wave momentum flux and forcing in the high latitude northern hemisphere mesopause region, *J. Atmos. Solar-Terr. Phys.*, doi: 10.1016/j.jastp.2014.10.002, 2014a.

de Wit, R. J., R. E. Hibbins, P. J. Espy, Y. J. Orsolini, V. Limpasuvan, and D. E. Kinnison, Observations of gravity wave forcing of the mesopause region during the January 2013 major Sudden Stratospheric Warming, *Geophys. Res. Lett.*, *41*, 4745–4752, doi: 10.1002/2014GL060501, 2014b.

Espy, P. J., and J. Stegman, Trends and variability of mesospheric temperature at high-latitudes, *Physics and Chemistry of the Earth*, *27*, 543–553, doi: 10.1016/S1474-7065(02)00036-0, 2002.

Eyring, V., T. G. Shepherd, and D. W. Waugh (Eds.), *SPARC CCMVal Report on the Evaluation of Chemistry-Climate Models, V.*, SPARC Report No. 5, WCRP-X, WMO/TD-No.X, 2010.

Forbes, J. M., Tidal and Planetary waves, in *The Upper Mesosphere and Lower Thermosphere: A Review of Experiment and Theory*, *Geophys. Monogr. Ser.*, vol. 87, edited by R. M. Johnson and T. L. Killeen, pp. 67–87, AGU, Washington, D.C., 1995.

Fritts, D. C., and M. J. Alexander, Gravity wave dynamics and effects in the middle atmosphere, *Rev. Geophys.*, *41*(1003), doi: 10.1029/2001RG000106, 2003.

Fritts, D. C., D. Janches, W. K. Hocking, N. J. Mitchell, and M. J. Taylor, Assessment of gravity wave momentum flux measurement capabilities by meteor radars having different transmitter power and antenna configurations, *J. Geophys. Res.*, *117*(D10108), doi: 10.1029/2011JD017174, 2012.

Garcia, R. R., and S. Solomon, The Effect of Breaking Gravity Waves on the Dynamics and Chemical Composition of the Mesosphere and Lower Thermosphere, *J. Geophys. Res.*, *90*(D2), 3850–3868, doi: 10.1029/JD090iD02p03850, 1985.

Goncharenko, L. P., J. L. Chau, H. L. Liu, and A. J. Coster, Unexpected connections between the stratosphere and ionosphere, *Geophys. Res. Lett.*, *37*, L10,101, doi: 10.1029/2010GL043125, 2010.

Greenwald, R. A., K. B. Baker, R. A. Hutchins, and C. Hanuise, An HF phase-array radar for studying small-scale structure in the high-latitude ionosphere, *Radio Sci.*, *20*(1), 63–79, doi: 10.1029/RS020i001p00063, 1985.

Greenwald, R. A., et al., DARN/SUPERDARN - A Global View of the Dynamics of High-Latitude Convection, *Space Sci. Rev.*, *71*(1-4), 761–796, doi: 10.1007/BF00751350, 1995.

Hall, G. E., J. W. MacDougall, D. R. Moorcroft, J. P. StMaurice, A. H. Manson, and C. E. Meek, Super Dual Auroral Radar Network observations of meteor echoes, *J. Geophys. Res.*, *102*(A7), 14,603–14,614, doi: 10.1029/97JA00517, 1997.

Hibbins, R. E., and M. J. Jarvis, A long-term comparison of wind and tide measurements in the upper mesosphere recorded with an imaging Doppler interferometer and SuperDARN radar at Halley, Antarctica, *Atmos. Chem. Phys.*, *8*(5), 1367–1376, doi: 10.5194/acp-8-1367-2008, 2008.

Hocking, W. K., B. Fuller, and B. Vandepeer, Real-time determination of meteor-related parameters utilizing modern digital technology, *J. Atmos. Solar-Terr. Phys.*, *63*(2-3), 155–169, doi: 10.1016/S1364-6826(00)00138-3, 2001.

Holton, J. R., The Influence of Gravity Wave Breaking on the General Circulation of the Middle Atmosphere, *J. Atmos. Sci.*, *40*, 2497–2507, doi: 10.1175/1520-0469(1983)040⟨2497:TIOGWB⟩2.0.CO;2, 1983.

Hussey, G. C., C. E. Meek, D. Andre, A. H. Manson, G. J. Sofko, and C. M. Hall, A comparison of Northern Hemisphere winds using SuperDARN meteor trail and MF radar wind measurements, *J. Geophys. Res.*, *105*(D14), 18,053–18,066, doi: 10.1029/2000JD900272, 2000.

Immel, T. J., E. Sagawa, S. L. England, S. B. Henderson, M. E. Hagan, S. B. Mende, H. U. Frey, C. M. Swenson, and L. J. Paxton, Control of equatorial ionospheric morphology by atmospheric tides, *Geophys. Res. Lett.*, *33*(L15108), doi: 10.1029/2006GL026161, 2006.

Jarvis, M. J., G. O. L. Jones, and B. Jenkins, New initiatives in observing the Antarctic mesosphere, *Adv. Space Res.*, *24*(5), 611 – 19, doi: 10.1016/S0273-1177(99)00479-2, 1999.

Kawahara, T. D., C. S. Gardner, and A. Nomura, Observed temperature structure of the atmosphere above Syowa Station, Antarctica (69S,39E), *J. Geophys. Res.*, *109*(D12103), doi: 10.102972003JD003918, 2004.

Kleinknecht, N. H., P. J. Espy, and R. E. Hibbins, The climatology of zonal wave numbers 1 and 2 planetary wave structure in the MLT using a chain of Northern Hemisphere SuperDARN radars, *J. Geophys. Res.*, *119*(3), 1292–1307, doi: 10.1002/2013JD019850, 2014.

Limpasuvan, V., D. W. J. Thompson, and D. L. Hartmann, The Life Cycle of the Northern Hemisphere Sudden Stratospheric Warmings, *J. Climate*, *17*, 2584–2596, doi: 10.1175/1520-0442(2004)017⟨2584:TLCOTN⟩2.0.CO;2, 2004.

Limpasuvan, V., J. H. Richter, Y. J. Orsolini, F. Stordal, and O.-K. Kvissel, The roles of planetary and gravity waves during a major stratospheric sudden warming as characterized in WACCM, *J. Atmos. Solar-Terr. Phys.*, *78-79*, 84–98, doi: 10.1016/j.jastp.2011.03.004, 2012.

Lindzen, R. S., Turbulence and Stress Owing to Gravity Wave and Tidal Breakdown, *J. Geophys. Res.*, *86*, 9707–9714, doi: 10.1029/JC086iC10p09707, 1981.

Liu, H.-L., and R. G. Roble, A study of a self-generated stratospheric sudden warming and its mesospheric-lower thermospheric impacts using the coupled TIME-GCM/CCM3, *J. Geophys. Res.*, *107*(D23), 4695, doi: 0.1029/2001JD001533, 2002.

Matsuno, T., A dynamical model of the stratospheric sudden warming, *J. Atmos. Sci.*, *28*, 1479–1494, doi: 10.1175/1520-0469(1971)028⟨1479:ADMOTS⟩2.0.CO;2, 1971.

Mitchell, N. J., H. R. Middleton, A. G. Beard, P. J. S. Williams, and H. G. Muller, The 16-day planetary wave in the mesosphere and lower thermosphere, *Ann. Geophys.*, *17*, 1447–1456, doi: 10.1007/s00585-999-1447-9, 1999.

Mitchell, N. J., D. Pancheva, H. R. Middleton, and M. E. Hagan, Mean winds and tides in the Arctic mesosphere and lower thermosphere, *J. Geophys. Res.*, *107*(A1), doi: 10.1029/2001JA900127, 2002.

Nielsen, K., D. E. Siskind, S. D. Eckermann, K. W. Hoppel, L. Coy, J. P. McCormack, S. Benze, C. E. Randall, and M. E. Hervig, Seasonal variation of the quasi 5 day planetary wave: Causes and consequences for polar mesospheric cloud variability in 2007, *J. Geophys. Res.*, *115*, D18,111, doi: 10.1029/2009JD012676, 2010.

Pan, W. L., and C. S. Gardner, Seasonal variations of the atmospheric temperature structure at South Pole, *J. Geophys. Res.*, *108*(D18), doi: 10.1029/2002JD003217, 2003.

Pancheva, D., and P. Mukhtarov, Stratospheric warmings: The atmosphere-ionosphere coupling paradigm, *J. Atmos. Solar-Terr. Phys.*, *73*(13), 1697–1702, doi: 10.1016/j.jastp.2011.03.006, 2011.

Pedatella, N. M., and J. M. Forbes, Evidence for stratosphere sudden warming-ionosphere coupling due to vertically propagating tides, *Geophys. Res. Lett.*, *37*, L11,104, doi: 10.1029/2010GL043560, 2010.

Pedlosky, J., *Geophysical Fluid Dynamics*, Spinger Verlag, Ch 7, 1979.

Press, W. H., and S. A. Teukolsky, Search algorithm for weak periodic signals in unevenly spaced data, *Comput. Phys.*, *2*(6), 77 – 80, 1988.

Rienecker, M. M., et al., MERRA: NASA's modern-era retrospective analysis for research and applications, *J. Climate*, *24*, 3624–3648, doi: 10.1175/JCLI-D-11-00015.1, 2011.

She, C. Y., S. Chen, Z. Hu, J. Sherman, J. D. Vance, V. Vasoli, J. White, M. A. ans Yu, and D. A. Krueger, Eight-year climatology of nocturnal temperature and sodium density in the mesopause region (80 to 105 km) over Fort Collins, CO (41N, 105W), *Geophys. Res. Lett.*, *27*(20), 3289–3292, doi: 10.1029/2000GL003825, 2000.

Smith, A. K., The Origin of Stationary Planetary Waves in the Upper Mesosphere, *J. Atmos. Sci.*, *60*, 3033–3041, doi: 10.1175/1520-0469(2003)060⟨3033:TOOSPW⟩2.0.CO;2, 2003.

Stray, N. H., R. J. de Wit, P. J. Espy, and R. E. Hibbins, Observational evidence for temporary planetary wave forcing of the MLT during fall equinox, *Geophys. Res. Lett.*, *41*(17), 6281–6288, doi: 10.1002/2014GL061119, 2014a.

Stray, N. H., P. J. Espy, V. Limpasuvan, and R. E. Hibbins, Characterisation of quasi-stationary planetary waves in the Northern MLT during summer, *J. Atmos. Solar-Terr. Phys.*, doi: 10.1016/j.jastp.2014.12.003, 2014b.

Stray, N. H., Y. J. Orsolini, P. J. Espy, V. Limpasuvan, and R. E. Hibbins, Observations of PW activity in the MLT during SSW events using a chain of SuperDARN radars and SD-WACCM, *15*(1), 393–413, doi: 10.5194/acpd-15-393-2015, 2015.

Swinbank, R., and A. A. O'Neill, A Stratosphere-Troposphere Data Assimilation System, *Monthy Weather Review*, *122*, 686–702, doi: http://dx.doi.org/10.1175/1520-0493(1994)122⟨0686:ASTDAS⟩2.0.CO;2, 1994.

Swinbank, R., et al., Stratospheric Assimilated Data, [Internet], *NCAS British Atmospheric Data Centre, 2006*, Available from http://badc.nerc.ac.uk/view/badc.nerc.ac.uk__ATOM__ dataent_ASSIM, 2013.

Taylor, M. J., W. R. Pendleton Jr., H. L. Liu, C. Y. She, L. C. Garnet, R. G. Roble, and V. Vasoli, Large amplitude perturbations in the mesospheric OH Meinel and 87-km Na lidar temperatures around the autumnal equinox, *Geophys. Res. Lett.*, *28*, 1899–1902, doi: 10.1029/2000GL012682, 2001.

Torrence, C., and G. P. Compo, A practical guide to wavelet analysis., *Bull. Amer. Meteor. Soc.*, *79*, 61–78, doi: 10.1175/1520-0477(1998)079⟨0061:APGTWA⟩2.0.CO;2, 1998.

Tweedy, O. V., et al., Nighttime secondary ozone layer during major stratospheric sudden warmings in specified-dynamics, *J. Geophys. Res.*, *118*, 1–13, doi: 10.1002/jgrd.50651, 2013.

Vincent, R. A., Gravity-wave motions in the mesosphere, *J. Atmos. Terr. Phys.*, *46*(2), 119–128, doi: 10.1016/0021-9169(84)90137-5, 1984.

Volland, H., *Atmospheric Tidal and Planetary Waves*, Kluwer Academic Publishers, Dordrecht, The Netherlands, 1988.

Wu, D. L., P. B. Hays, and S. W. R., A Least -Squares Method for Spectral-Analysis of Space-Time Series, *J. Atmos. Sci.*, *52*(20), 3501–3511, doi: 10.1175/1520-0469(1995)052⟨3501:ALSMFS⟩2.0.CO;2, 1995.

Yuan, T., B. Thurairajah, C.-Y. She, A. Chandran, R. L. Collins, and D. A. Krueger, Wind and temperature response of midlatitude mesopause region to the 2009 sudden stratospheric warming, *J. Geophys. Res.*, *117*(D09114), doi: 10.1029/2011JD017142, 2012.

Yukimatu, A. S., and M. Tsutsumi, A new SuperDARN meteor wind measurement: Raw time series analysis method and its application to mesopause region dynamics, *Geophys. Res. Lett.*, *29*(20), doi: 10.1029/2002GL015210, 2002.

A. Papers

Kleinknecht, N. H., P. J. Espy, and R. E. Hibbins, The climatology of zonal wave numbers 1 and 2 planetary wave structure in the MLT using a chain of Northern Hemisphere SuperDARN radars, *J. Geophys. Res.*, *119*(3), 1292–1307, doi: 10.1002/2013JD019850, 2014

Paper 1

AGU PUBLICATIONS

JGR

Journal of Geophysical Research: Atmospheres

RESEARCH ARTICLE

10.1002/2013JD019850

Key Points:

- Planetary wave zonal structure derived from network of SuperDARN meteor winds
- Robustness of extracting each zonal component compared to current techniques
- Mesospheric planetary waves used as possible precursor of stratospheric warmings

Correspondence to:
N. H. Kleinknecht,
nora.kleinknecht@ntnu.no

Citation:
Kleinknecht, N. H., P. J. Espy, and R. E. Hibbins (2014), The climatology of zonal wave numbers 1 and 2 planetary wave structure in the MLT using a chain of Northern Hemisphere SuperDARN radars, *J. Geophys. Res. Atmos.*, *119*, 1292–1307, doi:10.1002/2013JD019850.

Received 14 MAR 2013
Accepted 14 JAN 2014
Accepted article online 16 JAN 2014
Published online 13 FEB 2014

The climatology of zonal wave numbers 1 and 2 planetary wave structure in the MLT using a chain of Northern Hemisphere SuperDARN radars

Nora H. Kleinknecht[1], **Patrick J. Espy**[1,2], **and Robert E. Hibbins**[1,2]

[1]Department of Physics, NTNU, Trondheim, Norway, [2]Birkeland Centre for Space Science, Bergen, Norway

Abstract The zonal wave components 1 and 2 were extracted from the meridional wind along the latitude band of 51–66°N for the years 2000–2008 using eight Super Dual Auroral Radar Network (SuperDARN) radars spanning longitudes from 25°E to 150°W. Each extracted zonal component represents the superposition of all temporal periods with that zonal structure and indicates the total planetary wave energy available with that wave number. The Hovmöller diagrams show stationary as well as eastward and westward traveling planetary waves propagating in the background wind. The method used to detect the zonal planetary wave components in the SuperDARN data are detailed and validated using UK Meteorological Office data, which allows the evolution of S_1 and S_2 planetary wave energy between the stratosphere and mesosphere to be assessed. The climatology of zonal wave number 1 and 2 planetary wave activity in the mesosphere-lower thermosphere (MLT) is presented and compared to the activity in the stratosphere. The MLT climatology of the mean wind anomalies shows stronger planetary wave activity during winter and weaker activity during summer with enhancement around midsummer and autumn equinox. The climatology of the mean wind displays similar amplitudes apart from very strong S_1 planetary wave amplitudes during summer. In addition planetary wave activity during winters with major and minor stratospheric warming events are examined and contrasted.

1. Introduction

The interaction of radiation, dynamics, and chemistry, coupled with the curvature and rotation of the Earth, creates a complex structure in the atmosphere and a wide range of wave phenomena, such as tides, gravity, and planetary waves, with time scales in the range from a few minutes to several weeks. The cause and effect of planetary wave activity in the mesosphere-lower thermosphere (MLT) is still an open question. Some studies [e.g., *Dowdy et al.*, 2004; *Espy et al.*, 2005; *Chshyolkova et al.*, 2006; *McDonald et al.*, 2011] suggest an extension of the stratospheric wave field. Others found evidence for additional planetary wave activity through in situ generation by dissipation or breaking gravity waves and/or propagation of planetary wave activity from the winter hemisphere or equator to the summer MLT [e.g.,*Williams and Avery*, 1992; *Forbes*, 1995; *Espy et al.*, 1997; *Mitchell et al.*, 1999; *Smith*, 2003; *Garcia et al.*, 2005; *Pancheva et al.*, 2008].

In this study the wind field is separated into zonal wave numbers 1 (S_1) and 2 (S_2). The sum or superposition of all planetary wave modes of zonal structure 1 itself has zonal structure 1 with time-dependent amplitude, similarly for wave number 2. Because the atmosphere responds to the total superposition of all wave energy, not to a single period, wave number or propagation direction, the S_1 and S_2 wave energies have been used as a standard technique to assess the total wave forcing and its zonal character in stratospheric analyses [e.g., *Labitzke*, 1977, 1981; *Bancalá et al.*, 2012]. For that reason it has been adopted here. Not only does it give the total planetary wave energy available (and its longitudinal character), but it may easily be compared with stratospheric wave energy to assess the energy deposited in the background flow and its zonal structure. Comparison of the climatology of zonal wave numbers 1 and 2 planetary wave structures in the MLT and the stratosphere can be used to understand how MLT and stratospheric planetary wave activity are related. In addition, it indicates those seasons where mesospheric waves might be an extension of the stratospheric waves and when they are most likely generated locally in the mesosphere.

Planetary wave activity throughout the middle atmosphere has mainly been studied on a global scale by satellites [e.g., *Belova et al.*, 2008; *McDonald et al.*, 2011]. However, some studies have also used multiple ground-based radar stations to trace the propagation of planetary waves [e.g., *Espy et al.*, 2005; *Baumgaertner et al.*, 2008] and to compare that multiple-station data with satellite observations [e.g., *Bristow* *et al.*, 1999; *Pancheva et al.*, 2008]. Satellites give the opportunity to scan the whole Earth, making observations of the global behavior of planetary waves possible. The disadvantage of satellites is that they alias spatial and temporal information since it may take between 1 day and several weeks before a given geographic location is sampled at the same local time [e.g., *Wu et al.*, 1995]. In addition, if they operate in a Sun synchronous mode, only one phase of the migrating tide is observed.

Here the zonal wave numbers 1 and 2 planetary wave structures in the MLT have been observed using the Super Dual Auroral Radar Network (SuperDARN) [*Greenwald et al.*, 1985, 1995] around the North Pole operating as a so called "ground-based satellite." It has the spatial resolution required to trace longitudinal wave components, but in contrast to satellites, it also has very good temporal resolution (1 h) for a fixed point on Earth. This makes it possible to remove tides from the data accurately and give a global picture of longitudinal wave components at the latitude band between 51–66° N. Since many of the radars in the SuperDARN network have been in operation nearly continuously since the 1990's, it is possible to utilize a long time series of simultaneous data from 6–8 radars in order to determine individual longitudinal planetary wave components and compose climatologies of these components.

2. Data

SuperDARN radars [*Greenwald et al.*, 1985, 1995] were originally built for observation of the *F* region. Later it was shown [*Hall et al.*, 1997; *Jarvis et al.*, 1999; *Hussey et al.*, 2000; *Yukimatu and Tsutsumi*, 2002] that sporadic echoes received in the first few range gates are due to scatter from the ionization trails left by meteors ablating in the lower thermosphere and upper mesosphere. These trails travel with the neutral wind, which makes it possible to deduce the line of sight wind over the meteor ablation altitudes (80–100 km) [*Hocking et al.*, 2001]. Meteors observed in the lowest range gates of the multiple beams of the SuperDARN radars over $\sim$ 1 h are then combined in order to determine the vector neutral wind at the centroid location of the beams. Standard SuperDARN radars have no altitude discrimination within the lowest range gates used for meteor-trail detection, but the mean altitude of the meteor wind has been estimated to be 94 ($\pm$ 3) km by comparing the derived wind with that observed by a colocated MF radar [*Hall et al.*, 1997]. This has been verified by comparing winds from an imaging Doppler interferometer radar at Halley (75°S, 26°W) and a colocated SuperDARN radar [*Hibbins and Jarvis*, 2008]. Recently, *Chisham and Freeman* [2013] have developed a new method for calibrating SuperDARN interferometric data to estimate the meteor altitudes directly, finding a broad distribution between 75 and 125 km with a peak near 102–103 km. Although the peak of this meteor distribution is higher than the average derived through wind comparisons, *Chisham and Freeman* [2013] have suggested that this discrepancy is likely due to the averaging process. The hourly mean meridional winds and uncertainty estimate (number of meteors) are taken from the SuperDARN data base (http://psddb.nerc-bas.ac.uk/data/access/) and are processed as described in *Hibbins and Jarvis* [2008].

A more rigorous approach in determining accurate mean winds from a single SuperDARN radar would employ interferometric height finding [*Hussey et al.*, 2000] coupled with the techniques outlined in *Yukimatu and Tsutsumi* [2002], *Hussey et al.* [2000], and *Tsutsumi et al.* [2009] to eliminate any sidelobe contamination issues. However, not all the radars currently have this option, and those that do have have not been run continuously in this mode. The data need to be consistent, with good data coverage from one radar to the next and from 1 year to the next in order to attempt the planetary wave analysis. Therefore, in order to maximize the data coverage, while preserving the best longitudinal uniformity, the noninterferometric data was used to derive the mean winds from all radars. Previous studies [*Jenkins et al.*, 1998; *Jenkins and Jarvis*, 1999; *Hibbins and Jarvis*, 2008; *Hibbins et al.*, 2011] have taken this approach to meteor wind analysis and produced effective comparisons on short and long time scales with winds derived from other types of MLT radars that incorporated more conventional range determination of altitude.

The beam patterns of SuperDARN radars are known to have back lobes [*Milan et al.*, 1997], and contamination from meteors observed in the back lobes can lead to an underestimation of mean winds and tidal amplitudes from noninterferometric SuperDARN radars [*Yukimatu and Tsutsumi*, 2002; *Arnold et al.*, 2003]. If the horizontal winds observed in all SuperDARN radars are affected similarly, then the planetary wave amplitudes we derive will be similarly reduced. However, if the back lobe effects on the magnitude of the winds differ between the different radars, this could generate spurious stationary waves. Comparative studies of the mean wind have shown that the back lobe correction factors required for the SuperDARN radars are similar for radars at different locations and with different boresight directions [*Hussey et al.*, 2000; *Arnold*

Table 1. SuperDARNRadars Used in the Data Analysis[a]

Radar	Loc.(Geo)	Loc.(Mag)	Data Cov.
Hankasalmi	64.4 N, 25.2 E	61 N, 116 E	1995–2009
Pykkvibaer	65.7 N, −18.0 E	70 N, 77 E	1996–2008
Stokkseyri	64.7 N, −26.9 E	71 N, 62 E	1994–2008
Goose Bay	55.5 N, −60.3 E	65 N, 16 E	1995–2008
Kapuskasing	51.4 N, −83.3 E	61 N, −15 E	1993–2009
Saskatoon	54.2 N, −105.2 E	62 N, −44 E	1993–2008
Prince George	56.1 N, −123.2 E	61 N, −66 E	2000–2009
Kodiak	59.5 N, −150.1 E	60 N, −96 E	2000–2009

[a]Geographic (geo) and magnetic (mag) mean location (loc.) of scatter and data coverage (data cov.) of the SuperDARN radars used in the data analysis. Longitudinal wave components could only be retrieved during 2000–2008 when the longitudinal coverage was sufficient.

et al., 2003; *Hibbins and Jarvis*, 2008]. However, *Tsutsumi et al.* [2009] show that the meteors distributions seen in the back lobes may be different between the Iceland and Finland SuperDARN radars. Although wind differences induced by such site-specific back lobe effects in the SuperDARN radars have yet to be quantified, they could affect the planetary wave amplitudes derived from longitudinal chains of such radars if they prove to be significant.

Differences in the amplitude of the semidiurnal tide derived from noninterferometric SuperDARN radars and other MLT radar systems can largely be explained by the short vertical wavelength of this tide combined with the poor vertical resolution of the SuperDARN radar winds, with back lobe contamination of the SuperDARN radars playing a negligible role [e.g., *Hibbins et al.*, 2011]. Although there is relatively poorer agreement in the amplitude of the smaller diurnal tide between SuperDARN and other radars, these differences have been ascribed to the diurnal variation in meteor count rate, with low meteor counts in the evening creating large uncertainties in the inferred winds [*Hussey et al.*, 2000; *Thayaparan and Hocking*, 2002].

Table 1 shows the SuperDARN radars used in the study including the centroid location of the beam and years of data coverage used in the data analysis. All SuperDARN radars between 51–66°N with sufficient data coverage are used in the study.

3. Data Analysis

To assure data quality, the raw wind data from all SuperDARN radars used were quality checked before processing. Hourly mean winds above 100 m/s, winds with standard deviations of zero or a mean location different from the geometric centroid of the beams are excluded. These values are either unrealistic solutions or indicate a nonstandard operation mode of the radar [*Hibbins and Jarvis*, 2008]. To extract zonal planetary wave modes from the hourly averaged meridional wind of the eight radar stations, the data are processed through several steps as outlined below.

3.1. Daily Mean Wind

To produce daily mean winds that are not influenced by tides and quasi-two-day waves (QTDWs), data are treated in a similar fashion to *Hibbins and Jarvis* [2008]. First, the hourly mean winds are split into 4 day segments. Then a bias (mean wind) and 8 h, 12 h, 24 h, and 48 h sine waves, representing the strongest tidal components [*Hibbins et al.*, 2006] and the QTDW, are fitted to this segment of hourly winds. To ensure sufficient data coverage for the fit, only segments covering at least half of the hourly means and spanning at least 16 different hours are used [*Hibbins and Jarvis*, 2008]. In addition, 4 day segments that have data gaps >3 h occurring at the same hours in each day are excluded. Similarly, 4 day segments with data gaps >12 h that cover the same hours in both halves of the segment, are rejected. The 4 day segments are then stepped by 1 day intervals to build up a time series of 4 day running mean winds. Monthly averages of the mean wind and the QTDW as well as the amplitudes and phases of the tides for all eight radars are in broad agreement with other climatological observations for similar latitudes [e.g., *Manson et al.*, 1985; *Portnyagin et al.*, 2004; *Chshyolkova et al.*, 2005]. As an example, Figure 1 shows the monthly average fitting result for the meridional component of the wind recorded with the Hankasalmi SuperDARN radar (64°N, 25°E).

The mean wind is clearly equatorward during summer and turns more poleward during winter. The amplitude of the QTDW is observed to increase in summer, in agreement with *Salby* [1981]. The amplitude and phase of the 24 h tide is relatively constant, while the amplitude and phase of the 12 h tide are more variable. During equinox the amplitude of the 12 h tide is smallest and the local time of maximum phase occurs earlier. The amplitude of the 8 h tide is generally small with a maximum in October when the amplitude of the 12 h tide reaches a minimum. During summer the 8 h tide is nearly absent as indicated by small or insignificant amplitudes and nearly random phases. The behavior of the observed phases and amplitudes of

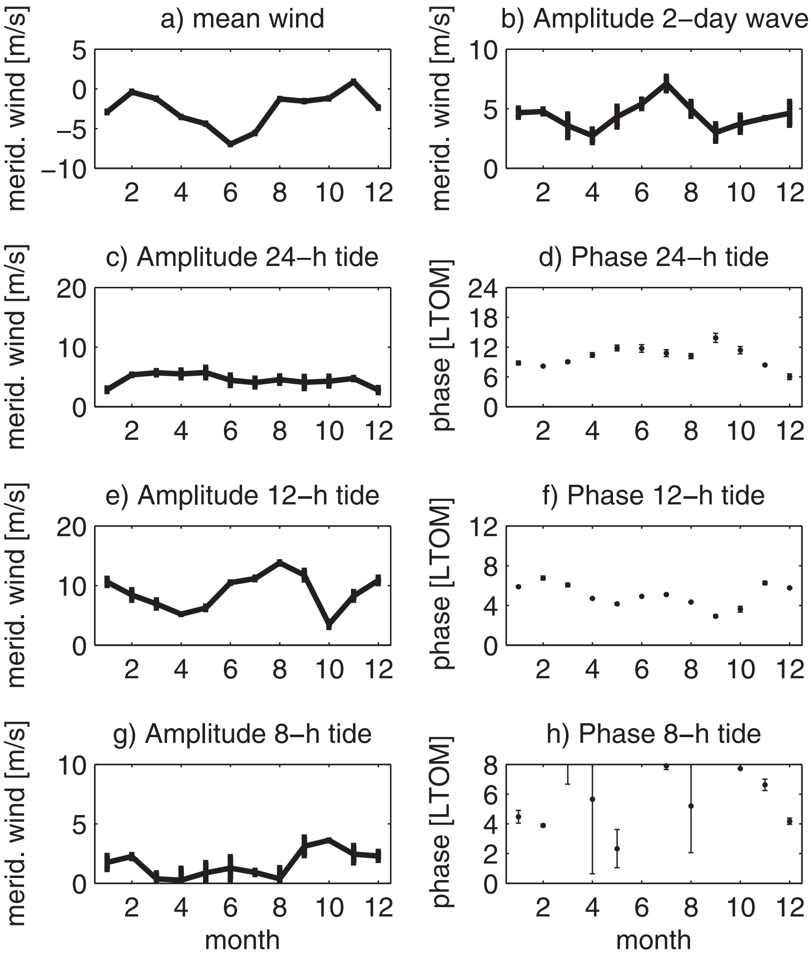

Figure 1. Monthly weighted mean of the mean wind, the 2 day wave and the 24 h, 12 h, and 8 h tides at Hankasalmi. The tidal phase represents the local solar time of the first maximum. The error bars shown are the standard errors of the weighted means.

the tides at Hankasalmi are similar to tides at 95 km altitude observed with an All-Sky Interferometric Meteor Radar at Esrange (68°N, 21°E) [*Mitchell et al.*, 2002]. The smaller tidal amplitude measured by the SuperDARN radars is a common feature that has been attributed to sidelobe effects [*Yukimatu and Tsutsumi*, 2002] or to the combination of the large vertical integration of the SuperDARN radar together with a finite vertical wavelength of the tide [*Hibbins et al.*, 2011].

3.2. Climatology and Daily Mean Wind Anomaly

To eliminate the seasonal variation of the mean wind, a smoothed meridional wind climatology over all years of the daily mean wind was produced for each of the eight radars. To form the climatology for each radar, the individual daily means, $V_{d,y}$, weighted by their individual fitting uncertainties, $\delta V_{d,y}$, were used to calculate the climatology over all years of data available, C_d, as shown in equation (1). Similarly, the corresponding standard error of the mean, δC_d, for each day of the climatology was calculated following equation (2).

$$C_d = \frac{\sum_y \frac{V_{d,y}}{(\delta V_{d,y})^2}}{\sum_y \frac{1}{(\delta V_{d,y})^2}} \quad (d = \text{day}, y = \text{year}) \tag{1}$$

$$\delta C_d = \frac{1}{\left(\sum_y \frac{1}{(\delta V_{d,y})^2}\right)^{1/2}} \tag{2}$$

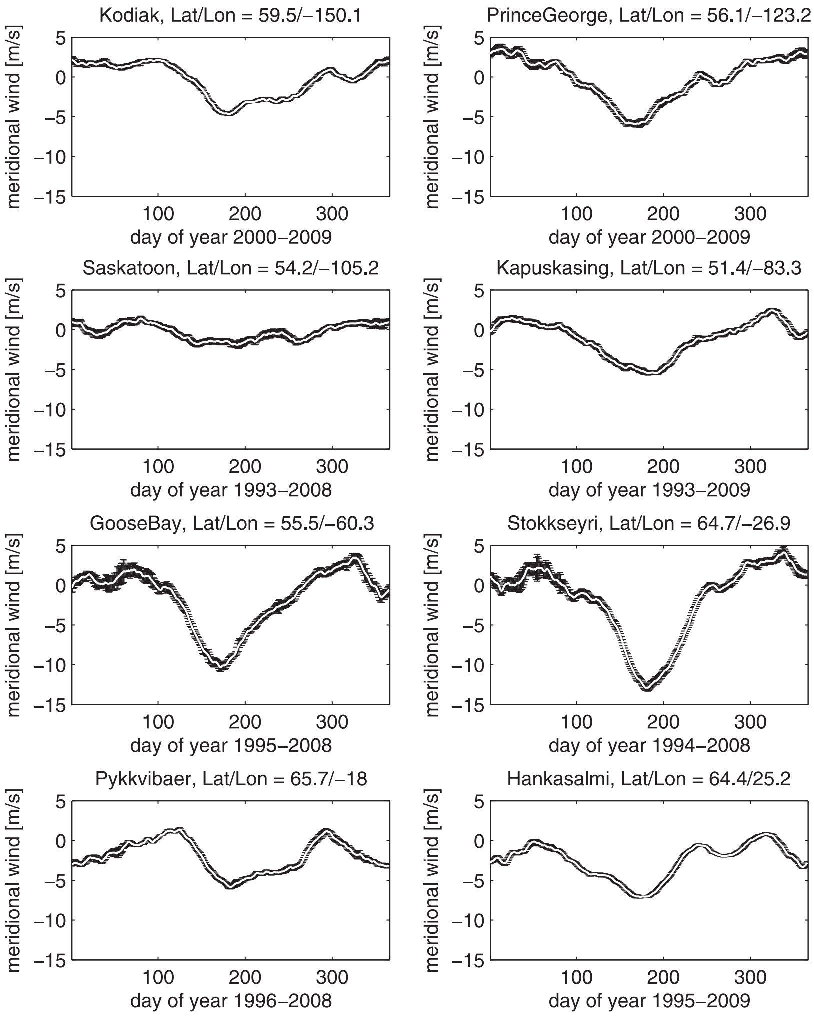

Figure 2. Smoothed (30 day running mean) climatology of all eight radar stations. Weighted mean (white line). Standard error of the weighted mean (black error bars).

A 30 day running mean was used to smooth the resulting climatology in order to remove any vestigial planetary wave effects. Figure 2 shows the smoothed meridional wind climatology for all stations, indicating their locations and the years used for the climatologies. Each day of the climatology includes at least 4 years of data.

Daily mean meridional wind anomalies ($V^{ano}_{d,y}$) and their estimated uncertainties, $\delta V^{ano}_{d,y}$, were then created by removing the smoothed climatology (C^s_d) from the individual daily mean wind data for each radar as shown in equations (3) and (4).

$$V^{ano}_{d,y} = V_{d,y} - C^s_d \tag{3}$$

$$\delta V^{ano}_{d,y} = \sqrt{(\delta V_{d,y})^2 + (\delta C_d)^2} \tag{4}$$

Both anomaly mean meridional winds and mean meridional winds as a function of longitude are fitted for planetary wave components as described below. A detailed discussion about similarity and difference between the retrieved wave components can be found in section 5.

3.3. Longitudinal Fit

Longitudinal wave components are retrieved by fitting two sinusoids with 360° and 180° spatial periods as a function of longitude to the daily mean wind anomaly at all available radar stations. These fitting components correspond to wave modes with zonal wave number $S = 1$ and 2, respectively. The fit was weighted with the uncertainty ($\delta V_{d,y}^{ano}$) of the daily mean wind anomaly given in equation (4). The strongest zonal wave number 3 component (a 120° sinusoid) represents the QTDW [*Salby*, 1981] which has already been removed in the detrending process. Thus, it and higher order waves, are taken to be insignificant and the fitting was stopped at $S = 2$. The zonal wave number $S = 0$ was calculated from the mean of the residual of the fit. Data are only fitted if the westernmost (Kodiak −150.1°) and most easterly (Hankasalmi 25°) stations are present, and at least four additional stations are available with no sequential data gaps (i.e., the missing stations are not located next to each other). The method described above is validated in the next section.

4. Validation

The longitudinal fitting technique used has been validated in three different ways.

4.1. Comparison With the Single Sites

The first validation compares the daily wind anomaly for the time period (1 January 2000 to 31 December 2008) at each station with the sum of the longitudinally fitted zonal wave components (S_1 and S_2) evaluated at the longitude of each station. Only days where both a longitudinal fit and the daily wind anomaly are available at the specific station were compared. The correlation coefficient between the daily wind anomaly and the sum of the fitted zonal components was statistically significant at >99% confidence level and greater than 0.75 at all but one station. The exception was Goose Bay where the correlation coefficient was still 0.61, significant at the 99% level. This high degree of correlation shows that the longitudinally fitted S_1 and S_2 components reproduce the majority of the observed variance in the daily wind at each station.

4.2. Comparison to a Full 360° Longitudinal Fit

A further validation of the technique was done by using meridional wind data from the UK Meteorological Office (UKMO)-Stratospheric Assimilated Data [*Swinbank and O'Neill*, 1994; *Met Office et al.*, 2013] at 6.8 hPa. As with the mesospheric analysis, the stratospheric anomaly meridional wind was calculated by removing a climatology for each longitude (2.5° spacing). A full 360° fit, using 2.5° longitudinal spacing, for the first four zonal wave numbers was done (S_0, S_1, S_2, S_3), at 51°N, 66°N, and for a latitude average between 51 and 66°N. These latitudes correspond to the southernmost, northernmost, and average latitude of the radar stations used in the SuperDARN analysis. Figure 3 (top left, top right, and bottom left) show Hovmöller diagrams for the first three zonal wave numbers during 2002 at 51°N, 66°N, and the average latitude band (51–66°N), respectively. From the similarity between the Hovmöller diagrams of the different latitudes and a correlation coefficient larger than 0.83, it is clear that the 15° latitudinal extent does not have a strong impact on the variability and phase of the S_1 and S_2 components as the phase progression is similar at all latitudes. The resulting amplitude lies between the larger northern and the weaker southern amplitudes. However, one should be aware that such a latitude span will have a larger effect in the midlatitudes and caution should be exercised when applying a similar method to midlatitude radars. Since the Hough functions of the normal modes which make up these wave components are not a function of altitude, the latitudinal extent of the radar chain used in the SuperDARN analysis should not affect the amplitudes and phases retrieved in the MLT. It is also clear from the plot that the S_0 component varies over the latitude band and that it is therefore not possible to retrieve a unique S_0 component.

To verify that the longitudinal extent of the SuperDARN radar network used is adequate to retrieve a zonal wave number $S = 1$ and $S = 2$, the meridional UKMO anomaly wind was sampled at the locations (longitude and latitude) of the radar stations and the wave number components were fit again repeating the aforementioned method. Figure 3 (bottom right) displays the resulting Hovmöller diagram for 2002. The S_3 component was removed from the data before the fit to emulate the removal of the 2 day wave in the SuperDARN winds. To verify this, fits with and without removal of the S_3 component were correlated and show a good agreement (correlation coefficients ≥ 0.83).

The variability, amplitude, and phase progression of the $S = 1$ and $S = 2$ wave number retrieved using only the radar locations compares well with the full, 360° fit. The correlation coefficients between the ideal 360° fits between 51° and 66°N and the fit at the coordinates of the SuperDARN stations for the amplitude and the phase of the zonal wave numbers 1 and 2 components are larger than 0.9 for both wave numbers. This indicates that the fit to the SuperDARN radar winds can accurately capture the temporal changes of the planetary wave components. The amplitude of S_1 retrieved at the stations is approximately 20 ± 20 % higher than the amplitudes retrieved from the ideal fit. The amplitude of the S_2 wave agrees within the 10%

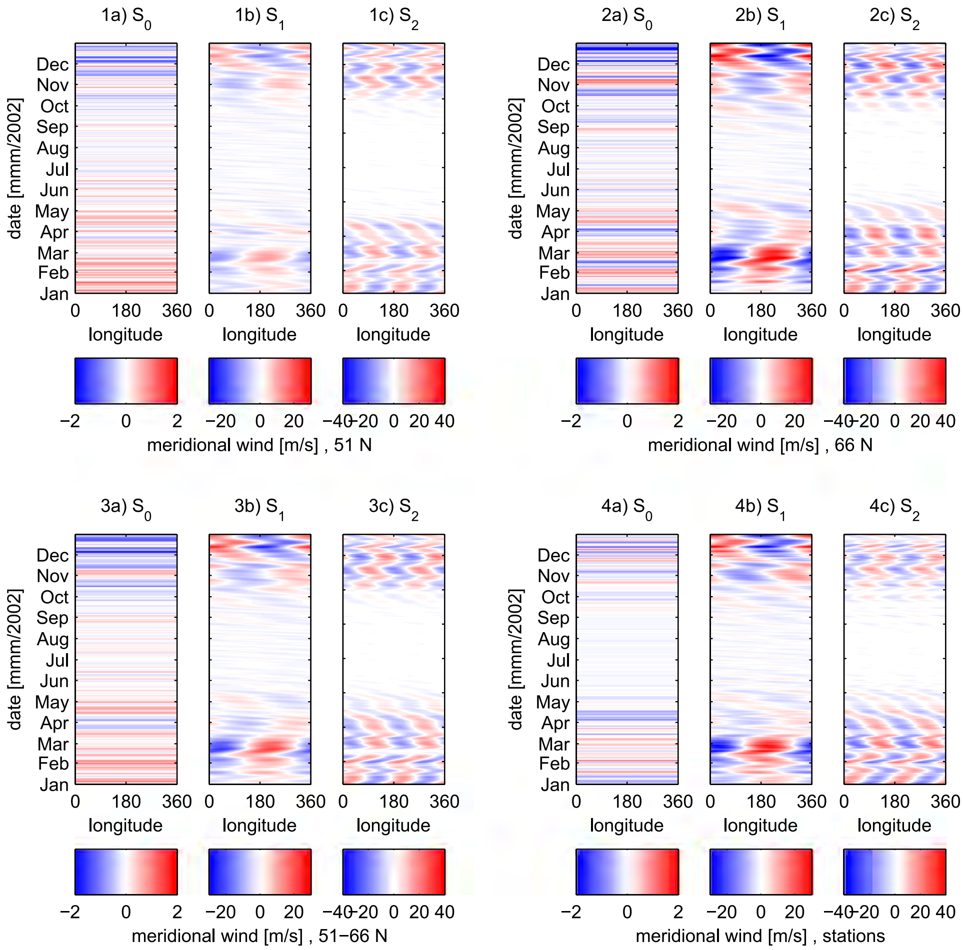

Figure 3. Hovmöller diagram of longitudinal wave components S_0 (a), S_1 (b), S_2 (c)) using the "ideal" longitudinal fit for anomaly meridional UKMO winds (top left) at 51°N, (top right) at 66°N, and for the latitude band (bottom left) 51–66°N for year 2002. (bottom right) Hovmöller diagram of longitudinal wave components using the anomaly meridional UKMO wind only at the coordinates of the SuperDARN chain for year 2002. Red and blue colors signify poleward and equatorward winds, respectively.

uncertainty of the two fits. Thus, the longitudinal extent of the SuperDARN radar stations can accurately reproduce the true amplitude of the S_2 component, but overestimates the S_1 component slightly.

4.3. Comparison to Hydroxyl Rotational Temperatures

For any given longitude, the different temporal components of each zonal wave number can be found by spectral analysis of the time series of the amplitudes and phases of that zonal component using Fourier, Lomb-Scargle, or wavelet techniques followed by band-pass filtering. Similar analysis has been applied to satellite- and ground-based data [e.g., *Grytsai et al.*, 2005; *McDonald et al.*, 2011; *Demissie et al.*, 2013]. While there could be some distortion of the waveform using a band-pass filter, their use to extract planetary waves has been demonstrated [e.g., *Belova*, 2008]. Figure 4 shows the quasi-16-day component of the zonal wave number one (a), two (b), and the sum of both (c) at 18°E for the time period 15 November 2001 to 15 March 2002.

This longitude and time period was chosen because temperatures derived from the hydroxyl (OH) nightglow from Stockholm (59.5°N,18.2°E) are available during that winter [*Espy et al.*, 1997]. To extract the quasi-16-day periodicity from the other wave components, a bidirectional fourth order Butterworth band-pass filter [*Stearns*, 1975] with a band pass between 14 and 18 days was chosen. This filter separates the quasi 16 day periodicity from other strong peaks in the power spectrum. The OH-temperatures at Stockholm can be filtered in the same way, and the extracted quasi-16-day wave can be compared to the sum of the zonal wave components from the longitudinal fit (Figure 4c). It can be seen

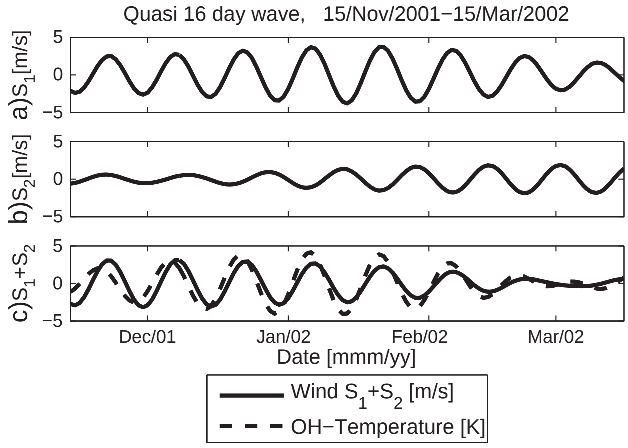

Figure 4. Quasi-16-day wave of the (a) S_1 and (b) S_2 anomaly meridional wind component at 18°E and (c) the sum of both components (solid line) together with the quasi-16-day component of the ground-based OH-temperature observation (dashed line) at Stockholm (59.5°N, 18.2 °E).

that the wave character of the quasi-16-day wave extracted from the wind is dominated by the zonal wave number 1 component and agrees well with the phase and relative amplitude of the wave in the OH rotational temperatures. Observation of the quasi-16-day wave at OH-temperature altitudes (∼87 km), at SuperDARN altitudes as well as in the lower stratosphere [e.g., *Alexander and Shepherd*, 2010], and throughout the whole stratosphere and mesosphere during winter [e.g., *McDonald et al.*, 2011] suggest an upward propagation of this wave component from the stratosphere into the MLT region.

5. Results and Discussion

The meridional wind anomalies from eight SuperDARN meteor radars between 51 and 66°N have been used to fit longitudinal planetary wave modes. Each resulting zonally fitted component (here S_1 and S_2) represents the superposition of stationary, as well as propagating and traveling normal mode waves with a variety of temporal periods. Wave components were fitted from January 2000 to December 2008 allowing the seasonal and interannual changes of the total planetary wave activity and its zonal character to be examined. Hovmöller diagrams of the fitted wave components for all years are shown in Figure 5. Red and blue colors signify poleward and equatorward winds, respectively. Throughout the 9 years of data, we typically see larger planetary wave activity during the winter month and weaker, but still significant, planetary wave activity during summer in both zonal wave components (S_1 and S_2). The phase of the zonal components are most stable during the summer months (see Figure 5) suggesting a quasi-stationary wave is the dominant wave component then.

Even though the longitudinal fits to each day's data are independent, Figure 5 shows that the phase of each fitted component is relatively stable from day to day. In addition, the phase can be seen to shift smoothly in time, indicating that the wave component is moving with respect to the ground-based stations. The change in time of the phase and amplitude of each zonal component are the result of both interaction with the background wind and the interaction of the different temporal components. At times the phase of the S_1 and S_2 waves seems to jump 180°, for example, on 3 March 2005. A closer look at these phase changes shows that the 180° phase transition occurs rapidly and systematically over the course of a few days. Similar 180° phase jumps can also be seen in analysis of total ozone from the Total Ozone Mapping Spectrometer [*Grytsai et al.*, 2005] and have been attributed to rapid bursts of the zonal wind speed and interaction of similarly strong eastward and westward wave packets with similar temporal periods.

The meridional wind climatologies at the different stations show large differences, especially in summer as can be seen in Figure 2. To investigate whether this behavior is the result of long-lasting wave features with a phase that is consistent year to year, zonal wave components were also fitted to the daily mean meridional winds, i.e., the winds where the climatologies were not removed. Hovmöller diagrams of the wave components for all 9 years are shown in Figure 6. Red and blue colors signify poleward and equatorward winds, respectively. The wave components are similar in amplitude and phase to the mean meridional wind

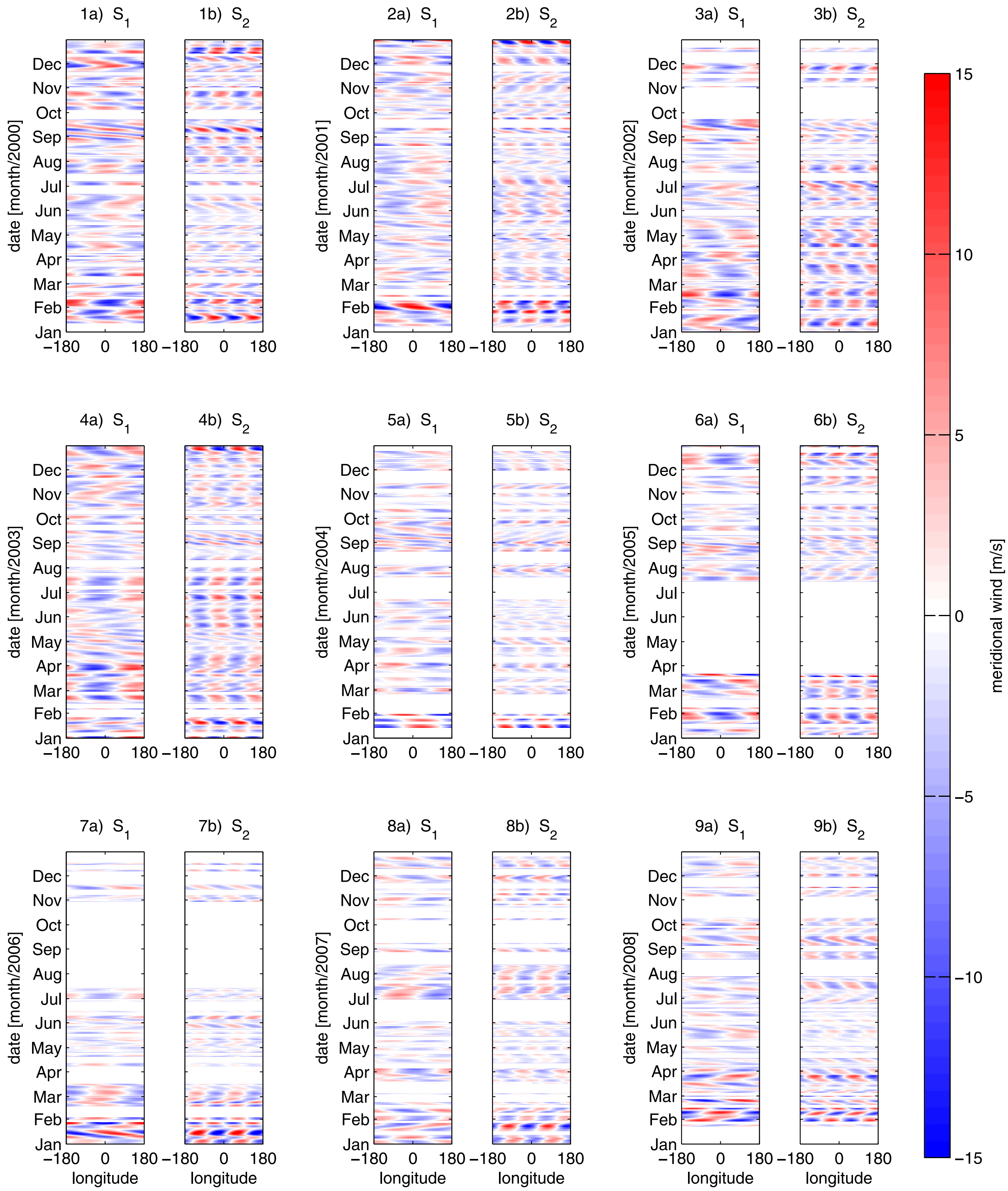

Figure 5. Longitudinal wave components (a) *S*1 and (b) *S*2 of the mean meridional wind anomalies for all years, 2000–2008 (1–9). Red and blue colors signify poleward and equatorward winds, respectively.

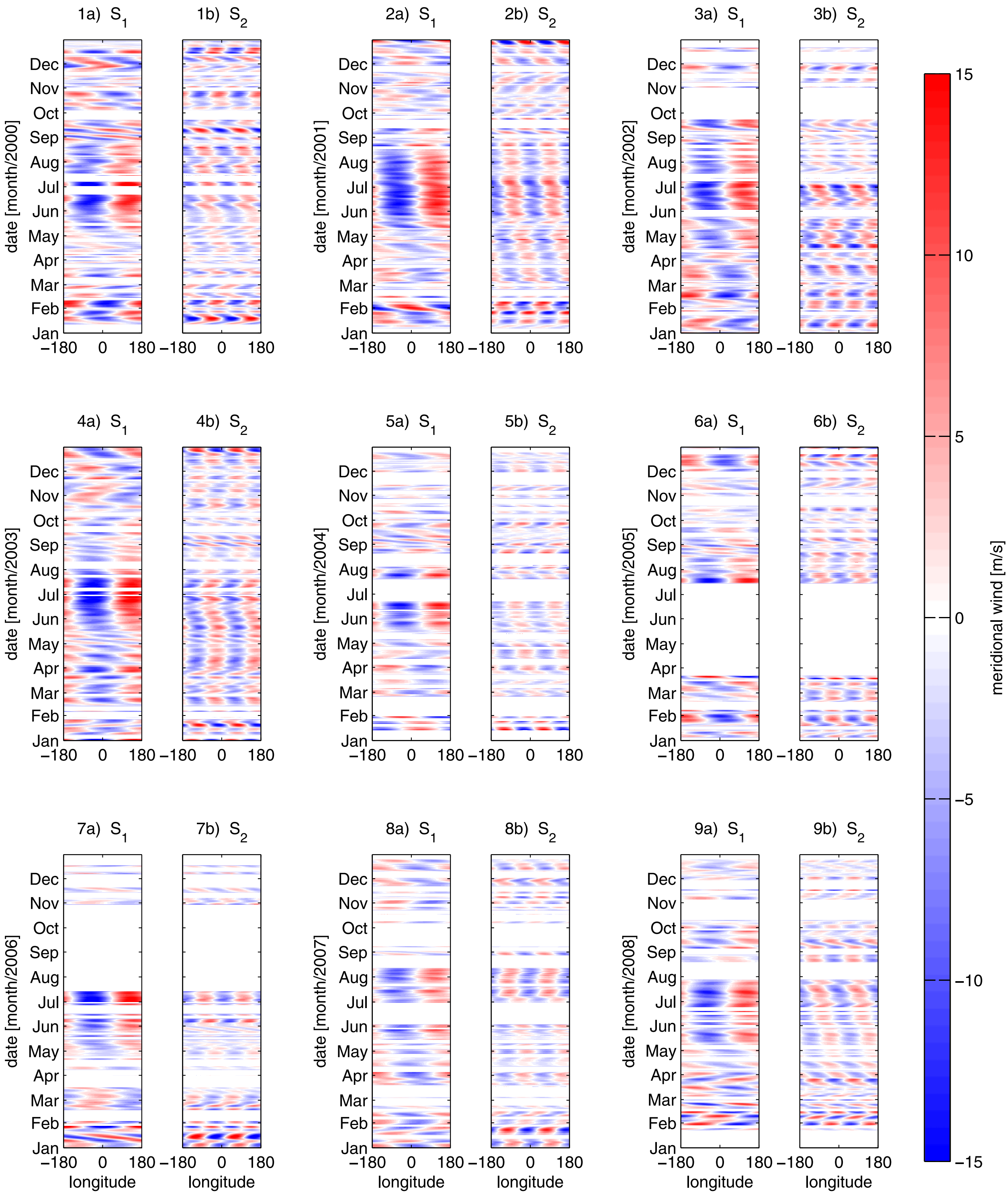

Figure 6. Longitudinal wave components (a) S_1 and (b) S_2 of the meridional wind for all years, 2000–2008 (1–9). Red and blue colors signify poleward and equatorward winds, respectively.

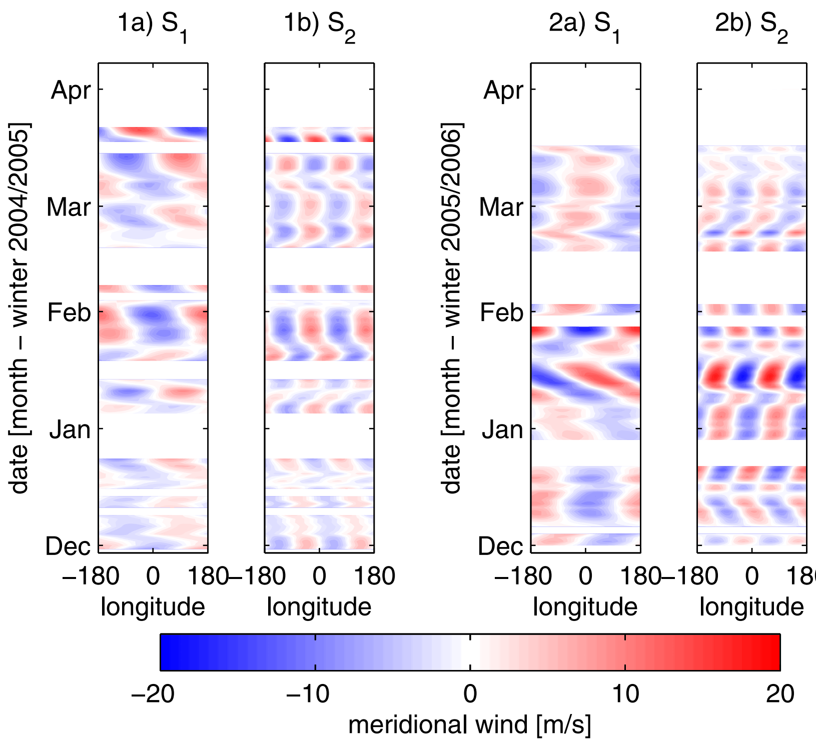

Figure 7. Longitudinal wave components (a) S_1 and (b) S_2 of the mean meridional wind anomalies, for (left) winter 2004–2005 and (right) winter 2005–2006. Red and blue colors signify poleward and equatorward winds, respectively.

anomalies throughout the year apart from the summer season. During all summers a strong stationary wave structure with a phase that is consistent year to year dominates the mean meridional wind wave components. It is unclear if this persistent year-to-year summer time wave structure is a stationary Rossby wave, or if it is produced by longitudinal differences in the gravity wave forcing [*Smith*, 2003]. It may even be the result of the underestimation of the S_0 component resulting from the limited longitudinal range of the radar chain, a limitation that will be relaxed as more SuperDARN radars are added to the chain in the future. The existence of a stationary Rossby wave in the polar summer MLT is puzzling since propagation from below is very unlikely due to the summertime westward stratospheric jet [*Charney and Drazin*, 1961]. However, longitudinally varying gravity wave forcing has been shown to produce planetary wave-like features in the MLT [*Smith*, 2003]. The appearance of a strong stationary S_1 wave only during the summer could be due to the stronger gravity forcing in the summer MLT resulting from the seasonal difference in wave breaking altitudes, i.e., approximately 80 km in summer and 50 km in winter [*Lindzen*, 1981]. Evidence for seasonally persistent S_1-like structures have also been found in other studies of the meridional wind in the MLT region. For example *Dowdy et al.* [2007] observed evidence for similar structures in the climatology of the meridional wind measured using two MF radars in the northern polar region which are approximately 180° apart (Poker Flat and Andenes). The effect maximized at approximately 90 km around summer solstices and approximately 70 km around winter solstices (see Figure 4) [*Dowdy et al.*, 2007]. This seasonal variation with altitude is consistent with gravity wave breaking as the cause of this phase-stable S_1 structure.

5.1. Interannual Planetary Wave Variability

Applying this longitudinal fitting technique to several years of data shows both eastward and westward traveling waves as well as stationary waves. Shown in Figure 7 are examples for the winters (left) 2004/2005 and (right) 2005/2006. Evident in these data is a strong interannual variability of the mesospheric planetary waves that may be associated with stratospheric warming events. For example, the wave activity during the winter of 2005/2006, where a major stratospheric warming was observed [*Manney et al.*, 2009a; *Lima et al.*, 2012], is stronger and more stationary than during the winter of 2004/2005 when only a minor warming occurred. This strong stationary wave activity during 2005/2006 is consistent with the generally weak polar vortex, higher stratospheric temperatures, and high ozone concentrations that occurred in the stratosphere

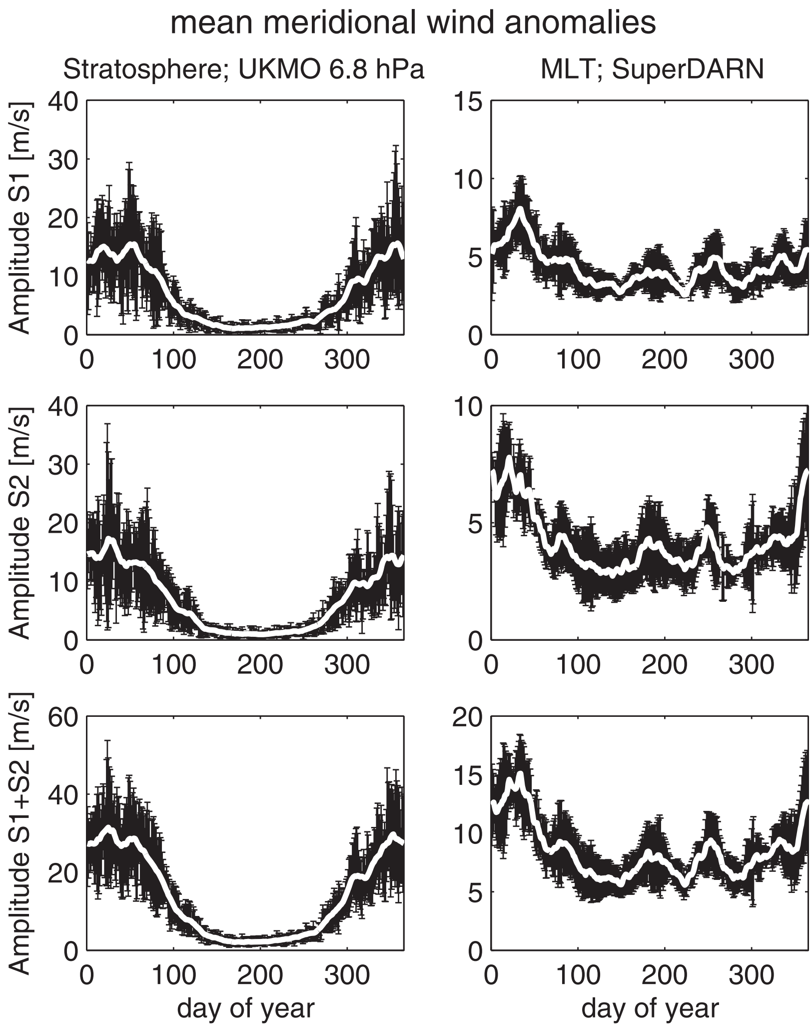

Figure 8. (left) Stratospheric planetary wave climatology from UKMO and (right) mesospheric planetary wave climatology from SuperDARN radar chain derived from the mean meridional wind anomalies. The white line shows the climatology of the 15 day smoothed (top) S_1, (middle) S_2 and (bottom) the sum of both. The black error bars depict the year-to-year variability of the zonal wave numbers.

during that winter [*Angell et al.*, 2006], as suggested by *Holton and Tan* [1980]. Furthermore, a persistent eastward traveling S_2 zonal wave packet in the mesosphere intensifies just before the start of the major stratospheric warming event that occurred in January/February 2006 (zonal wind reversal onset at 10hPa, 60°N on 21 January 2006). *Ushimaru and Tanaka* [1992] have shown that an eastward traveling S_2 planetary wave can interact with a strong stationary S_1 planetary wave in the stratosphere and create a major impact on the zonal mean flow there.

In contrast to the winter of 2005/2006, the mesospheric wave activity observed here during the winter of 2004/2005 is generally weaker, as can be seen in Figure 7 (right). Rather than a strong stationary S_1 component, this winter is characterized instead by a weaker westward traveling S_1 wave packet. Additionally, there is an absence of a strong eastward traveling S_2 component in January. This generally weak wave activity, as well as the absence of stationary S_1 and eastward traveling S_2 wave components in the mesosphere, is consistent with the anomalously strong polar vortex conditions observed during 2004/2005. This includes low stratospheric temperatures, ozone concentrations [*Angell et al.*, 2005], and the absence of a major stratospheric warming event [*Lima et al.*, 2012]. However, strong planetary wave activity in both wave numbers can be seen in mid-March during the final warming events. A more complete analysis of the MLT planetary wave evolution during major stratospheric warming events will be the subject of a future paper.

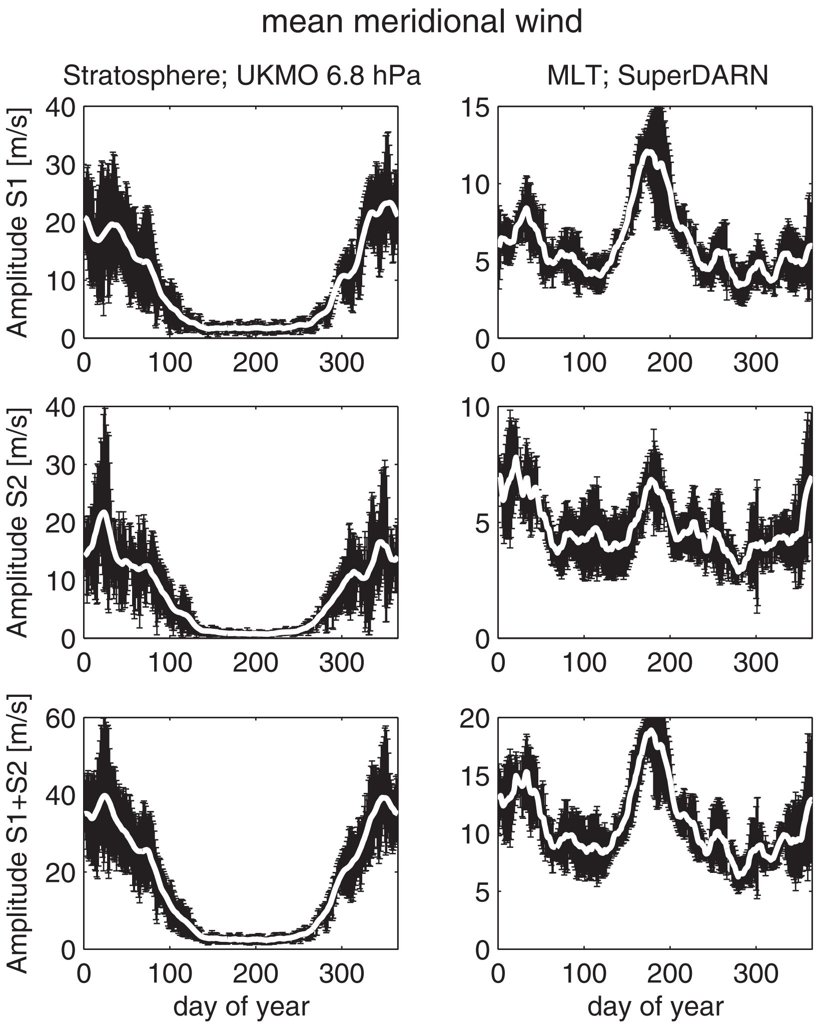

Figure 9. (left) Stratospheric planetary wave climatology from UKMO and (right) mesospheric planetary wave climatology from SuperDARN radar chain derived from the mean meridional wind. The white line shows the climatology of the 15 day smoothed (top) S_1, (middle) S_2, and (bottom) the sum of both. The black error bars depict the year-to-year variability of the zonal wave numbers.

5.2. Planetary Wave Climatologies

In order to examine the climatological seasonal behavior of the zonal wave numbers 1 and 2 components in both the stratosphere and the MLT, the daily average of the amplitudes retrieved in the fitting process were calculated. Climatologies (2000–2005) of planetary wave amplitudes fitted to the UKMO 6.8 hPa (~ 35 km) anomaly data at the radar stations are shown in Figure 8 (left) for the S_1, S_2 and the sum of S_1 and S_2. Similarly, climatologies (2000–2008) of wave amplitudes resulting form the fit to the SuperDARN radar anomaly winds are shown in the right-hand panels. The wave activity is smoothed with a 15 day running mean before averaging for better visibility of the general behavior.

In general the planetary wave activity of the zonal wave numbers 1 and 2 components has a similar magnitude and year-to-year variability. In the stratosphere (Figure 8 (left)) the planetary wave activity in both zonal wave numbers is low in summer and high in winter. This behavior reflects the filtering effect of the zonal background wind in the lower stratosphere. *Charney and Drazin* [1961] showed for a simplified, analytically solvable system that planetary waves can propagate only into regions where the zonal mean wind ($\bar{u}$) is both larger (more eastward) than the zonal velocity (c) of the wave and smaller (more westward) than the Rossby critical velocity (U_c), where U_c depends on the horizontal scale of the wave. The intrinsic wave velocity of Rossby waves is always westward and their propagation is therefore strongly prohibited by the stratospheric summertime westward jets. This explains the low values for both zonal wave numbers in the summer stratosphere. The higher values in the winter stratosphere are related to general eastward zonal background winds and propagation of planetary waves from below. A strong year-to-year variability is visible during winter as has been observed in previous studies [e.g., *McDonald et al.*, 2011].

Large year-to-year variability can also be observed in the planetary wave activity of zonal wave numbers 1 and 2 in the MLT (Figure 8 (right)). The MLT magnitudes of both planetary wave zonal wave numbers are smaller than in the stratosphere. The seasonal variation of the MLT planetary wave activity is similar to that in the stratosphere but with smaller winter-summer ratios. In addition, the winter enhancement is more restricted in the MLT, generally occurring from late December until the beginning of March. This period represents times when stratospheric sudden warmings frequently occur in the Northern Hemisphere [e.g., *Manney et al.*, 2009a, 2009b; *Lima et al.*, 2012; *Matthias et al.*, 2012]. This supports the idea that sudden stratospheric warmings increase the vertical coupling. During sudden stratospheric warmings the stratospheric background wind is strongly reduced, or reversed during major events, and this favors the propagation of stratospheric planetary waves into the MLT.

In addition to the winter-time enhancement an increase in planetary wave activity can be seen during midsummer and around autumn equinox. Strong perturbations in the temperature near 87 km have been seen during the autumn equinox [*Taylor et al.*, 2001] and have been interpreted and modeled [*Liu et al.*, 2001] as an increase in planetary wave activity at these altitudes. The midsummer increase in planetary wave activity might be related to interhemispheric coupling above the strong summertime westward wind regime or to planetary wave generation in the upper atmosphere [e.g., *Williams and Avery*, 1992; *Forbes*, 1995; *Espy et al.*, 1997; *Mitchell et al.*, 1999; *Garcia et al.*, 2005; *Pancheva et al.*, 2008].

Figure 9 shows the climatologies of wave components for the mean meridional winds (station climatologies not removed). The seasonal behavior is similar to the climatology-removed case, with in general ~15% higher amplitudes. The only exception is the MLT summer, where strong S_1 wave amplitudes appear. These high amplitudes are related to the stationary summertime wave feature seen in Figure 6 arising from the differences in the station climatologies seen in Figure 2. As mentioned before, this consistent wave feature can be interpreted as a result of longitudinal differences in gravity wave forcing [e.g., *Smith*, 2003].

6. Conclusion

Planetary wave activity in the MLT has been observed using meridional winds from the high northern latitude (51–66°N) SuperDARN network used as a "ground-based satellite." The zonal wave numbers 1 and 2 components have been extracted from daily mean meridional winds and wind anomalies from 25°E to 150°W for the years 2000–2008. The technique was validated over the entire data range by first using the wave components fitted over the entire longitude range to reconstruct the original observed wind at each individual station. The correlation between the reconstructions and the original data exceeded a correlation coefficient of 0.61, significant at >99% confidence level, for all stations. Further validation was done by applying the fit to meridional UKMO wind data at just the longitudes of the radar stations and comparing it to an ideal fit covering 360° (2.5° spacing) longitude. Finally, the planetary wave perturbation in the meridional wind at a single longitude derived from the SuperDARN chain was compared with an independent observation of OH-airglow temperatures over Stockholm. All three validation techniques indicate that the longitudinal fitting method applied to the SuperDARN meridional wind data is able to extract accurate planetary wave amplitudes that account for 40%–60% of the variation seen in the wind.

The climatology of planetary wave activity of zonal wave numbers 1 and 2 in the MLT (from SuperDARN) and stratosphere (from UKMO) indicates vertical coupling throughout the middle atmosphere around the autumn equinox and during winter when sudden stratospheric warming events occur frequently. The planetary wave amplitudes observed during winter are approximately halved between the stratosphere (~ 35 km) and the MLT, indicating significant planetary wave energy dissipation in the middle atmosphere. Thus, the use of this method provides a way of monitoring the planetary wave activity in the MLT during stratospheric sudden warmings allowing a better understanding of stratospheric warming effects and mesospheric precursors [*Lee et al.*, 2009; *Manney et al.*, 2009b; *Kurihara et al.*, 2010; *Coy et al.*, 2011]. Finally, the difference between the mesospheric and stratospheric planetary wave activity during the summer indicates that any MLT wave activity due to transfer of planetary wave activity from the winter hemisphere [*Forbes*, 1995] occurs above the stratopause. However, it is also consistent with the regeneration of planetary waves in the

MLT due to the forcing by breaking gravity waves whose transmission through the stratosphere have been modulated by planetary waves in the lower stratosphere [*Holton*, 1984].

The SuperDARN chain is capable of providing a reliable measure of mesospheric planetary wave activity, allowing a quantitative assessment of wave strength, propagation direction, and evolution throughout the season. Furthermore, as the availability of SuperDARN and other wind measurements grows in both hemispheres, the method will be an important tool in assessing interhemispheric coupling.

Acknowledgments
The authors acknowledge the use of SuperDARN data. SuperDARN is a collection of radars funded by the national scientific funding agencies of Australia, Canada, China, France, Japan, South Africa, United Kingdom, and United States of America. The UK Meteorological Office assimilated data set was made available by the stratospheric British Atmospheric Data Centre. The authors are thankful for constructive comments provided during review.

References

Alexander, S. P., and M. G. Shepherd (2010), Planetary wave activity in the polar lower stratosphere, *Atmos. Chem. Phys.*, *10*(2), 707–718.
Angell, J. K., L. T. Flynn, M. E. Gelman, D. Hofmann, C. S. Long, A. J. Miller, and S. Zhou (2005), *Northern Hemisphere Winter Summary*, Oltmans, S. http://www.cpc.ncep.noaa.gov/products/stratosphere/winter_bulletins/nh_04-05/.
Angell, J. K., L. T. Flynn, M. E. Gelman, D. Hofmann, C. S. Long, A. J. Miller, S. Oltmans, and S. Zhou (2006), *Northern Hemisphere Winter Summary*. http://www.cpc.ncep.noaa.gov/products/stratosphere/winter_bulletins/nh_05-06/.
Arnold, N. F., P. A. Cook, T. R. Robinson, M. Lester, P. J. Chapman, and N. Mitchell (2003), Comparison of D-region Doppler drift winds measured by the SuperDARN Finland HF radar over an annual cycle using the Kiruna VHF meteor radar, *Ann. Geophys.*, *21*(10), 2073–2082.
Bancalá, S., K. Krüger, and M. Giorgette (2012), The preconditioning of major sudden stratospheric warmings, *J. Geophys. Res.*, *117*, D04101, doi:10.1029/2011JD016769.
Baumgaertner, A. J. G., A. J. McDonald, R. E. Hibbins, D. C. Fritts, D. J. Murphy, and R. A. Vincent (2008), Short-period planetary waves in the Antarctic middle atmosphere, *J. Atmos. Solar-Terr. Phys.*, *70*(10), 1336–1350, doi:10.1016/j.jastp.2008.04.007.
Belova, A. (2008), Studies of planetary waves in ozone and temperature fields as observed by the Odin satellite in 2002–2007, *IRF Scientific Report*, *298*, 35.
Belova, A., S. Kirkwood, D. Murtagh, N. Mitchell, W. Singer, and W. Hocking (2008), Five-day planetary waves in the middle atmosphere from Odin satellite data and ground-based instruments in Northern Hemisphere summer 2003, 2004, 2005 and 2007, *Ann. Geophys.*, *26*(11), 3557–3570.
Bristow, W. A., J. H. Yee, X. Zhu, and R. A. Greenwald (1999), Simultaneous observations of the July 1996 2-day wave event using the Super Dual Auroral Radar Network and the High Resolution Doppler Imager, *J. Geophys. Res.*, *104*(A6), 12,715–12,721, doi:10.1029/1999JA900030.
Charney, J. G., and P. G. Drazin (1961), Propagation of planetary-scale disturbance from lower into upper atmophere, *Geophys. Res. Lett.*, *66*(1), 83–109.
Chisham, G., and M. P. Freeman (2013), A reassessment of SuperDARN meteor echoes from the upper mesosphere and lower thermosphere, *J. Atmos. Solar-Terr. Phys.*, *102*, 207–221, doi:10.1016/j.jastp.2013.05.018.
Chshyolkova, T., A. H. Manson, and C. E. Meek (2005), Climatology of the quasi two-day wave over Saskatoon (52 degrees N, 107 degrees W): 14 Years of MF radar observations, in *Coupling Process in the MLT Region, Advances in Space Research*, vol. 35, edited by B. Clemesha and M. Taylor, pp. 2011–2016, 35th COSPAR Scientific Assembly, Paris, FRANCE, doi:10.1016/j.asr.2005.03.040.
Chshyolkova, T., A. H. Manson, C. E. Meek, S. K. Avery, D. Thorsen, J. W. MacDougall, W. Hocking, Y. Murayama, and K. Igarashi (2006), Planetary wave coupling processes in the middle atmosphere (30–90 km): A study involving MetO and MFR data, *J. Atmos. Solar-Terr. Phys.*, *68*(3–5), 353–368, doi:10.1016/j.jastp.2005.05.011.
Coy, L., S. D. Eckermann, K. W. Hoppel, and F. Sassi (2011), Mesospheric precursors to the major stratospheric sudden warming of 2009: Validation and dynamical attribution using a ground-to-edge-of-space data assimilation system, *J. Adv. Model. Earth Syst.*, *3*(4), M10002, doi:10.1029/2011MS000067.
Demissie, T. D., N. H. Kleinknecht, R. E. Hibbins, P. J. Espy, and C. Straub (2013), Quasi-16 day planetary-wave oscillations observed in ozone and temperature data from Antarctica, *Ann. Geophys.*, *31*, 1–6, doi:10.5194/angeo-31-1-2013.
Dowdy, A. J., R. A. Vincent, M. Tsutsumi, K. Igarashi, Y. Murayama, W. Singer, and D. J. Murphy (2007), Polar mesosphere and lower thermosphere dynamics: Mean wind and gravity wave climatologies, *J. Geophys. Res.*, *112*, D17104, doi:10.1029/2006JD008126.
Dowdy, A. J., R. A. Vincent, D. J. Murphy, M. Tsutsumi, D. M. Riggin, and M. J. Jarvis (2004), The large-scale dynamics of the mesosphere-lower thermosphere during the Southern Hemisphere stratospheric warming of 2002, *Geophys. Res. Lett.*, *31*, L14102, doi:10.1029/2004GL020282.
Espy, P. J., J. Stegman, and G. Witt (1997), Interannual variations of the quasi-16-day oscillation in the polar summer mesospheric temperature, *J. Geophys. Res.*, *102*(D2), 1983–1990, doi:10.1029/96JD02717.
Espy, P. J., R. E. Hibbins, D. M. Riggin, and D. C. Fritts (2005), Mesospheric planetary waves over Antarctica during 2002, *Geophys. Res. Lett.*, *32*, L21804, doi:10.1029/2005GL023886.
Forbes, J. M. (1995), Tidal and planetary waves, in *The Upper Mesosphere and Lower Thermosphere: A Review of Experiment and Theory, Geophys. Monogr. Ser.*, vol. 87, pp. 67–87, AGU, Washington, D. C.
Garcia, R. R., R. Lieberman, J. M. Russell, and M. G. Mlynczak (2005), Large-scale waves in the mesosphere and lower thermosphere observed by SABER, *J. Atmos. Sci.*, *62*(12), 4384–4399, doi:10.1175/JAS3612.1.
Greenwald, R. A., K. B. Baker, R. A. Hutchins, and C. Hanuise (1985), An HF phase-array radar for studying small-scale structure in the high-latitude ionosphere, *Radio Sci.*, *20*(1), 63–79, doi:10.1029/RS020i001p00063.
Greenwald, R. A., et al. (1995), DARN/SUPERDARN—A global view of the dynamics of high-latitude convection, *Space Sci. Rev.*, *71*(1–4), 761–796, doi:10.1007/BF00751350.
Grytsai, A., Z. Grytsai, A. Evtushevsky, G. Milinevsky, and N. Leonov (2005), Zonal wave numbers 1–5 in planetary waves from the TOMS total ozone at 65 degrees S, *Ann. Geophys.*, *23*(5), 1565–1573.
Hall, G. E., J. W. MacDougall, D. R. Moorcroft, J. P. St.-Maurice, A. H. Manson, and C. E. Meek (1997), Super Dual Auroral Radar Network observations of meteor echoes, *J. Geophys. Res.*, *102*(A7), 14,603–14,614, doi:10.1029/97JA00517.
Hibbins, R. E., and M. J. Jarvis (2008), A long-term comparison of wind and tide measurements in the upper mesosphere recorded with an imaging Doppler interferometer and SuperDARN radar at Halley, Antarctica, *Atmos. Chem. Phys.*, *8*(5), 1367–1376, doi:10.5194/acp-8-1367-2008.
Hibbins, R. E., P. J. Espy, and M. J. Jarvis (2006), Mean winds and tides in the mesosphere and lower thermosphere above Halley, Antarctica, *J. Atmos. Solar-Terr. Phys.*, *68*(3–5), 436–444, doi:10.1016/j.jastp.2005.02.030.

Hibbins, R. E., M. P. Freeman, S. E. Milan, and J. M. Ruohoniemi (2011), Winds and tides in the mid-latitude Southern Hemisphere upper mesosphere recorded with the Falkland Islands SuperDARN radar, *Ann. Geophys.*, *29*(11), 1985–1996, doi:10.5194/angeo-29-1985-2011.

Hocking, W. K., B. Fuller, and B. Vandepeer (2001), Real-time determination of meteor-related parameters utilizing modem digital technology, *J. Atmos. Solar-Terr. Phys.*, *63*(2–3), 155–169, doi:10.1016/S1364-6826(00)00138-3.

Holton, J. R. (1984), The generation of mesospheric planetary-waves by zonally asymmetric greavity-wave breaking, *J. Atmos. Sci.*, *41*(23), 3427–3430, doi:10.1175/1520-0469(1984)041<3427:TGOMPW>2.0.CO;2.

Holton, J. R., and H. C. Tan (1980), The influenced of the equatorial quasi-biennial oscillation on the global circulation at 50 mb, *J. Atmos. Sci.*, *37*(10), 2200–2208, doi:10.1175/1520-0469(1980)037<2200:TIOTEQ>2.0.CO;2.

Hussey, G. C., C. E. Meek, D. Andre, A. H. Manson, G. J. Sofko, and C. M. Hall (2000), A comparison of Northern Hemisphere winds using SuperDARN meteor trail and MF radar wind measurements, *J. Geophys. Res.*, *105*(D14), 18,053–18,066, doi:10.1029/2000JD900272.

Jarvis, M. J., G. O. L. Jones, and B. Jenkins (1999), New initiatives in observing the Antarctic mesosphere, *Adv. Space Res.*, *24*(5), 611–619, doi:10.1016/S0273-1177(99)00479-2.

Jenkins, B., and M. J. Jarvis (1999), Mesospheric winds derived from SuperDARN HF radar meteor echoes at Halley, Antarctica, *Earth Planets Space*, *51*(7–8), 685–689.

Jenkins, B., M. J. Jarvis, and D. M. Forbes (1998), Mesospheric wind observations derived from Super Dual Auroral Radar Network (SuperDARN) HF radar meteor echoes at Halley, Antarctica: Preliminary results, *Radio Sci.*, *33*(4), 957–965, doi:10.1029/98RS01113.

Kurihara, J., Y. Ogawa, S. Oyama, S. Nozawa, M. Tsutsumi, C. M. Hall, Y. Tomikawa, and R. Fujii (2010), Links between a stratospheric sudden warming and thermal structures and dynamics in the high-latitude mesosphere, lower thermosphere, and ionosphere, *Geophys. Res. Lett.*, *37*, L13806, doi:10.1029/2010GL043643.

Labitzke, K. (1977), Innerannual variability of the winter stratosphere in the northern hemisphere, *Mon. Weather Rev.*, *105*, 762–770.

Labitzke, K. (1981), The amplification of height wave 1 in January 1979: A characteristic precondition for major warming in February, *Mon. Weather Rev.*, *109*, 983–989.

Lee, J. N., D. L. Wu, G. L. Manney, and M. J. Schwartz (2009), Aura microwave limb sounder observations of the northern annular mode: From the mesosphere to the upper troposphere, *Geophys. Res. Lett.*, *36*, L20807, doi:10.1029/2009GL040678.

Lima, L. M., E. O. Alves, P. P. Batista, B. R. Clemesha, A. F. Medeiros, and R. A. Buriti (2012), Sudden stratospheric warming effects on the mesospheric tides and 2-day wave dynamics at 7 degrees S, *J. Atmos. Solar-Terr. Phys.*, *78–79*(SI), 99–107, doi:10.1016/j.jastp.2011.02.013.

Lindzen, R. S. (1981), Turbulence and stress owing to gravity wave and tidal breakdown, *J. Geophys. Res.*, *86*, 9707–9714.

Liu, H. L., R. G. Roble, M. J. Taylor, and W. R. Pendleton Jr. (2001), Mesospheric planetary waves at northern hemisphere fall equinox, *Geophys. Res. Lett.*, *28*, 1903–1906.

Manney, G. L., et al. (2009a), Satellite observations and modeling of transport in the upper troposphere through the lower mesosphere during the 2006 major stratospheric sudden warming, *Atmos. Chem. Phys.*, *9*(14), 4775–4795, doi:10.5194/acp-9-4775-2009.

Manney, G. L., M. J. Schwartz, K. Krüger, M. L. Santee, S. Pawson, J. N. Lee, W. Daffer, R. A. Fuller, and N. J. Livesey (2009b), Aura microwave limb sounder observations of dynamics and transport during the record-breaking 2009 arctic stratospheric major warming, *Geophys. Res. Lett.*, *36*, L12815, doi:10.1029/2009GL038586.

Manson, A. H., C. E. Meek, M. J. Smith, and G. J. Fraser (1985), Direct comparisons of prevailing winds and tital wind fiels (24-h, 12-h) in the upper middle armosphere(60–105 km) during 1978–1980 Saskatoon (52-degrees-n, 107-degrees-w) and Christchurch (44-degrees-s, 173-degree-e), *J. Atmos. Terr. Phys.*, *47*(5), 463–476, doi:10.1016/0021-9169(85)90112-6.

Matthias, V., P. Hoffmann, M. Rapp, and G. Baumgarten (2012), Composite analysis of the temporal development of waves in the polar MLT region during stratospheric warmings, *J. Atmos. Solar-Terr. Phys.*, *90–91*(SI), 86–96, doi:10.1016/j.jastp.2012.04.004.

McDonald, A. J., R. E. Hibbins, and M. J. Jarvis (2011), Properties of the quasi 16 day wave derived from EOS MLS observations, *J. Geophys. Res.*, *116*, D06112, doi:10.1029/2010JD014719.

Met Office et al. (2013), Stratospheric assimilated data, [internet], NCAS British Atmospheric Data Centre, 2006, Available from http://badc.nerc.ac.uk/view/badc.nerc.ac.uk__ATOM__dataent_ASSIM.

Milan, S. E., T. B. Jones, T. R. Robinson, E. C. Thomas, and T. K. Yeoman (1997), Interferometric evidence for the observation of ground backscatter originating behind the cutlass coherent hf radars, *Ann. Geophys.*, *15*, 29–39, doi:10.1007/s00585-997-0029-y.

Mitchell, N. J., H. R. Middleton, A. G. Beard, P. J. S. Williams, and H. G. Muller (1999), The 16-day planetary wave in the mesosphere and lower thermosphere, *Ann. Geophys.*, *17*, 1447–1456, doi:10.1007/s00585-999-1447-9.

Mitchell, N. J., D. Pancheva, H. R. Middleton, and M. E. Hagan (2002), Mean winds and tides in the Arctic mesosphere and lower thermosphere, *J. Geophys. Res.*, *107*(A1), 1004, doi:10.1029/2001JA900127.

Pancheva, D., et al. (2008), Planetary waves in coupling the stratosphere and mesosphere during the major stratospheric warming in 2003/2004, *J. Geophys. Res.*, *113*, D12105, doi:10.1029/2007JD009011.

Portnyagin, Y. I., et al. (2004), Monthly mean climatology of the prevailing winds and tides in the Arctic mesosphere/lower thermosphere, *Ann. Geophys.*, *22*(10), 3395–3410.

Salby, M. L. (1981), The 2-day wave in the middle atmophere: Observations and theory, *J. Geophys. Res.*, *86*(C10), 9654–9660, doi:10.1029/JC086iC10p09654.

Smith, A. K. (2003), The origion of stationary planetary waves in the upper mesosphere, *J. Atmos. Sci.*, *60*, 3033–3041.

Stearns, S. D. (1975), *Digital signal analysis*, Hayden book, Rochelle Park, New Jersey.

Swinbank, R., and A. A. O'Neill (1994), A stratosphere-troposphere data assimilation system, *Mon. Weather Rev.*, *122*, 686–702.

Taylor, M. J., W. R. Pendleton Jr., H. L. Liu, C. Y. She, L. C. Garnet, R. G. Roble, and V. Vasoli (2001), Large amplitude pertubationa in the mesospheric OH meinel and 87-km Na lidar temperatures around the autumnal equinox, *Geophys. Res. Lett.*, *28*, 1899–1902.

Thayaparan, T., and W. K. Hocking (2002), A long-term comparison of winds and tides measured at London, Canada (43N, 81W) by co-located MF and meteor radars, *J. Atmos. Solar-Terr. Phys.*, *64*(8–11), 931–946, doi:10.1016/S1364-6826(02)00048-2.

Tsutsumi, M., A. S. Yukimatu, D. A. Holdsworth, and M. Lester (2009), Advanced SuperDARN meteor wind observations based on raw time series analysis technique, *Radio Sci.*, *44*, RS2006, doi:10.1029/2008RS003994.

Ushimaru, S., and H. Tanaka (1992), A numerical study of the interaction between stationary rossby waves and eastward-traveling waves in the southern hemisphere stratosphere, *J. Atmos. Sci.*, *49*(15), 1354–1373, doi:10.1175/1520-0469(1992)049<1354:ANSOTI>2.0.CO;2.

Williams, C. R., and S. K. Avery (1992), Analysis of long-period waves using the mesosphere-stratosphere-troposphere radar at Poker Flat, Alaska, *J. Geophys. Res.*, *97*(D18), 20,855–20,861.

Wu, D. L., P. B. Hays, and Wilbert R. S. (1995), A least-squares method for spectral-analysis of space-time series, *J. Atmos. Sci.*, *52*(20), 3501–3511, doi:10.1175/1520-0469(1995)052<3501:ALSMFS>2.0.CO;2.

Yukimatu, A. S., and M. Tsutsumi (2002), A new SuperDARN meteor wind measurement: Raw time series analysis method and its application to mesopause region dynamics, *Geophys. Res. Lett.*, *29*(20), 1981, doi:10.1029/2002GL015210.

Stray, N. H., R. J. de Wit, P. J. Espy, and R. E. Hibbins, Observational evidence for temporary planetary wave forcing of the MLT during fall equinox, *Geophys. Res. Lett.*, *41*(17), 6281–6288, doi: 10.1002/2014GL061119, 2014a

Paper 2

AGU PUBLICATIONS

Geophysical Research Letters

RESEARCH LETTER
10.1002/2014GL061119

Key Points:
- Planetary wave activity increases during NH fall equinox in the MLT
- Temporary planetary wave forcing of the mesospheric residual circulation
- Previously observed meridional wind and temperature increases are explained

Correspondence to:
N. H. Stray,
nora.kleinknecht@ntnu.no

Citation:
Stray, N. H., R. J. de Wit, P. J. Espy, and R. E. Hibbins (2014), Observational evidence for temporary planetary wave forcing of the MLT during fall equinox, *Geophys. Res. Lett.*, *41*, 6281–6288, doi:10.1002/2014GL061119.

Received 4 JUL 2014
Accepted 11 AUG 2014
Accepted article online 14 AUG 2014
Published online 2 SEP 2014

Observational evidence for temporary planetary wave forcing of the MLT during fall equinox

Nora H. Stray[1], Rosmarie J. de Wit[1], Patrick J. Espy[1,2], and Robert E. Hibbins[1,2]

[1]Department of Physics, NTNU, Trondheim, Norway, [2]Birkeland Centre for Space Science, Bergen, Norway

Abstract We present direct observations of zonal wave numbers 1 and 2 planetary wave activity in the mesopause region derived from a longitudinal chain of high-latitude Northern Hemisphere (51–66°N) Super Dual Auroral Radar Network radars. Over a 9 year period (2000–2008), the planetary wave activity observed shows a consistent increase around the fall equinox. This is shown to be coincident with a minimum in the magnitude of the stratospheric winds and consequently a minimum in the stratospheric gravity wave filtering and the subsequent momentum deposition in the mesopause region. Despite this, the observed meridional winds are shown to be perturbed poleward and mesopause temperatures rise temporarily, suggesting that westward momentum deposition from planetary waves temporarily becomes the dominant forcing on the mesopause region each fall equinox.

1. Introduction

The mesosphere and lower thermosphere (MLT) is driven far from radiative equilibrium by the deposition of momentum by waves [*Fritts and Alexander*, 2003]. Generally, this forcing is due to gravity waves (GWs), generated in all directions in the lower atmosphere, but filtered by stratospheric background winds as they propagate upward. As GWs propagate into the MLT and break, they provide a net momentum source to the region [e.g., *Lindzen*, 1981; *Holton*, 1982, 1983; *Garcia and Solomon*, 1985] and force the residual meridional circulation. During equinox, when the zonal stratospheric winds approach zero, little net gravity wave filtering takes place, and subsequently, little net momentum is deposited into the mesosphere by GWs. Hence, the atmosphere should approach radiative equilibrium in the MLT around equinox [*Andrews*, 2010].

In this paper we present observations of enhanced planetary wave (PW) activity in the MLT during fall equinox that occurs concurrently with increased poleward meridional flow and reduced gravity wave forcing. Mean meridional winds as well as the zonal wave numbers 1 and 2 PW structures in the Northern Hemisphere MLT have been extracted using a longitudinal chain of Super Dual Auroral Radar Network (SuperDARN) radars. These are combined with winds from the UK Meteorological Office (UKMO) Stratospheric Assimilated Data [*Swinbank et al.*, 2013] to investigate the relationship between the PW activity in the MLT and the underlying wind field. A momentum flux meteor radar is also used to assess the forcing of the MLT winds by gravity wave momentum deposition during the fall equinox [*Hocking et al.*, 2001; *Hocking*, 2005; *Fritts et al.*, 2010]. Although some of these features have been previously modeled or observed in isolation, here a suite of observations is presented and combined in order to examine the primary forcing mechanism of the MLT residual circulation and its contribution to the mesospheric temperature enhancements that have previously been reported [*Taylor et al.*, 2001; *Espy and Stegman*, 2002; *French and Burns*, 2004].

2. Data

PW activity with zonal wave numbers 1 and 2 for years 2000–2008 was extracted from daily mesospheric meridional meteor wind anomalies using a longitudinal chain (150°W–25°E) of SuperDARN radars [*Greenwald et al.*, 1985, 1995] spanning latitudes from 51 to 66°N as described by *Kleinknecht et al.* [2014]. Tidal effects and effects of the 2 day wave were removed using the techniques outlined in *Hibbins and Jarvis* [2008] and *Kleinknecht et al.* [2014] before the retrieval of the PW structures. Figure 1 shows Hovmöller diagrams of wave numbers 1 and 2 PW components for the year 2000 as an example. Blue and red colors signify equatorward and poleward wind, respectively. Figures for all other years can be found in *Kleinknecht et al.* [2014, Figure 5].

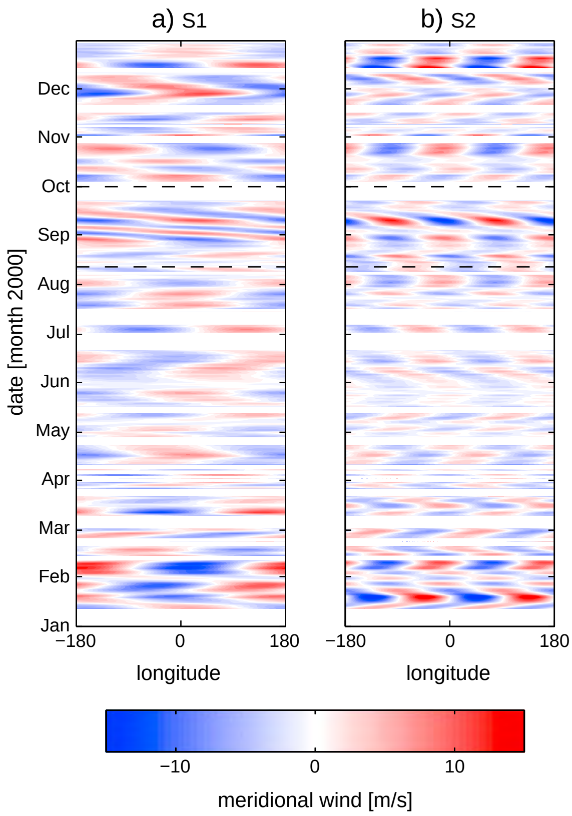

Figure 1. Hovmöller diagrams of zonal wave numbers 1 and 2 (S_1, S_2) of the mesospheric (mean altitude around 95 km) meridional wind, year 2000. Blue and red colors signify poleward and equatorward wind, respectively. A period of westward propagating wave activity can clearly be seen around fall equinox in the S_1 mode. Adapted from *Kleinknecht et al.* [2014].

The UK Meteorological Office (UKMO) Stratospheric Assimilated Data winds [*Swinbank et al.*, 2013] from the years 2000–2008 were used to quantify the tropospheric and stratospheric wind regimes. UKMO wind data are available for pressure levels between 1000 and 0.1 hPa (0.3 hPa before 28 October 2003 and 0.4 hPa between 14 March 2006 and 14 May 2007) and a horizontal resolution of 2.5° × 3.75° (latitude × longitude).

Vertical profiles of the density-weighted GW momentum fluxes of zonal momentum, $\rho\,\overline{u'\,w'}$, have been determined using a new generation All-Sky Interferometric (SKiYMET) meteor radar [*Hocking et al.*, 2001; *Fritts et al.*, 2010] located in Trondheim (63°N, 10°E), Norway [*de Wit et al.*, 2014]. The system, operating at a frequency of 34.21 MHz, is optimized to measure momentum fluxes by the use of a circular transmitter array consisting of eight antennas, which directs most of the 30 kW peak power between zenith angles of 15° and 50°. Maximum meteor count rates are observed around 90 km, and daily count rates range between 6000 and 12,000 unambiguous meteors at zenith angles between 15° and 50° and altitudes of 70–100 km. Momentum fluxes are derived in four altitude ranges (80–85 km, 85–90 km, 90–95 km, and 95–100 km) after removing the background winds [*Andrioli et al.*, 2013] using the method proposed by *Hocking* [2005] to estimate their vertical divergence using densities, ρ, taken from the COSPAR International Reference Atmosphere 1986 monthly mean density data set [*Fleming et al.*, 1990].

3. Results

Figure 2 shows the observed mesospheric PW activity (the sum of zonal wave numbers 1 and 2) at high northern latitudes (51–66°N) between 1 March and 15 October for the years 2000–2008. The PW activity is also shown smoothed over 10 days for better visualization. These data are representative of the PW activity around an altitude of ∼ 95 km [e.g., *Hall et al.*, 1997; *Hibbins and Jarvis*, 2008]. The maximum eastward (red) and westward (green) zonal mean zonal wind speed in the height column from 1000 to 0.1 hPa (ground to ∼ 65 km) and at the latitude band between 51 and 66°N are displayed for the same time periods. These winds are extracted from the zonal mean zonal UKMO winds.

Increased PW activity can be observed after spring equinox, during midsummer and around fall equinox. The enhancements in spring and summer show strong interannual variability in both timing and strength. The spring enhancements are related to the final breakdowns of the polar vortex, as discussed by *Manson et al.* [2002] and *Shepherd et al.* [2002] who found good agreement between (final) stratospheric warming events and springtime temperature perturbations. The midsummer peak in PW activity is consistent with interhemispheric propagation of PW's into the summer mesosphere [e.g., *Forbes et al.*, 1995; *Espy et al.*, 1997; *Hibbins et al.*, 2007; *Ford et al.*, 2009; *Hibbins et al.*, 2009] or in situ generated waves [*Nielsen et al.*, 2010]. A detailed description of this feature will be the subject of a subsequent publication. Although there is some interannual variability in both the start date and peak amplitude, there is a persistent PW enhancement that

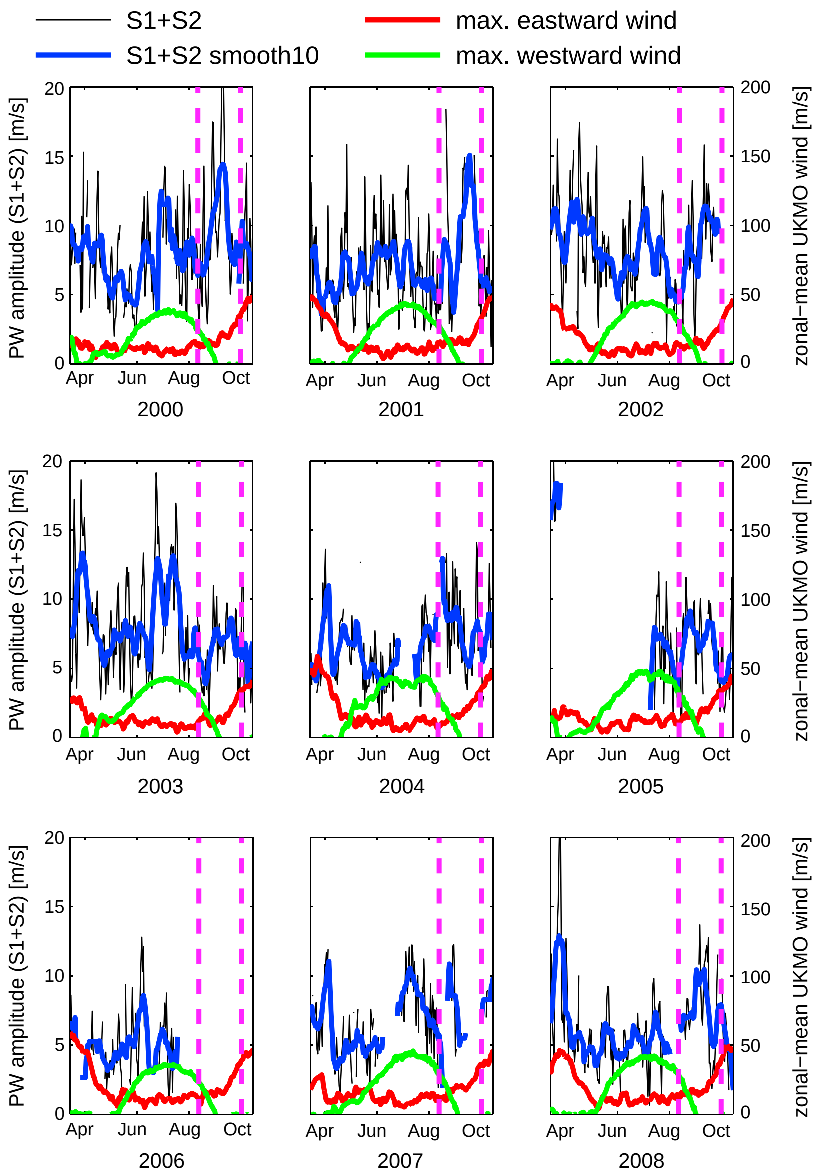

Figure 2. Ten day smoothed (blue, left axis) and unsmoothed (black, left axis) mesospheric (mean altitude around 95 km) PW activity (S_1+S_2) and maximum UKMO zonal mean eastward (red, right axis) and westward (green, right axis) wind below (~65 km) between 1 March and 15 October for years 2000–2008. The vertical dashed lines mark the start and end of the PW enhancement seen in Figure 3.

occurs around fall equinox (~days 230–270) in all years where data are available. To extract seasonal features from the year-to-year variability, the PW amplitude and the maximum wind values between 1 March and 15 October have been averaged over all 9 years. This climatology of PW activity is shown in Figure 3 and shows the enhancement around fall equinox to be a climatologically consistent feature. It is also clear that the observed enhancement in high-latitudinal mesosphere PW activity (the sum of zonal wave numbers 1 and 2) in fall occurs simultaneously with the climatological minimum in the zonal background wind observed in the underlying column.

Coincident with this burst of PW activity, a temporary poleward wind perturbation can be seen in the daily mean meridional wind of individual SuperDARN radars. As an example, Figure 4 shows the climatology of the daily mean meridional wind (blue) in the mesosphere (~ 95 km) measured by the SuperDARN radar at Stokkseyri (64.7°N, 26.9°W) and the 20 day smoothing of the climatology (green). The strength and direction

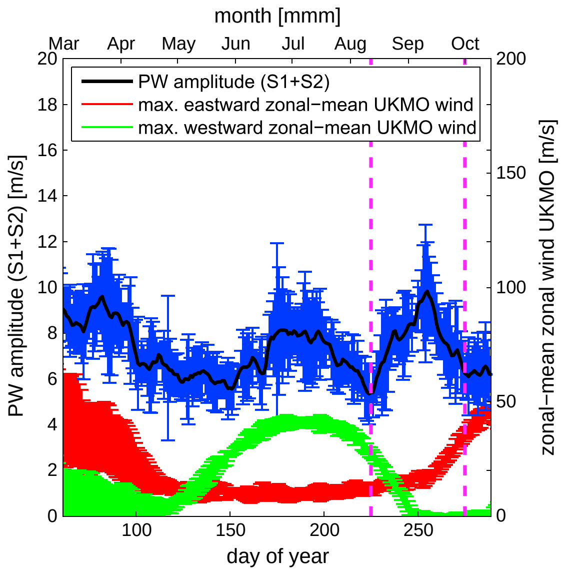

Figure 3. Ten day smoothed climatology (2000–2008) of mesospheric (mean altitude around 95 km) PW activity (black, left axis) with error bars of 1σ (blue) and climatology (2000–2008) of maximum eastward (red) and westward (green) zonal mean UKMO wind below ~65 km (right axis) between 1 March and 15 October.

of the gravity wave forcing is related to the net filtering below the MLT and hence the difference between the maximum eastward and westward wind in the height column below the MLT. Fourier decomposition of this difference reveals only an annual and semiannual component (not shown). The expected meridional wind in the mesosphere can therefore be constructed by a fit of a bias, an annual, and a semiannual component. This expected wind is shown as the red line in Figure 4. There are clear perturbations in the measured mean wind (difference between green and red line) that cannot be explained by the effect of gravity wave forcing and radiation alone. During autumn a poleward meridional wind perturbation is seen to occur just prior to day 250 coincident with the enhancement in PW activity shown in Figures 2 and 3.

4. Discussion

The vertical propagation of a PW depends on its phase speed relative to the zonal background wind in the atmosphere [e.g., *Salby*, 1996]. The maximum wind velocity in the stratosphere therefore gives an indication as to when and which waves can propagate through the stratosphere into the mesosphere. *Charney and Drazin* [1961] showed for a simplified analytically solvable system that PWs can only propagate into regions where the zonal mean wind ($\bar{u}$) is both larger (more eastward) than the zonal wave velocity (c) of the wave and smaller (more westward) than the Rossby critical velocity (U_c), where U_c is dependent on the horizontal scale of the wave. PW activity in the middle atmosphere is generally observed to be weaker in summer than in winter [e.g., *Alexander and Shepherd*, 2010; *McDonald et al.*, 2011; *Day and Mitchell*, 2010], since the intrinsic PW velocity is always westward and their propagation is therefore strongly reduced by the summertime westward jets in the stratosphere. However, during the fall equinox, stratospheric zonal winds are generally low, resulting in a high atmospheric transmission and the enhancement of PW propagation into the MLT seen in Figures 2 and 3.

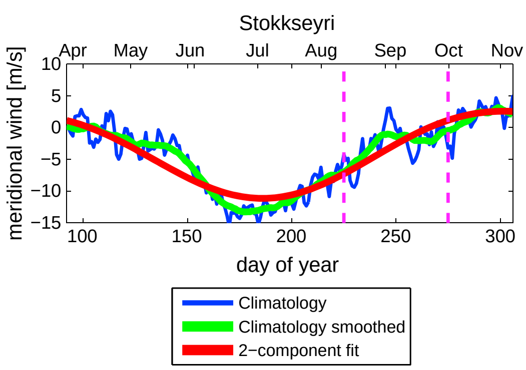

Figure 4. Climatology of planetary wave activity (blue) and 20 day smoothed climatology (green) from the Stokkseyri (64.7°N, 26.9°W) SuperDARN radar. The red curve depicts the expected seasonal variation of the meridional wind due to pure radiative and gravity wave forcing. A poleward perturbation away from the standard picture is clearly visible around fall equinox.

Bursts of 5 day and 16 day PW activity during the fall equinox have previously been observed in mesospheric winds derived from single northern hemispheric meteor radars at, e.g., Sheffield (53°N, 4°W), Esrange (68°N, 21°E), and Bear Lake (42°N, 11°W) by *Mitchell et al.* [1999], *Day and Mitchell* [2010], and *Day et al.* [2012], respectively. *Day and Mitchell* [2010] present the seasonal behavior of the quasi 5 day (4–7 days) wave in the MLT showing a clear enhancement of its amplitude in fall. This enhancement of a single temporal component occurs at the same time as the enhancement of the zonal wave numbers 1 and 2 PW structures observed here (Figure 3). Indeed, spectral analysis of the PW observed by the SuperDARN chain around fall equinox reveals quasi 5, 10, and 16 day oscillations in agreement with other PW observations at

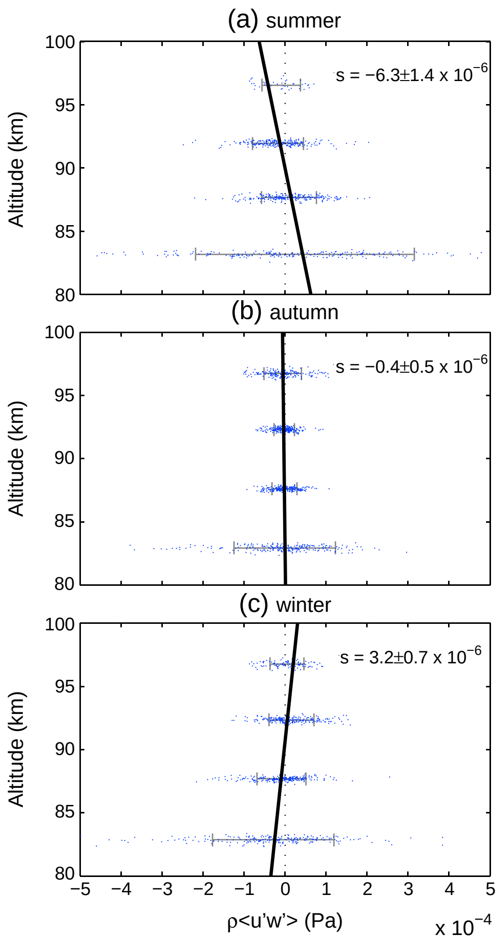

Figure 5. Vertical profile of hourly values of $\rho\overline{u'w'}$ (blue dots) and their $\pm 1\sigma$ standard deviation (grey line) together with a linear best fit (black, slope $s\left[\frac{\text{km}}{\text{Pa}}\right] \pm 1\sigma$ shown in figure) through all available data points for (a) days 156–166, (b) days 252–262, and (c) days 334–344 in the year 2013.

single stations around the fall equinox [e.g., *Day and Mitchell*, 2010; *Day et al.*, 2012]. In addition, Hovmöller diagrams (Figure 1 and *Kleinknecht et al.*, 2014, Figure 5) of the PW structures show that the wavefield during fall (August–September) often exhibits a strong phase shift and westward traveling wave components with periods shorter than 20 days become dominant in both zonal wave numbers. The strong wave transition toward the west at the time of the wave enhancement agrees with model simulations [*Liu et al.*, 2001].

Riggin et al. [2003] observed an autumn equinox enhancement of semidiurnal tidal amplitudes from MF radar observations at these latitudes which was localized between 82 and 90 km at the preferred altitudes for these radars. The amplitude decay above this altitude was attributed to refraction of the tide by the background wind field. However, *Mitchell et al.* [2002], using a SKiYMET meteor radar system located at Esrange (68°N, 21°E), observed the amplitude of the autumn equinox semidiurnal tide to continue to grow up to 97 km altitude. Although refraction of the wave energy would be expected to produce a westward and poleward forcing of the background winds, the tendency for MF radars to progressively underestimate the winds and tidal amplitudes above 90 km is well documented [e.g., *Manson et al.*, 2004; *Portnyagin et al.*, 2004]. So although tidal forcing of the background wind may play a role during the autumn equinox, the SuperDARN radars lack the altitude resolution to quantify its contribution.

Upward propagation of gravity waves is also prohibited if the background wind matches the phase velocity of the wave [*Fritts and Alexander*, 2003]. However, since GWs can have both eastward and westward phase velocities, the seasonal change of the stratospheric background wind leads to the transmission of westward GWs in winter and, correspondingly, eastward waves in summer. Those GWs that reach the MLT and break deposit their momentum. The resulting drag creates a meridional flow that redirects the wind away from the summer and toward the winter pole [*Lindzen*, 1981; *Holton*, 1982, 1983; *Garcia and Solomon*, 1985]. During equinox the zonal winds are generally low, and therefore, the filtering is at a minimum for gravity waves. Hence, GW forcing in the MLT would be expected to minimize around equinox as the GW forcing makes a smooth transition from positive (summer) to negative (winter) forcing [*Andrews et al.*, 1987].

The net effect of GWs on the zonal momentum budget of the mesopause region can be derived from the vertical divergence of the density-weighted vertical flux of horizontal momentum [e.g., *Fritts and Vincent*, 1987]. To illustrate how the GW forcing characteristically varies between solstice and equinox conditions, vertical profiles of density-weighted GW fluxes of zonal momentum, $\rho\,\overline{u'\,w'}$, determined using the meteor radar located in Trondheim [*Hocking*, 2005; *de Wit et al.*, 2014] are presented in Figure 5. Figure 5b shows $\rho\,\overline{u'\,w'}$ (blue dots) over a period of 10 days around fall equinox (days 252–262) in 2013 and their 1σ standard deviation (horizontal grey lines) at each altitude bin, together with a linear best fit through all available data points representing the vertical profile of $\rho\,\overline{u'\,w'}$ (black line). For comparison, vertical profiles of $\rho\,\overline{u'\,w'}$ representative of summertime (days 156–166 2013) and wintertime (days 334–344 2013) forcing conditions are shown in Figures 5a and 5c, respectively. During summer (winter) $\rho\,\overline{u'\,w'}$ decreases (increases) significantly with height, indicating an eastward (westward) GW forcing. However, around the fall equinox, the vertical divergence of $\rho\,\overline{u'\,w'}$ is not statistically significantly different from zero, indicating no net zonal GW forcing of the MLT region. Consequently, in the absence of other MLT dynamic forcing, the atmosphere should relax toward radiative equilibrium around equinox with MLT meridional winds close to zero [*Andrews*, 2010].

In contrast, meridional wind observations in the MLT show a poleward directed perturbation during equinox, as can be seen in Figure 4. Such poleward bursts of MLT meridional winds during the fall equinox have previously been reported at similar northern and southern latitudes [e.g., *Sandford et al.*, 2010] but not related to specific forcing mechanisms. In addition, mesosphere temperature enhancements near equinox have been observed at a variety of longitudes in both hemispheres [e.g., *Taylor et al.*, 2001; *Manson et al.*, 2002; *Shepherd et al.*, 2002; *Espy and Stegman*, 2002; *French and Burns*, 2004]. Both the enhanced poleward flow and the temperature enhancement are evidence that the MLT is driven away from radiative equilibrium by westward wave forcing during the observed enhancement of PW amplitudes at the fall equinox, when the net GW forcing minimizes. It appears that the westward momentum carried by PWs temporarily dominates the forcing of the meridional wind, driving it toward the pole and enhancing temperatures in the mesosphere during the fall equinox due to convergence and subsequent downwelling.

It should be noted that the observed enhancement of PW amplitude seems to occur slightly earlier than climatological OH-temperature perturbations that have been observed [*Taylor et al.*, 2001; *Espy and Stegman*, 2002; *French and Burns*, 2004]. However, LIDAR temperature observations [*She et al.*, 2000; *Pan and Gardner*, 2003; *Kawahara et al.*, 2004] tend to show that the fall temperature maximum occurs first at the higher altitudes of the SuperDARN wind observations (95 km) and progresses downward in time to where the OH-temperature observations take place (87 km). This downward phase progression of the temperature perturbation is again indicative of a wave-breaking source [*Plumb and Semeniuk*, 2003].

Together, these observations indicate that the temporary increase in the westward momentum carried by the PWs temporarily drives the ageostrophic meridional circulation when GW forcing is weak and in a transition from positive (summer) to negative (winter) forcing during the fall equinox. This results in a temporary increase in the poleward flow, increasing mesospheric temperatures beyond that which the weak GW forcing alone would produce. As the stratospheric winds become steadily more eastward, the increasingly filtered GWs again assume control of the meridional residual circulation and the mesospheric temperature. Although a similar process occurs during spring equinox, its timing in the Northern Hemisphere is more variable due to the timing of the final warming of the stratosphere. Hence, the climatological mean of the springtime temperature enhancement in the Northern Hemisphere [*Espy and Stegman*, 2002; *Manson et al.*, 2002; *Shepherd et al.*, 2002] is less pronounced. Thus, the enhanced flux of westward momentum carried by PWs temporarily provides the main forcing of the MLT residual circulation, resulting in enhanced poleward flow and the adiabatic heating observed in OH airglow and LIDAR temperature measurements in the MLT during fall equinox.

5. Conclusion

Evidence for temporary PW forcing of the MLT during the fall equinox has been presented and discussed as a possible cause of a concurrent poleward wind perturbation and subsequent temperature enhancement in the MLT around fall equinox. PW activity of zonal wave numbers 1 and 2 has been extracted using a longitudinal chain of high-latitude Northern Hemisphere SuperDARN radars over 9 years (2000–2008). A clear and significant enhancement of the PW amplitudes in the MLT is observed each year, as well as in the climatological composite, during the fall equinox. At this time the low zonal wind speeds in the underlying atmosphere provide reduced filtering of the GWs and PWs. While the resulting enhanced transmission of PWs increases the westward momentum carried to the MLT, the net momentum deposition of the more isotropic GWs is observed to decrease due to the reduced filtering. This temporary increase of westward momentum transmitted to the MLT by the PWs then controls the meridional residual circulation, resulting in the increased poleward flows observed here and by other studies. This, in turn, raises mesospheric temperatures beyond that which the weakened momentum flux provided by the GWs would provide and results in the enhanced mesospheric temperatures that have been observed previously. In the future the proposed mechanism to characterize the role of PW forcing on the meridional circulation will be tested by appropriate modeling efforts.

Acknowledgments

The authors acknowledge the use of SuperDARN data. SuperDARN is a collection of radars funded by the national scientific funding agencies of Australia, Canada, China, France, Japan, South Africa, United Kingdom, and United States of America. The UK Meteorological Office assimilated data set was made available by the British Atmospheric Data Centre. This study was partly supported by the Research Council of Norway/CoE under contract 223252/F50.

The Editor thanks two anonymous reviewers for their assistance in evaluating this paper.

References

Alexander, S. P., and M. G. Shepherd (2010), Planetary wave activity in the polar lower stratosphere, *Atmos. Chem. Phys.*, *10*(2), 707–718, doi:10.5194/acp-10-707-2010.

Andrews, D. G. (2010), *An Introduction to Atmospheric Physics,* 2nd ed., Cambridge Univ. Press, Cambridge, U. K.

Andrews, D. G., J. R. Holton, and C. B. Leovy (1987), *Middle Atmosphere Dynamics*, Academic Press, London, U. K.

Andrioli, V. F., D. C. Fritts, P. P. Batista, and B. R. Clemesha (2013), Improved analysis of all-sky meteor radar measurements of gravity wave variances and momentum fluxes, *Ann. Geophys.*, *31*(5), 889–908, doi:10.5194/angeo-31-889-2013.

Charney, J. G., and P. G. Drazin (1961), Propagation of planetary-scale disturbance from lower into upper atmosphere, *Geophys. Res. Lett.*, *66*(1), 83–109, doi:10.1029/JZ066i001p00083.

Day, K. A., and N. J. Mitchell (2010), The 5-day wave in the Arctic and Antarctic mesosphere and lower thermosphere, *J. Geophys. Res.*, *115*, D01109, doi:10.1029/2009JD012545.

Day, K. A., M. J. Taylor, and N. J. Mitchell (2012), Mean winds, temperatures and the 16-and 5-day planetary waves in the mesosphere and lower thermosphere over Bear Lake Observatory (42°N, 111°W), *Atmos. Chem. Phys.*, *12*(3), 1571–1585, doi:10.5194/acp-12-1571-2012.

de Wit, R. J., R. E. Hibbins, P. J. Espy, Y. J. Orsolini, V. Limpasuvan, and D. E. Kinnison (2014), Observations of gravity wave forcing of the mesopause region during the January 2013 major Sudden Stratospheric Warming, *Geophys. Res. Lett.*, *41*, 4745–4752, doi:10.1002/2014GL060501.

Espy, P. J., and J. Stegman (2002), Trends and variability of mesospheric temperature at high-latitudes, *Phys. Chem. Earth*, *27*, 543–553, doi:10.1016/S1474-7065(02)00036-0.

Espy, P. J., J. Stegman, and G. Witt (1997), Interannual variations of the quasi-16-day oscillation in the polar summer mesospheric temperature, *J. Geophys. Res.*, *102*(D2), 1983–1990, doi:10.1029/96JD02717.

Fleming, E. L., S. Chandra, J. J. Barnett, and M. Corney (1990), Zonal mean temperature, pressure, zonal wind, and geopotential height as functions of latitude, COSPAR International Reference Atmosphere: 1986. Part II: Middle atmosphere models, *Adv. Space Res.*, *10*(12), 11–59, doi:10.1016/0273-1177(90)90386-E.

Forbes, J. M., M. E. Hagan, S. Miyahara, F. Vial, A. H. Manson, C. E. Meek, and Y. I. Portnyagin (1995), Quasi 16-day oscillation in the mesosphere and lower thermosphere, *J. Geophys. Res.*, *100*, 9149–9163, doi:10.1029/94JD02157.

Ford, E. A. K., R. E. Hibbins, and M. J. Jarvis (2009), QBO effects on Antarctic mesospheric winds and polar vortex dynamics, *Geophys. Res. Lett.*, *36*, L20801, doi:10.1029/2009GL039848.

French, W. J. R., and G. B. Burns (2004), The influence of large-scale oscillations on long-term trend assessment in hydroxyl temperature over Davis, Antarctica, *J. Atmos. Sol. Terr. Phys.*, *66*, 493–506, doi:10.1016/j.jastp.2004.01.027.

Fritts, D., and R. Vincent (1987), Mesospheric momentum flux studies at Adelaide, Australia—Observations and a gravity wave-tidal interaction-model, *J. Atmos. Sci.*, *44*(3), 605–619, doi:10.1175/1520-0469(1987)04<0605:MMFSAA>2.0.CO;2.

Fritts, D., D. Janches, and W. Hocking (2010), Southern Argentina Agile Meteor Radar (SAAMER): Initial assessment of gravity wave momentum fluxes, *J. Geophys. Res.*, *115*, D19123, doi:10.1029/2010JD013891.

Fritts, D. C., and M. J. Alexander (2003), Gravity wave dynamics and effects in the middle atmosphere, *Rev. Geophys.*, *41*(1), 1003, doi:10.1029/2001RG000106.

Garcia, R. R., and S. Solomon (1985), The effect of breaking gravity waves on the dynamics and chemical composition of the mesosphere and lower thermosphere, *J. Geophys. Res.*, *90*(D2), 3850–3868, doi:10.1029/JD090iD02p03850.

Greenwald, R. A., K. B. Baker, R. A. Hutchins, and C. Hanuise (1985), An HF phase-array radar for studying small-scale structure in the high-latitude ionosphere, *Radio Sci.*, *20*(1), 63–79, doi:10.1029/RS020i001p00063.

Greenwald, R. A., et al. (1995), DARN/SUPERDARN—A global view of the dynamics of high-latitude convection, *Space Sci. Rev.*, *71*(1-4), 761–796, doi:10.1007/BF00751350.

Hall, G. E., J. W. MacDougall, D. R. Moorcroft, J. P. StMaurice, A. H. Manson, and C. E. Meek (1997), Super dual auroral radar network observations of meteor echoes, *J. Geophys. Res.*, *102*(A7), 14,603–14,614, doi:10.1029/97JA00517.

Hibbins, R. E., and M. J. Jarvis (2008), A long-term comparison of wind and tide measurements in the upper mesosphere recorded with an imaging Doppler interferometer and SuperDARN radar at Halley, Antarctica, *Atmos. Chem. Phys.*, *8*(5), 1367–1376, doi:10.5194/acp-8-1367-2008.

Hibbins, R. E., P. J. Espy, and M. J. Jarvis (2007), Quasi-biennial modulation of the semidiurnal tide in the upper mesosphere above Halley, Antarctica, *Geophys. Res. Lett.*, *34*, L21804, doi:10.1029/2007GL031282.

Hibbins, R. E., M. J. Jarvis, and E. A. K. Ford (2009), Quasi-biennial oscillation influence on long-period planetary waves in the Antarctic upper mesosphere, *J. Geophys. Res.*, *114*, D09109, doi:10.1029/2008JD011174.

Hocking, W. K. (2005), A new approach to momentum flux determinations using SKiYMET meteor radars, *Ann. Geophys.*, *23*(7), 2433–2439, doi:10.5194/angeo-23-2433-2005.

Hocking, W. K., B. Fuller, and B. Vandepeer (2001), Real-time determination of meteor-related parameters utilizing modern digital technology, *J. Atmos. Sol. Terr. Phys.*, *63*(2-3), 155–169, doi:10.1016/S1364-6826(00)00138-3.

Holton, J. R. (1982), The role of gravity wave induced drag and diffusion in the momentum budget of the mesosphere, *J. Atmos. Sci.*, *39*, 791–799, doi:10.1175/1520-0469(1982)039<0791:TROGWI>2.0.CO;2.

Holton, J. R. (1983), The influence of gravity wave breaking on the general circulation of the middle atmosphere, *J. Atmos. Sci.*, *40*, 2497–2507, doi:10.1175/1520-0469(1983)040<2497:TIOGWB>2.0.CO;2.

Kawahara, T. D., C. S. Gardner, and A. Nomura (2004), Observed temperature structure of the atmosphere above Syowa Station, Antarctica (69S,39E), *J. Geophys. Res.*, *109*, D12103, doi:10.1029/72003JD003918.

Kleinknecht, N. H., P. J. Espy, and R. E. Hibbins (2014), The climatology of zonal wave numbers 1 and 2 planetary wave structure in the MLT using a chain of Northern Hemisphere SuperDARN radars, *J. Geophys. Res. Atmos.*, *119*, 1292–1307, doi:10.1002/2013JD019850.

Lindzen, R. S. (1981), Turbulence and stress owing to gravity wave and tidal breakdown, *J. Geophys. Res.*, *86*, 9707–9714, doi:10.1029/JC086iC10p09707.

Liu, H.-L., R. G. Roble, M. J. Taylor, and W. R. Pendleton Jr. (2001), Mesospheric planetary waves at northern hemisphere fall equinox, *Geophys. Res. Lett.*, *28*, 1903–1906, doi:10.1029/2000GL012689.

Manson, A. H., C. E. Meek, J. Stegman, P. J. Espy, R. G. Roble, C. M. Hall, P. Hoffmann, and C. Jacobi (2002), Springtime transitions in mesopause airglow and dynamics: Photometer and MF radar observations in the Scandinavian and Canadian sectors, *J. Atmos. Sol. Terr. Phys.*, *64*(8-11), 1131–1146, doi:10.1016/S1364-6826(02)00064-0.

Manson, A. H., C. E. Meek, C. M. Hall, S. Nozawa, N. J. Mitchell, D. Pancheva, W. Singer, and P. Hoffmann (2004), Mesopause dynamics from the Scandinavian Triangle of radars within the PSMOS-DATAR Project, *Ann. Geophys.*, *22*, 367–386, doi:10.5194/angeo-22-367-2004.

McDonald, A. J., R. E. Hibbins, and M. J. Jarvis (2011), Properties of the quasi 16 day wave derived from EOS MLS observations, *J. Geophys. Res.*, *116*, D06112, doi:10.1029/2010JD014719.

Mitchell, N. J., H. R. Middleton, A. G. Beard, P. J. S. Williams, and H. G. Muller (1999), The 16-day planetary wave in the mesosphere and lower thermosphere, *Ann. Geophys.*, *17*, 1447–1456, doi:10.1007/s00585-999-1447-9.

Mitchell, N. J., D. Pancheva, H. R. Middleton, and M. E. Hagan (2002), Mean winds and tides in the Arctic mesosphere and lower thermosphere, *J. Geophys. Res.*, *107*(A1), SIA 2-1–2-14, doi:10.1029/2001JA900127.

Nielsen, K., D. E. Siskind, S. D. Eckermann, K. W. Hoppel, L. Coy, J. P. McCormack, S. Benze, C. E. Randall, and M. E. Hervig (2010), Seasonal variation of the quasi 5 day planetary wave: Causes and consequences for polar mesospheric cloud variability in 2007, *J. Geophys. Res.*, *115*, D18111, doi:10.1029/2009JD012676.

Pan, W. L., and C. S. Gardner (2003), Seasonal variations of the atmospheric temperature structure at South Pole, *J. Geophys. Res.*, *108*(D18), 4564, doi:10.1029/2002JD003217.

Plumb, R. A., and K. Semeniuk (2003), Downward migration of extratropical zonal wind anomalies, *J. Geophys. Res.*, *108*(D7), 4223, doi:10.1029/2002JD002773.

Portnyagin, Y. I., et al. (2004), Monthly mean climatology of the prevailing winds and tides in the Arctic mesosphere/lower thermosphere, *Ann. Geophys.*, *22*(10), 3395–3410, doi:10.5194/angeo-22-3395-2004.

Riggin, D. M., C. K. Meyer, D. C. Fritts, M. J. Jarvis, Y. Murayama, W. Singer, R. A. Vincent, and D. J. Murphy (2003), MF radar observations of seasonal variability of semidiurnal motions in the mesosphere at high northern and southern latitudes, *J. Atmos. Sol. Terr. Phys.*, *65*(4), 483–493, doi:10.1016/S1364-6826(02)00340-1.

Salby, M. L. (1996), *Fundamentals of Atmospheric Physics*, Academic Press, San Diego, Calif.

Sandford, D. J., C. L. Beldon, R. E. Hibbins, and N. J. Mitchell (2010), Dynamics of the Antarctic and Arctic mesosphere and lower thermosphere—Part 1: Mean winds, *Atmos. Chem. Phys.*, *10*(21), 10,273–10,289, doi:10.5194/acp-10-10273-2010.

She, C. Y., S. Chen, Z. Hu, J. Sherman, J. D. Vance, V. Vasoli, M. A. White, J. Yu, and D. A. Krueger (2000), Eight-year climatology of nocturnal temperature and sodium density in the mesopause region (80 to 105 km) over Fort Collins, CO (41N, 105W), *Geophys. Res. Lett.*, *27*(20), 3289–3292, doi:10.1029/2000GL003825.

Shepherd, M. G., P. J. Espy, C. Y. She, W. Hocking, P. Keckhut, G. Gavrilyeva, G. G. Shepherd, and B. Naujokat (2002), Springtime transition in upper mesospheric temperature in the Northern Hemisphere, *J. Atmos. Sol. Terr. Phys.*, *64*(8-11), 1183–1199, doi:10.1016/S1364-6826(02)00068-8.

Swinbank, R., et al. (2013), Stratospheric assimilated data, NCAS British Atmospheric Data Centre, 2006. [Available from http://badc.nerc.ac.uk/view/badc.nerc.ac.uk__ATOM__dataent_ASSIM.]

Taylor, M. J., W. R. Pendleton Jr., H. L. Liu, C. Y. She, L. C. Garnet, R. G. Roble, and V. Vasoli (2001), Large amplitude perturbations in the mesospheric OH Meinel and 87-km Na lidar temperatures around the autumnal equinox, *Geophys. Res. Lett.*, *28*, 1899–1902, doi:10.1029/2000GL012682.

Stray, N. H., P. J. Espy, V. Limpasuvan, and R. E. Hibbins, Characterisation of quasi-stationary planetary waves in the Northern MLT during summer, *J. Atmos. Solar-Terr. Phys.*, doi: 10.1016/j.jastp.2014.12.003, 2014b

Paper 3

Journal of Atmospheric and Solar-Terrestrial Physics ∎ (∎∎∎∎) ∎∎∎–∎∎∎

Contents lists available at ScienceDirect

Journal of Atmospheric and Solar-Terrestrial Physics

journal homepage: www.elsevier.com/locate/jastp

Characterisation of quasi-stationary planetary waves in the Northern MLT during summer

Nora H. Stray [a,*], Patrick J. Espy [a,b], Varavut Limpasuvan [c], Robert E. Hibbins [a,b]

[a] Department of Physics, NTNU, Trondheim, Norway
[b] Birkeland Centre for Space Science, Bergen, Norway
[c] School of Coastal and Marine Systems Science, Coastal Carolina University, SC, USA

ARTICLE INFO

Article history:
Received 1 July 2014
Received in revised form
11 November 2014
Accepted 5 December 2014

Keywords:
Planetary waves
MLT
SuperDARN
Meteor winds

ABSTRACT

Observations of planetary wave (PW) activity in the northern hemisphere, polar summer mesosphere and lower thermosphere (MLT) are presented. Meteor winds from a northern hemisphere chain of SuperDARN radars have been used to monitor the meridional wind along a latitude band (51–66°N) in the MLT. A stationary PW-like longitudinal structure with a strong zonal PW number 1 characteristic is persistently observed year-to-year during summer. Here we characterize the amplitude and the phase structure of this wave in the MLT. The Modern-Era Retrospective Analysis for Research and Application (MERRA) of the NASA Global Modelling and Assimilation Office has been used to evaluate possible sources of the observed longitudinal perturbation in the mesospheric meridional wind by investigating the amplitudes and phases of PWs in the underlying atmosphere. The investigation shows that neither gravity wave modulation by lower atmospheric PWs nor direct propagation of PWs from the lower atmosphere are a significant cause of the observed longitudinal perturbation. However, the data are not of sufficient scope to investigate longitudinal differences in gravity wave sources, or to separate the effects of instabilities and inter-hemispheric propagation as possible causes for the large PW present in the summer MLT.

1. Introduction

Planetary waves are global scale waves where the latitudinal gradient of the Coriolis force serves as the restoring force. They can be generated in the lower atmosphere and, due to their westward intrinsic phase speeds (Forbes, 1995), they transport energy and westward momentum as they propagate upward, growing in amplitude.

Charney and Drazin (1961) showed using a simplified analytical solvable system of the atmosphere that planetary waves can only propagate into regions where the zonal mean wind is more eastward than the zonal phase velocity of the wave. The strong westward stratospheric winds that form during summer at mid- to high-latitudes should inhibit the upward propagation of planetary waves from below. More detailed analyses showed that the relationship is more complex and that vertical planetary wave propagation can be related to the effective refractive index (e.g. Smith, 1983; McDonald et al., 2011). In the quasi-geostrophic approximation, this refractive index depends primarily on the zonal wind and its latitudinal and vertical gradients (Smith, 1983). Nevertheless, vertical planetary wave propagation through the stratosphere from below is still unlikely during summer, and several studies have shown that there is little planetary wave activity present in the middle atmosphere during summer (e.g. Alexander and Shepherd, 2010; McDonald et al., 2011).

In spite of this, signatures of planetary waves in the summer mesosphere and lower thermosphere (MLT) have been modelled and observed (e.g. Forbes et al., 1995; Espy et al., 1997; Wang et al., 2000; Smith, 2003). Since vertical propagation through the stratosphere is unlikely during summer, the existence of planetary waves in the summertime MLT is puzzling. It has been suggested that the planetary wave signatures in the MLT might arise from the breaking of gravity waves whose momentum flux has been modulated by the selective filtering of the planetary waves present in the lower atmosphere (Smith, 2003). That is, gravity waves with eastward momentum would reach their critical levels in the eastward phase of the planetary waves (as manifested in the zonal wind field), allowing gravity waves carrying westward momentum to reach the MLT, and vice versa. The gravity waves that reach and break in the MLT would deposit their momentum and force the mean wind, imprinting in the MLT a mirror image of the planetary wave in the lower atmosphere.

* Corresponding author.
E-mail address: Nora.Kleinknecht@ntnu.no (N.H. Stray).

http://dx.doi.org/10.1016/j.jastp.2014.12.003
1364-6826/

Free travelling planetary waves are also possible in the summer mesosphere. These waves are considered to be global normal (resonant) modes that are not maintained by particular travelling forcing effects (Andrews, 1987). As shown by Salby (1981), the amplitudes of these wave disturbances can become large locally when the background wind speed approaches their phase speeds. The most prominent travelling wave in the summer mesosphere is the so-called 2-day wave (e.g. Limpasuvan and Wu, 2003). These features take on zonal wave numbers 2–4 and tend to amplify shortly after the solstice. As discussed below, fluctuations associated with the 2-day wave are removed in our analyses so their impacts are not relevant to our results.

Additionally, in situ generation of planetary waves by the baroclinic and barotropic instabilities created by the steep wind and temperature gradients in the middle atmosphere near solstice (e.g. Plumb, 1983; Baumgaertner et al., 2008) have also been proposed as a possible source of planetary waves in the MLT. Finally, it has been suggested that the source of the planetary waves in the summertime MLT might be the winter hemisphere, where the waves duct along the near-zero wind line that stretches from the winter stratosphere into the summer mesosphere (e.g. Forbes, 1995; Espy et al., 1997; Hibbins et al., 2009). While all these mechanisms are plausible and fit the existing measurements, there has been a lack of simultaneous observations of planetary wave amplitudes and phases, as well as the underlying wind field during summer that could be used to separate the relative importance of these proposed mechanisms.

Here observations of summertime wave number 1 (S_1) and 2 (S_2) planetary wave activity in the MLT (~95 km) are derived from meteor winds recorded with a chain of SuperDARN radars using the technique described by Kleinknecht et al. (2014). The possible sources of these planetary wave-like longitudinal perturbations of the MLT meridional wind that show a stable phase behaviour from year to year are evaluated using the underlying winds from the Modern-Era Retrospective Analysis for Research and Application (MERRA) of the NASA Global Modelling and Assimilation Office (Rienecker et al., 2011). By combining these data sets we discuss which of the proposed mechanisms for the appearance of planetary waves in the summertime MLT are likely.

2. Data

In order to examine the wind and planetary wave field in the mesosphere and the lower thermosphere (MLT), meridional winds have been retrieved from the meteor winds at each of 8 SuperDARN radars (Greenwald et al., 1985, 1995) at high northern latitudes (51–66°N). Since the orientation of most of the SuperDARN radars is toward the north, the meridional component derived from the line of sight winds of all beams is used due to its smaller uncertainty. Planetary wave amplitudes with wave numbers 1 and 2 in the mesopause region (~95 km) have been retrieved from these meridional meteor winds by taking advantage of the longitudinal chain (150°W–25°E) formed by these 8 SuperDARN radars. The technique is fully described and the validation studies are presented in Kleinknecht et al. (2014). Briefly, after an initial quality check, a daily mean wind, the 24-h, 12-h and 8-h sinusoidal tidal periods and a 2-day wave period were fitted to a 4-day sliding window of the hourly meridional wind for each of the 8 SuperDARN stations. The window was shifted in 1 day intervals to retrieve the time series of daily mean meridional winds at each station. These daily mean meridional winds at each station are then fitted as a sinusoidal function of longitude with 360° (S_1) and 180° (S_2) spatial periods to retrieve the amplitude and the phase of the wave number 1 and 2 components for each day.

To quantify the lower atmosphere, the zonal and meridional winds from MERRA (Rienecker et al., 2011) have been used to monitor the wind structure in the troposphere and the stratosphere. The horizontal resolution of the MERRA data used in this study is 0.5° × 3.3° (latitude × longitude). The vertical grid consists of 72 pressure levels from the ground to 0.015 hPa (~80 km). MERRA is measurement driven up to approximately 50 km (~1 hPa), above which it is free running. For this analysis only the measurement driven region of MERRA has been used. Since MERRA outputs are produced four times a day (0, 6, 12, and 18 UT), the daily means of the meridional wind averaged over the latitude band between 51°N and 66°N were produced to minimise tidal effects and to obtain wind profiles at latitudes similar to the latitude coverage of the SuperDARN chain.

Fig. 1 shows an altitude–longitude profile of the meridional (left panel) and the zonal (right panel) wind produced by MERRA for the 18 July 2000 between the ground and 1 hPa averaged over the latitude band of 51–66°N.

Red and blue colours signify poleward (eastward) and equatorward (westward) meridional (zonal) winds, respectively. While the zonal-mean zonal wind is predominantly eastward in the troposphere and turns westward in the stratosphere due to surface and ozone heating, the zonal-mean meridional wind is close to zero throughout the troposphere and the stratosphere due to geostrophic balance. Fig. 1 also shows that there are strong

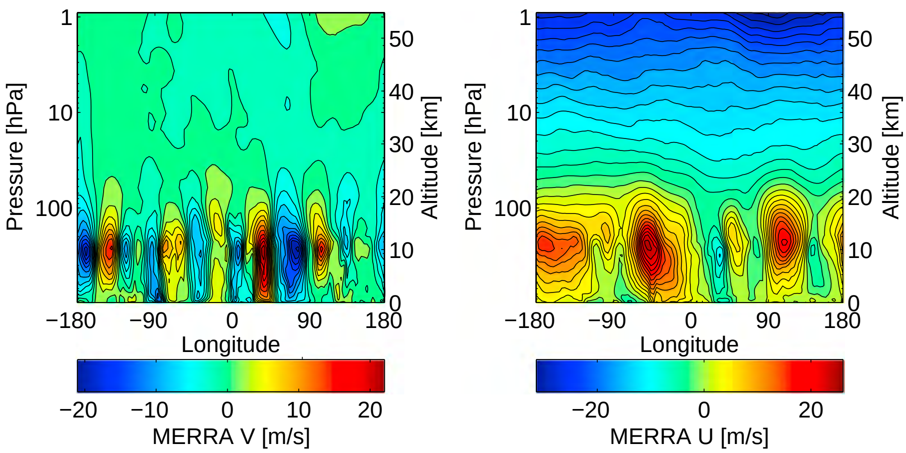

Fig. 1. MERRA meridional (left) and zonal (right) wind (m/s) for the 18 July 2000 between the ground and 1 hPa (~50 km) averaged over the latitude band between 51°N and 66°N. Red and blue colours signify poleward (eastward) and equatorward (westward) winds, respectively.

longitudinal perturbations in both the tropospheric zonal and the meridional wind. These perturbations are indicative of planetary waves and reach a maximum amplitude around the tropopause (~230 hPa, ~10 km) before rapidly falling in amplitude in the stratosphere. To quantify the planetary wave amplitudes in the lower atmosphere a longitudinal fit of the first four zonal wave numbers (S_0, S_1, S_2, and S_3) of the meridional and the zonal wind was calculated for each day and pressure level by fitting a mean (S_0), and sine functions with 360° (S_1), 180° (S_2) and 120° (S_3) spatial periods as follows:

$$S_0 + \sum_{i=1}^{3} S_i^{Amplitude} \cdot \sin\left(2\pi \cdot \left[\frac{i \cdot longitude}{360} + S_i^{Phase}\right]\right) \tag{1}$$

3. Results

Fig. 2(a) shows the climatology of the daily mean meridional wind at each of the 8 SuperDARN radar stations. The meridional wind is generally directed into the pole in winter (positive values) and out of the pole in summer. This is due to the residual mesospheric meridional circulation caused by the breaking of gravity waves that have been selectively filtered in the stratosphere (e.g Lindzen, 1981; Garcia and Solomon, 1985).

The climatology of the different stations also shows that the magnitude of the wintertime poleward meridional wind is generally smaller than the summertime equatorward winds. Model studies and observations (e.g. Lindzen, 1981) have shown that the gravity wave breaking altitude, and hence the strongest meridional forcing, varies between about 50 km in winter and 70 km in summer due to the different vertical temperature profiles in the middle atmosphere during winter and summer. Hence the meridional wind in the MLT observed in the SuperDARN measurements (~95 km) is generally stronger in summer than in winter.

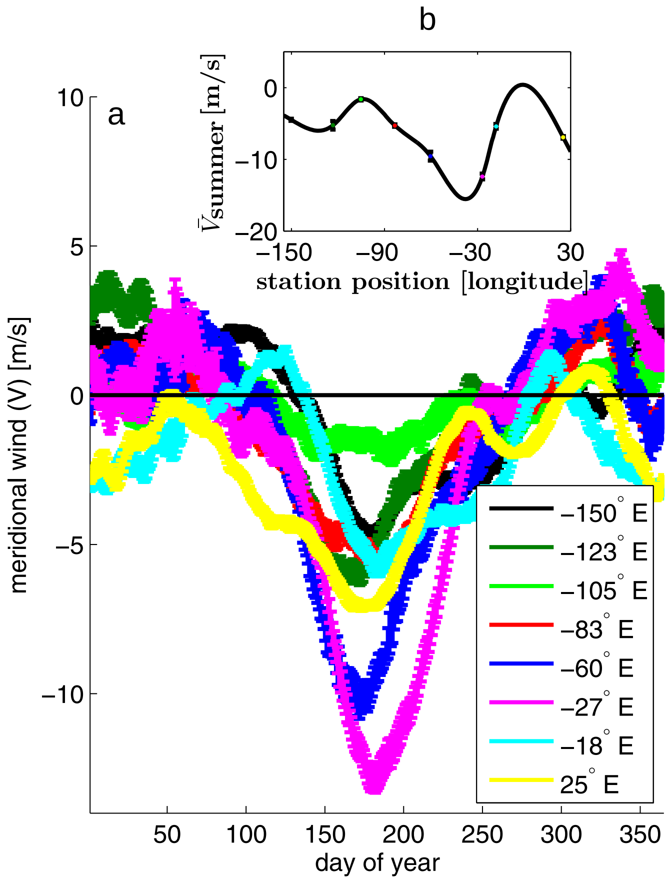

Fig. 2. (a) Climatology of daily mean meridional meteor winds for each of the 8 SuperDARN radar stations. The legend depicts the centroid longitude of the meteor wind measurements for each station. (b) A 20-day average about summer solstice of the daily mean climatological winds shown in (a) for each of the 8 stations, plotted as a function of the station longitude.

Even though the SuperDARN radars are closely spaced in latitude, Fig. 2(a) shows that the summer wind varies markedly as a function of the different longitudinal locations of the radars. Stations that are located close to each other in longitude however show similar wind magnitudes during summer as demonstrated in Fig. 2(b). The equatorward meridional wind during summer is observed to be strongest at longitudes around Greenland (30–60°W) with values of up to −13 m/s. In contrast, at other longitudes the climatological meridional wind falls to less than half this amount. Evidence for a longitudinal variation in the summertime MLT meridional wind that is stable from year to year has also been observed by e.g. Dowdy et al. (2007).

This longitudinal variation of the meridional wind, visible in Fig. 2(b), can also be seen on a daily basis and can be represented by the planetary wave number 1 and 2 components that have been retrieved for all days in summertime (May–August) for the years 2000–2008 as described in the previous section. The daily wave components fitted are presented as a function of time and longitude in the Hovmöller diagrams in Fig. 3. The longitudinal difference observed in the climatology of the different stations is clearly visible here as a quasi-stationary wave in both wave components with a longitudinal phase during mid-summer that is consistent year to year for all 9 years. The mean (summer solstice ±20 days) longitudinal position of the minimum (most southward) meridional wind in the observed S_1 wave component varies only between −64°E (year 2001) and −46°E (year 2007) and the mean amplitude of the S_1 wave component varies between 5 m/s (year 2007) and 13 m/s (year 2000).

The existence of such phase-stable wave components during summer adds a perturbation to the general equatorward meridional circulation. This results in a stronger meridional wind blowing out of the pole above the Atlantic sector while the equatorward winds are weaker over Russia. This longitudinal variation in meridional wind would then result in stronger outflow and more adiabatic lifting over the Atlantic sector, resulting in colder mesopause summer temperatures there compared to warmer temperatures above Russia. The longitudinal temperature perturbations associated with the meridional wind anomalies observed here have been reported by Chandran et al. (2010) using SABER temperatures as well as a temperature proxy, the occurrence frequency of Polar Mesospheric Clouds (PMC).

4. Discussion

As noted earlier, possible sources of the mesospheric planetary wave-like perturbation of the meridional wind observed here are (1) vertical propagation of the planetary waves from below, in situ generation through either (2) modulation of gravity wave filtering by planetary waves in the lower atmosphere, (3) longitudinal difference in gravity wave sources or (4) baroclinic and barotropic instabilities, and finally (5) inter-hemispheric coupling of planetary waves from the winter stratosphere. These different mechanisms will be evaluated for consistency with the observed wind and wave fields observed in both the MLT and the lower atmosphere.

4.1. Vertical propagation

Vertical propagation of planetary waves from the troposphere through the summertime stratosphere is unlikely due to the

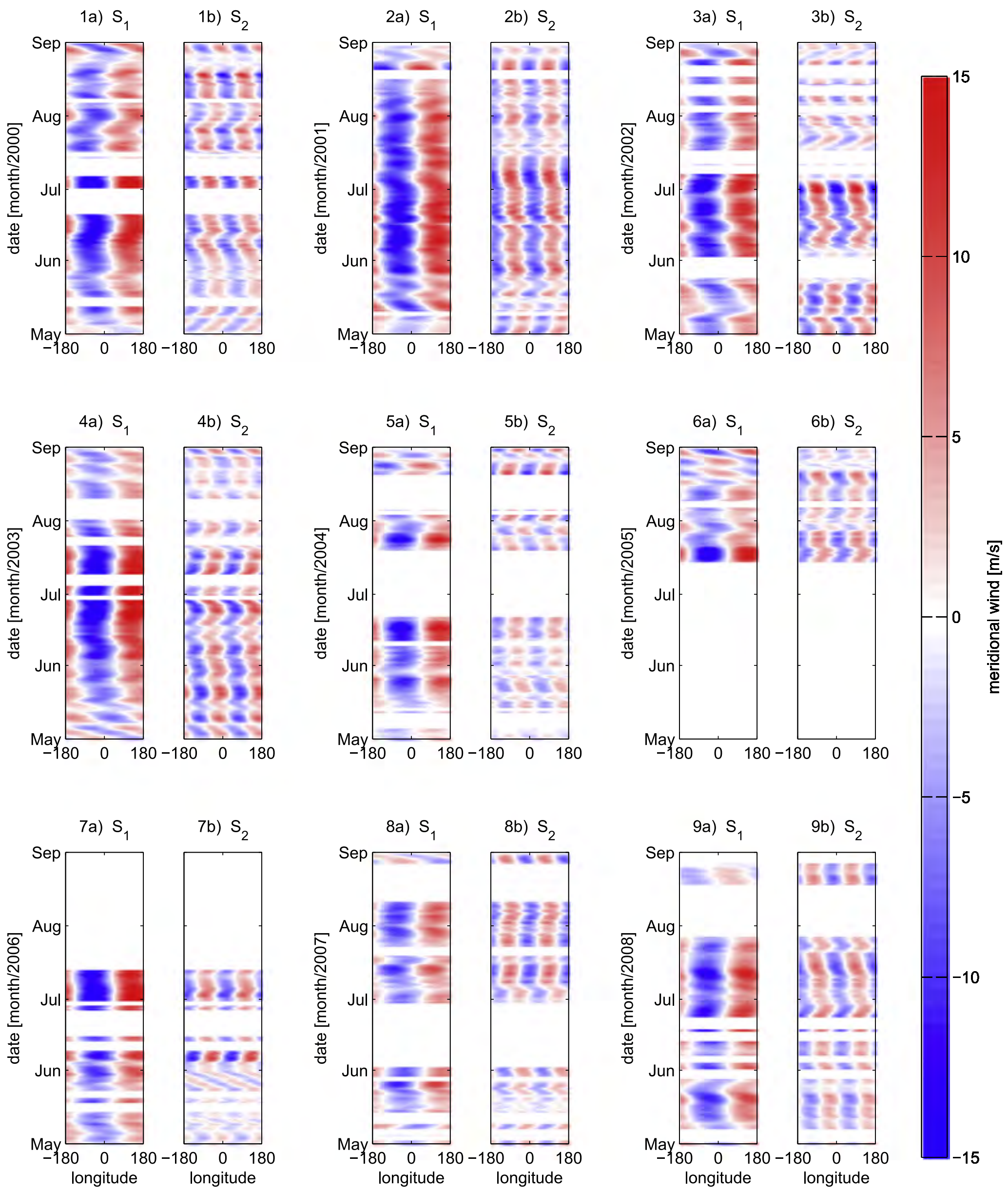

Fig. 3. Longitudinal wave components S_1 (a) and S_2 (b) of the mean meridional wind for summertime (May–August), years 2000–2008 (1–9). Red and blue colours signify poleward and equatorward wind, respectively. Adapted from Kleinknecht et al. (2014).

strong westward jet that theoretically inhibits vertical planetary wave propagation (Charney and Drazin, 1961). MERRA meridional winds have been used to monitor planetary-wave activity in the lower and the middle atmosphere to investigate if direct planetary wave propagation into the MLT from lower altitudes is possible. Fig. 4 shows the climatology of wave number 1 and 2 amplitudes. The upper panel shows the amplitudes in the MLT that have been extracted from the SuperDARN chain, while the lower panel shows planetary wave amplitudes in the troposphere and the stratosphere (up to 1 hPa, ~50 km) extracted from the data driven region of MERRA. The left panels show the climatology of the S_1 planetary wave component and the right panels the climatology of the S_2 planetary wave component.

In the troposphere and the stratosphere planetary wave amplitudes maximise in summer near the tropopause around 200–300 hPa (10–12 km) together with the zonal-mean zonal wind (Fig. 1). Above, the vertical gradient of the zonal wind becomes negative as the mean wind adjusts to the westward stratospheric wind regime, inhibiting vertical planetary wave propagation. This leads to a summertime minimum of planetary wave activity in the stratosphere. In contrast, observations in the MLT (~95 km) by the SuperDARN network show an increase of planetary wave amplitudes in summer. This indicates that direct propagation through the stratosphere is an ineffective source of the year-to-year persistent planetary waves observed in the MLT.

4.2. Modulation of gravity wave filtering by planetary waves in the lower atmosphere

Zonal winds from MERRA have been used to investigate if the filtering of gravity waves can be modulated by stationary planetary waves in the lower atmosphere during summer and result in a mapping of these planetary waves into the MLT when the gravity waves break and deposit their momentum at mesospheric altitudes. Such a mechanism has been shown to be a possible source of stationary planetary waves in the wintertime mesosphere

Please cite this article as: Stray, N.H., et al., Characterisation of quasi-stationary planetary waves in the Northern MLT during summer. Journal of Atmospheric and Solar-Terrestrial Physics (2014), http://dx.doi.org/10.1016/j.jastp.2014.12.003

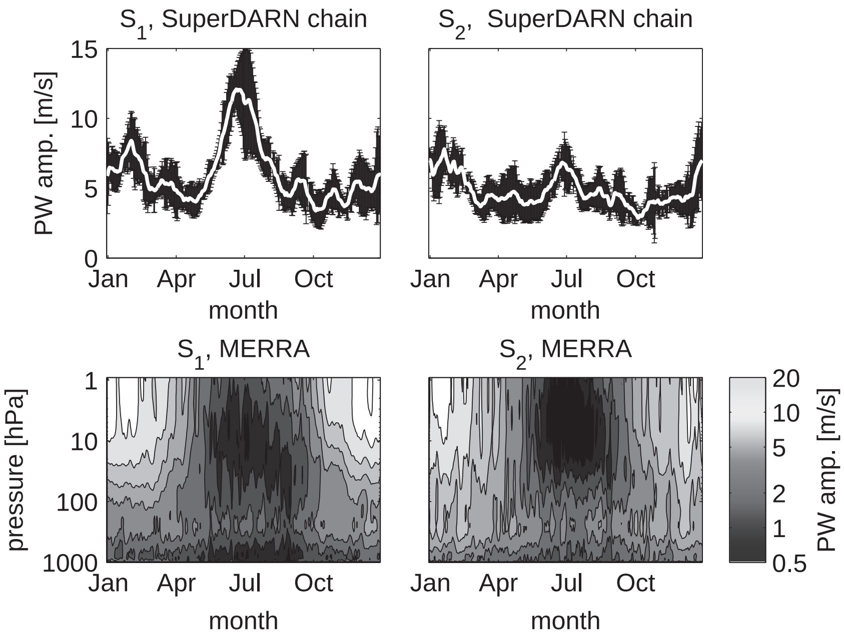

Fig. 4. Climatology of planetary wave amplitudes of the wave number 1 (left panels) and wave number 2 (right panels) components from the SuperDARN observations (upper panels) and MERRA (lower panels).

(Smith, 2003). During summer the planetary wave amplitudes are weakest in the stratosphere due to the westward winds there (Charney and Drazin, 1961). Thus, the strongest PW amplitudes that would modulate the filtering of gravity waves occur near the tropopause (~230 hPa ~10–12 km) where the winds are eastward. At this altitude the zonal-mean eastward wind as well as the planetary wave magnitudes maximizes in summer, as can be seen in Figs. 1 and 4, respectively, and any modulation of the gravity wave filtering by planetary waves would be expected to be strongest there. Fig. 5 (upper panel) shows the climatologically stable S_1 planetary wave component around the tropopause (~230 hPa, 10–12 km) retrieved from MERRA (a) and at the MLT (~95 km) retrieved from the SuperDARN network (b). At the tropopause the observed wave component shows a maximum amplitude of 6 m/s with the eastward phase of the wave above the Atlantic sector (~0–60°W). The mean summertime background wind at this altitude is eastward with a magnitude around 10 m/s.

Above the tropopause, the zonal wind turns westward in summer throughout the middle atmosphere, and wind speeds exceeding −30 m/s (Fig. 1) effectively filter the bulk of westward propagating gravity waves (Lindzen, 1981). It has been shown that the deposition of eastward momentum from the remaining eastward gravity waves in the mesosphere increases drag on the zonal wind and increases the resulting residual circulation equatorwards, with the strength of the effect dependent on the amount of eastward momentum deposition (e.g. Lindzen, 1981; Fritts and Alexander, 2003). The wind fluctuations associated with planetary waves near the tropopause could modulate the upward gravity-wave momentum flux, thereby modulating the momentum transferred to the mesosphere by gravity waves.

Stronger eastward winds near the tropopause (red regions in Fig. 5a) will filter more eastward gravity waves and hence lead to less eastward momentum deposition in the MLT. This, in turn, will decrease the associated residual MLT equatorward wind, producing a poleward (red) perturbation of the meridional wind. Conversely, decreased eastward winds at the troposphere (blue regions in Fig. 5a) will result in less filtering and hence stronger momentum deposition in the MLT. This will result in a stronger equatorward residual circulation in the MLT, resulting in an equatorward (blue) perturbation of the meridional wind.

If the modulation of the filtering described above were to have a significant effect on the longitudinal modulation of meridional wind in the MLT one would expect to see poleward (red) wind perturbations above stronger eastward (red) wind at the tropopause. Similarly there should be an equatorward (blue) wind perturbations above less strong eastward (blue) winds at the tropopause. However exactly the opposite is the case as can be seen from Fig. 5(b). Modulation of the gravity wave filtering by zonal wave number 1 stationary planetary waves near the tropopause seems therefore not to be the primary mechanism behind the stationary summertime planetary wave-like longitudinal perturbation of the meridional wind observed in the MLT. In addition, the phase of the S_1 component at the tropopause can vary widely throughout summer and shows strong inter-annual variations. However, the S_1 wave in the MLT shows a stable phase throughout the summer, and is consistent year to year. As an example, the zonal wind at the tropopause (MERRA) and the meridional wind in the MLT (SuperDARN) during summer 2001 are shown in Fig. 5 (c) and (d), respectively.

4.3. Longitudinal difference in gravity wave sources

In the previous section it has been shown that the westward portion of the gravity wave spectrum will be nearly completely filtered by the strong westward winds in the stratosphere. Thus, the eastward gravity wave spectrum in the troposphere should dictate the momentum delivered to the MLT (Fritts and Alexander, 2003). As this spectrum of tropospheric gravity waves will grow and break in the mesosphere and force the mesospheric wind, any longitudinal variation in the tropospheric eastward gravity wave source spectrum could map into the mesosphere to provide the longitudinal modulation of the meridional wind observed in the MLT. For the longitudinal variations of the eastward gravity wave spectra to be a possible source of the meridional wind modulation observed by the SuperDARN chain in the MLT (~95 km) a strong source of free eastward propagating gravity waves above the Atlantic sector (30–60°W) has to exist. Studies by e.g. Limpasuvan et al. (2007) show that there is strong gravity wave generation

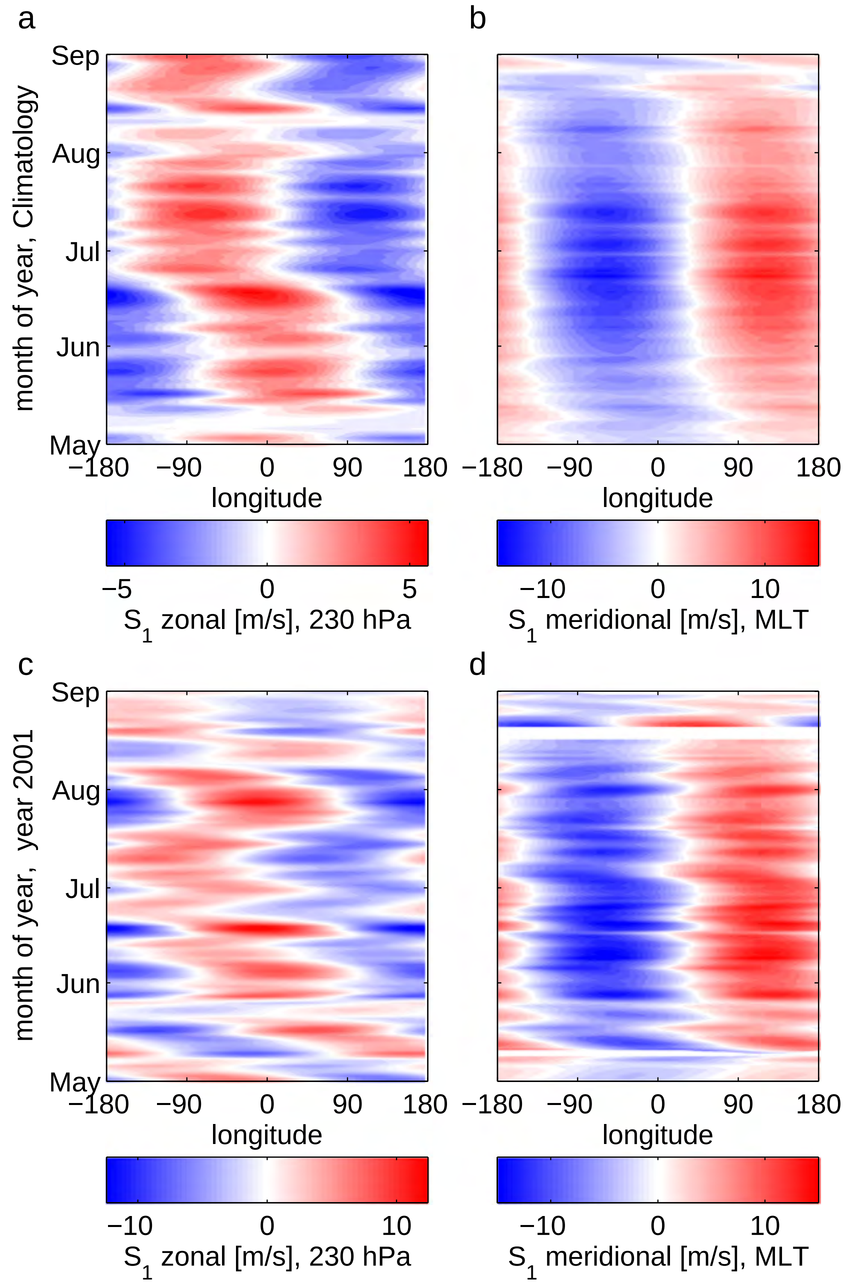

Fig. 5. Upper panel: climatology (year 2000–2008) of the longitudinal S_1 planetary wave component during summertime (May–August) retrieved from (a) the zonal wind from MERRA at the tropopause (230 hPa, ~10–12 km) averaged over 51–66°N and (b) the meridional wind from the SuperDARN network at MLT altitudes (~95 km). Lower panel: longitudinal S_1 planetary wave component during summer 2001 at (c) the tropopause (zonal wind, MERRA) and (d) at the MLT (meridional wind, SuperDARN). Red and blue colours signify eastward (poleward) and westward (equatorward) wind, respectively.

above Greenland. However a detailed analysis of the gravity wave source spectrum and its longitudinal distribution at these latitudes would be necessary to test this mechanism and is beyond the scope of this study.

4.4. Generation through baroclinic and barotropic instabilities

No observational or theoretical evidence of baroclinic and barotropic jet instabilities forcing climatologically stationary and phase-stable waves has been reported. However baroclinic and barotropic instabilities have been shown to be the cause of fast travelling planetary waves in the mesosphere during summer (Plumb, 1983; Limpasuvan and Wu, 2003; Baumgaertner et al., 2008) and it is therefore mentioned as a possible source. The necessary condition for instability states that the meridional gradient of the zonal mean (quasi-geostrophic) potential vorticity becomes negative. This condition reflects the zonal-mean zonal wind changing rapidly in the meridional direction (leading to barotropic instability) and/or vertical direction (related to thermal meridional gradient and leading thus to baroclinic instability). Initial results using the Whole Atmospheric Community Climate model with Specified Dynamics (WACCM-SD, Tweedy et al., 2013) indicate that there are potential source regions for the generation of instabilities near 70–90°N above 80 km (not shown). However, a thorough instability analysis is needed to examine unstable wave growth rates (in the face of damping) and the corresponding background conditions. Such analysis will be the subject of future work.

Please cite this article as: Stray, N.H., et al., Characterisation of quasi-stationary planetary waves in the Northern MLT during summer. Journal of Atmospheric and Solar-Terrestrial Physics (2014), http://dx.doi.org/10.1016/j.jastp.2014.12.003

4.5. Inter-hemispheric coupling

Evidence for inter-hemispheric coupling of planetary waves has been shown in several studies (e.g. Forbes, 1995; Espy et al., 1997; Hibbins et al., 2009; Day and Mitchell, 2010). These studies focus mostly on travelling wave components. However one should keep in mind that the longitudinal wave components observed in this paper are the sum of all stationary and travelling planetary waves with the same longitudinal structure. While strong stationary wave components might exist in the winter mesosphere and migrate to the summer along the near-zero wind line, we currently lack the data needed to test this hypothesis. This would require a characterization of southern hemispheric stationary wave amplitudes and a theoretical model of horizontal wave transport that is beyond the scope of this paper. In addition several observational studies suggest large inter-annual variability in the inter-hemispheric propagation of PWs (e.g. Espy et al., 1997; Hibbins et al., 2009), which is inconsistent with the relatively stable stationary wave reported here. Thus, this must be considered as a viable, albeit untested mechanism which will be subject of future modelling work.

5. Summary and conclusion

Planetary wave observations in the mesosphere–lower thermosphere using meridional meteor winds from a chain of SuperDARN radars show strong quasi-stationary planetary wave activity of the zonal wave numbers 1 and 2 during mid-summer. The observed planetary wave activity shows a year-to-year consistent quasi-stationary phase. Supporting longitudinal wind and temperature variations in the mesosphere have been observed in other studies and show the impact of these structures on the longitudinal variability of PMC. Winds from the Modern-Era Retrospective Analysis for Research and Application (MERRA) of the NASA Global Modelling and Assimilation Office are used to investigate the source of the stationary planetary wave-like perturbations of the meridional wind observed in the MLT. The analysis downplays the role of planetary wave modulated filtering of gravity waves as well as vertical propagation through the stratosphere as a source. However, longitudinal differences in gravity wave sources, barotropic and baroclinic instabilities as well as inter-hemispheric coupling remain as possible explanations for the longitudinal structure in the meridional wind in the MLT and will be investigated further.

Acknowledgments

The authors acknowledge the use of SuperDARN data. SuperDARN is a collection of radars funded by the National Scientific Funding Agencies of Australia, Canada, China, France, Japan, South Africa, United Kingdom and United States of America. Support for Varavut Limpasuvan (V.L.) was provided by the National Science Foundation (NSF) under Grants AGS-1116123 and AGS-MRI-0958616 as well as by the Coastal Carolina University's Kerns Palmetto Professor Endowment. This study was partly supported by the Research Council of Norway/CoE under Contract 223252/F50.

References

Alexander, S.P., Shepherd, M.G., 2010. Planetary wave activity in the polar lower stratosphere. Atmos. Chem. Phys. 10 (2), 707–718. http://dx.doi.org/10.5194/acp-10-707-2010.

Andrews, D.G., 1987. Middle Atmosphere Dynamics. Academic Press, London, UK.

Baumgaertner, A.J.G., McDonald, A.J., Hibbins, R.E., Fritts, D.C., Murphy, D.J., Vincent, R.A., 2008. Short-period planetary waves in the Antarctic middle atmosphere. J. Atmos. Solar-Terr. Phys. 70 (10), 1336–1350. http://dx.doi.org/10.1016/j.jastp.2008.04.007.

Chandran, A., Rusch, D.W., Merkel, A.W., Thomas, G.E., Taylor, M.J., Bailey, S.M., Russell, J.M., 2010. Polar mesospheric cloud structures observed from the cloud imaging and particle size experiment on the Aeronomy of Ice in the Mesosphere spacecraft: atmospheric gravity waves as drivers for longitudinal variability in polar mesospheric cloud occurrence. J. Geophys. Res. 115 (D13), 102. http://dx.doi.org/10.1029/2009JD013185.

Charney, J.G., Drazin, P.G., 1961. Propagation of planetary-scale disturbance from lower into upper atmosphere. Geophys. Res. Lett. 66 (1), 83–109.

Day, K.A., Mitchell, N.J., 2010. The 5-day wave in the Arctic and Antarctic mesosphere and lower thermosphere. J. Geophys. Res. 115 (D01109), http://dx.doi.org/10.1029/2009JD012545.

Dowdy, A.J., Vincent, R.A., Tsutsumi, M., Igarashi, K., Murayama, Y., Singer, W., Murphy, D.J., 2007. Polar mesosphere and lower thermosphere dynamics: mean wind and gravity wave climatologies. J. Geophys. Res. 112 (D17), http://dx.doi.org/10.1029/2006JD008126.

Espy, P.J., Stegman, J., Witt, G., 1997. Interannual variations of the quasi-16-day oscillation in the polar summer mesospheric temperature. J. Geophys. Res. 102 (D2), 1983–1990. http://dx.doi.org/10.1029/96JD02717.

Forbes, J.M., 1995. Tidal and Planetary waves. In: Johnson, R.M., Killeen, T.L. (Eds.), The Upper Mesosphere and Lower Thermosphere: A Review of Experiment and Theory, Geophysical Monograph Series, vol. 87. AGU, Washington, DC.

Forbes, J.M., Hagan, M.E., Miyahara, S., Vial, F., Manson, A.H., Meek, C.E., Portnyagin, Y.I., 1995. Quasi 16-day oscillation in the mesosphere and lower thermosphere. J. Geophys. Res. 100, 9149–9163. http://dx.doi.org/10.1029/94JD02157.

Fritts, D.C., Alexander, M.J., 2003. Gravity wave dynamics and effects in the middle atmosphere. Rev. Geophys. 41 (1), http://dx.doi.org/10.1029/2001RG000106.

Garcia, R.R., Solomon, S., 1985. The effect of breaking gravity waves on the dynamics and chemical composition of the mesosphere and lower thermosphere. J. Geophys. Res. 90 (D2), 3850–3868. http://dx.doi.org/10.1029/JD090iD02p03850.

Greenwald, R.A., Baker, K.B., Hutchins, R.A., Hanuise, C., 1985. An HF phase-array radar for studying small-scale structure in the high-latitude ionosphere. Radio Sci. 20 (1), 63–79. http://dx.doi.org/10.1029/RS020i001p00063.

Greenwald, R.A., et al., 1995. DARN/SUPERDARN—a global view of the dynamics of high-latitude convection. Space Sci. Rev. 71 (1–4), 761–796. http://dx.doi.org/10.1007/BF00751350.

Hibbins, R.E., Jarvis, M.J., Ford, E.A.K., 2009. Quasi-biennial oscillation influence on long-period planetary waves in the Antarctic upper mesosphere. J. Geophys. Res. 114, http://dx.doi.org/10.1029/2008JD011174.

Kleinknecht, N.H., Espy, P.J., Hibbins, R.E., 2014. The climatology of zonal wave numbers 1 and 2 planetary wave structure in the MLT using a chain of Northern Hemisphere SuperDARN radars. J. Geophys. Res. 119 (3), 1292–1307. http://dx.doi.org/10.1002/2013JD019850.

Limpasuvan, V., Wu, D.L., 2003. Two-day wave observations of UARS-MLS mesospheric water vapor and temperature. J. Geophys. Res. 108 (D10), 4307. http://dx.doi.org/10.1029/2002JD002903.

Limpasuvan, V., Wu, D.L., Alexander, M.J., Xue, M., Hu, M., Pawson, S., Perkins, J.R., 2007. Stratospheric gravity wave simulation over greenland during 24 January 2005. J. Geophys. Res. 112 (D10), 115. http://dx.doi.org/10.1029/2006JD007823.

Lindzen, R.S., 1981. Turbulence and stress owing to gravity wave and tidal breakdown. J. Geophys. Res. 86, 9707–9714. http://dx.doi.org/10.1029/JC086iC10p09707.

McDonald, A.J., Hibbins, R.E., Jarvis, M.J., 2011. Properties of the quasi 16 day wave derived from EOS MLS observations. J. Geophys. Res. 116, http://dx.doi.org/10.1029/2010JD014719.

Plumb, R.A., 1983. Baroclinic instability of the summer mesosphere—a mechanism for the quasi-2-day wave. J. Atmos. Sci. 40 (1), 262–270, doi:10.1175/1520-0469(1983)040 < 0262:BIOTSM > 2.0.CO;2.

Rienecker, M.M., et al., 2011. MERRA: NASA's modern-era retrospective analysis for research and applications. J. Climate 24, 3624–3648. http://dx.doi.org/10.1175/JCLI-D-11-00015.1.

Salby, M.L., 1981. Rossby normal modes in nonuniform background configurations. II. Equinox and solstice conditions. J. Atmos. Sci. 38 (9), 1827–1840, doi:10.1175/1520-0469(1981)038 < 1827:RNMINB > 2.0.CO;2.

Smith, A.K., 1983. Stationary waves in the winter stratophere—seasonal and interannual varibility. J. Atmos. Sci. 40 (1), 245–261, doi:10.1175/1520-0469(1983)040 < 0245:SWITWS > 2.0.CO;2.

Smith, A.K., 2003. The origin of stationary planetary waves in the upper mesosphere. J. Atmos. Sci. 60, 3033–3041, doi:10.1175/1520-0469(2003)060 < 3033:TOOSPW > 2.0.CO;2.

Tweedy, O.V., et al., 2013. Nighttime secondary ozone layer during major stratospheric sudden warmings in specified-dynamics. J. Geophys. Res. 118, 1–13. http://dx.doi.org/10.1002/jgrd.50651.

Wang, D.Y., Ward, W.E., Shepherd, G.G., Wu, D.L., 2000. Stationary planetary waves inferred from WINDII wind data taken within altitudes 90–120 km during 1991–1996. J. Atmos. Sci. 57 (12), 1906–1918, doi:10.1175/1520-0469(2000)057 < 1906:SPWIFW > 2.0.CO;2.

Stray, N. H., Y. J. Orsolini, P. J. Espy, V. Limpasuvan, and R. E. Hibbins, Observations of PW activity in the MLT during SSW events using a chain of SuperDARN radars and SD-WACCM, *15*(1), 393–413, doi: 10.5194/acpd-15-393-2015, 2015

Paper 4

Atmos. Chem. Phys. Discuss., 15, 393–413, 2015
www.atmos-chem-phys-discuss.net/15/393/2015/
doi:10.5194/acpd-15-393-2015

Atmospheric Chemistry and Physics Discussions

Observations of PW activity in the MLT during SSW events using a chain of SuperDARN radars and SD-WACCM

N. H. Stray[1], Y. J. Orsolini[2,3], P. J. Espy[1,3], V. Limpasuvan[4], and R. E. Hibbins[1,3]

[1]Department of Physics, NTNU, Trondheim, Norway
[2]Norwegian Institute for Air Research, Kjeller, Norway
[3]Birkeland Centre for Space Science, Bergen, Norway
[4]School of Coastal and Marine Systems Science, Coastal Carolina University, South Carolina, USA

Received: 1 October 2014 – Accepted: 5 December 2014 – Published: 7 January 2015

Correspondence to: N. H. Stray (nora.kleinknecht@ntnu.no)

Published by Copernicus Publications on behalf of the European Geosciences Union.

Abstract

This study investigates the effect of Stratospheric Sudden Warmings (SSWs) on Planetary Wave (PW) activity in the Mesosphere-Lower Thermosphere (MLT). PW activity near 95 km is derived from meteor wind data using a chain of 8 SuperDARN radars at high northern latitudes that span longitudes from 150° W to 25° E and latitudes from 51 to 66° N. Zonal wave number 1 and 2 components were extracted from the meridional wind for the years 2000–2008. The observed wintertime PW activity shows common features associated with the stratospheric wind reversals and the accompanying stratospheric warming events. Onset dates for seven SSW events accompanied by an elevated stratopause (ES) were identified during this time period using the Specified Dynamics Whole Atmosphere Community Climate Model (SD-WACCM). For the seven events, a significant enhancement in wave number 1 and 2 PW amplitudes near 95 km was found to occur after the wind reversed at 50 km, with amplitudes maximizing approximately 5 days after the onset of the wind reversal. This PW enhancement in the MLT after the event was confirmed using SD-WACCM. When all cases of polar cap wind reversals at 50 km were considered, a significant, albeit moderate, correlation of 0.4 was found between PW amplitudes near 95 km and westward polar-cap stratospheric winds at 50 km, with the maximum correlation occurring ~ 3 days after the maximum westward wind. These results indicate that the enhancement of PW amplitudes near 95 km are a common feature of SSWs irrespective of the strength of the wind reversal.

1 Introduction

Stratospheric Sudden Warmings (SSWs) are dramatic breakdowns of the polar vortex occurring in the polar wintertime that can dynamically couple the atmosphere all the way from the troposphere into the ionosphere (e.g. Limpasuvan et al., 2004; Goncharenko et al., 2010; Pancheva and Mukhtarov, 2011; Yuan et al., 2012). They occur frequently in the northern polar hemisphere but vary in strength and time of occurrence. SSWs are caused by the interaction of Planetary Waves (PWs) with the mean flow (Matsuno, 1971) that leads to an abrupt reversal of the zonal-mean winds in the middle atmosphere as well as to a sudden warming (cooling) of the stratosphere (mesosphere) (e.g. Manney et al., 2008; Chandran et al., 2014, and references therein).

A total breakdown of the polar vortex during a SSW can lead to a nearly isothermal region around the stratopause, with the stratopause subsequently re-forming at higher altitudes (Manney et al., 2008). Such an event is known as an elevated stratopause (ES) event. Based on a case study with the WACCM model, (Limpasuvan et al., 2012) suggested that during a strong warming accompanied by an ES event, PWs appear in the Mesosphere-Lower Thermosphere (MLT). These are instrumental in initiating the descent of the elevated stratopause, before the westward gravity wave forcing is re-established. The sudden changes in atmospheric conditions related to an SSW alter the transmission of planetary and gravity waves and result in large vertical and horizontal temperature and velocity gradients that can lead to the generation of new waves (Chandran et al., 2013b). In a high-resolution model study, Tomikawa et al. (2012) demonstrated that the generation of the MLT planetary waves could arise from large-scale flow instabilities. In a climatological analysis using both the WACCM model and the MERRA analysis data, Chandran et al. (2013a) found that over half of the SSW events were accompanied by an ES, and $\sim 87\,\%$ of these combined events showed enhanced planetary wave activity in the upper mesosphere.

In addition to these model results, Chandran et al. (2013b) also observed an enhancement of PW amplitudes and a change of their longitudinal propagation speed in the MLT in connection with a strong SSW event in January 2012 using the Specified Dynamics Whole Atmosphere Community Climate Model (SD-WACCM) and temperatures from the Sounding of the Atmosphere using Broadband Emission Radiometry (SABER) instrument. This event was noteworthy in that it was strong, with the total zonal-mean zonal wind at 50 km (averaged from 50–77° N) reaching westward wind speeds of more than $40\,\mathrm{m\,s^{-1}}$ during the reversal. In addition it was accompanied by

an elevated stratopause event. Chandran et al. (2013b) inferred that the PWs in the MLT were generated in-situ by the instabilities associated with the large wind and temperature gradients that resulted from this strong SSW event.

Here we examine whether PW enhancements in the MLT are a general feature connected to SSWs or whether they are only associated with strong events. To do so, PW activity around 95 km was examined during several SSW events that were characterized by a range of wind reversal magnitudes (-2 to $-50\,\mathrm{m\,s^{-1}}$). The PW amplitudes were derived using the meridional meteor winds from a northern high latitude chain of SuperDARN meteor radars for the winter seasons between 2000 and 2008.

2 Data

PW activity near 95 km has been derived from meteor winds measured by a chain of SuperDARN radars at high northern latitudes (51–66° N). SD-WACCM has been used to model PW activity throughout the middle atmosphere and monitor atmospheric background conditions of wind and temperature.

2.1 Observational data (SuperDARN)

Hourly meridional meteor winds from eight SuperDARN radars (Greenwald et al., 1985, 1995) located between 51–66° N and 150° W–25° E have been used to extract the longitudinal structure of PWs with zonal wave number 1 and 2 (S_1 and S_2) in the MLT, at approximately 95 km (Hall et al., 1997; Hibbins and Jarvis, 2008) for all winters (November–March) between January 2000 and December 2008. This has been done following the technique described and validated in Kleinknecht et al. (2014). Briefly, after an initial quality check, daily mean winds are produced by fitting and removing tidal (8, 12, 24 h) and 2 day wave components to 4 day segments of the hourly winds which are stepped in 1 day intervals. These resulting daily winds are then fitted as a function of longitude to provide the amplitude and phase of the S_1 and S_2 PWs. The wave num-

Discussion Paper | Discussion Paper | Discussion Paper | Discussion Paper |

ber one (S_1) and two (S_2) components resulting from the fit to the chain of SuperDARN radars are shown in Fig. 1 for all winter seasons (November–March) between 2000 and 2008. The independent fits from the individual days are presented in the form of a Hovmöller diagram, where the phase vs. longitude of the S_1 and S_2 components can be seen to evolve in time. Red and blue colors signify poleward and equatorward wind, respectively. Each wave component represents the superposition of all stationary as well as eastward and westward travelling waves with that zonal wavenumber. The temporal changes in the amplitude and longitudinal phase of each wave component, shown in the Hovmöller diagram, indicate the interaction of the different temporal components of the PW as they propagate in the zonal background wind.

2.2 Model data (SD-WACCM)

WACCM is a global circulation model of the National Center of Atmospheric Research (NCAR) extending from the surface to 150 km (88 pressure levels) with fully coupled chemistry and dynamics. Its horizontal resolution is 1.9° × 2.5° (latitude × longitude). The WACCM version used in this study is a specified dynamics version of WACCM4 called SD-WACCM. The dynamics and temperature of the specified dynamics version are nudged to MERRA, the Modern-Era Retrospective Analysis for Research and Application of the NASA Global Modeling and Assimilation Office (Rienecker and et al., 2011) up to 0.79 hPa (~ 50 km). Meteorological fields above this altitude are fully interactive with linear transition in between. Due to the nudging SD-WACCM is capable of representing atmospheric temperature and dynamics for individual dates and has been shown to respresent ES events well (Eyring et al., 2010; Chandran et al., 2013a; Tweedy et al., 2013).

3 Data analysis

SSWs occur frequently in the Northern Hemisphere during winters (November–March). However their time of occurrence and their strength vary due to differences in the stratospheric wave forcing. To investigate the effect of SSWs on PW activity in the MLT, a threshold to define an SSW event has to be set. Here, the onset day of an event was defined as the point when the zonal-mean zonal polar cap (70–90° N) wind at 0.7 hPa (~ 50 km) reversed from eastward to westward and persisted reversed for at least 4 days. These criteria are similar to the criteria chosen by Tweedy et al. (2013) who showed that this onset date corresponds to the day when the polar wind reverses direction over an extended range of altitudes in the mesosphere. Zonal wind data from MERRA were used to identify SSW events in the zonal-mean polar cap zonal winds. In addition SSWs were divided into SSWs with and without elevated stratopause (ES) events. An ES event was defined as having a temperature below 185 K at 80 km immediately after the wind reversal, and a stratopause elevation of at least 10 km after the onset of the wind reversal. Here SD-WACCM was used to define the events due to the limited top altitude of MERRA. Using these criteria, in total 23 SSW event have been found during the years 2000–2008, among which 7 of these events were followed by an ES event (11 December 2000, 29 January 2001, 22 December 2001, 29 December 2002, 19 December 2003, 9 January 2006, 23 January 2008). It should be noticed that all the 7 SSW ES events occurred during undisturbed winter conditions; that is, there were no polar cap wind reversals (lasting at least 4 days) that occurred in the 40 days preceding the selected events. Composites of these 7 SSW ES events were made for the modelled temperature, wind and PW activity using SD-WACCM and for the PW activity observed by the SuperDARN chain.

4 Modelled wind and temperature during a composite SSW ES event

The composite of the SD-WACCM background conditions (temperature and wind) using these 7 SSW ES events is shown in Fig. 2 and demonstrates the general behaviour of the atmospheric zonal-mean temperature and winds during an SSW ES event. The upper panel depicts the zonal-mean zonal wind. Red and blue colors signify eastward and westward winds, respectively. The lower panel shows the zonal-mean temperature with red and blue colors signifying temperatures above and below 220 K, respectively.

The first days of the composite fields reflect undisturbed winter conditions. Briefly, the zonal-mean zonal wind is eastward in the stratosphere, which leads to filtering of the eastward-propagating gravity waves and hence westward gravity wave momentum deposition and westward zonal-mean winds in the mesosphere. The vertical temperature gradient is positive (increasing with altitude) in the stratosphere and negative in the mesosphere, with the stratopause clearly visible as a temperature maximum around 60 km.

A SSW is created by the interaction of PWs with the mean flow that leads to a deceleration of the polar vortex and hence a reversal of the zonal-mean zonal wind (Matsuno, 1971). In Fig. 2a this reversal of the zonal wind can be seen as a strong, westward wind regime in the stratosphere starting at day zero of the composite and lasting for several days. This distortion of the polar vortex leads to sinking motion and hence to adiabatic heating in the stratosphere, and a descent of the stratopause as can be seen in Fig. 2b. In addition the distortion of the polar vortex leads to a change in gravity wave filtering. During the wind reversal eastward gravity waves can reach the mesosphere while westward gravity waves are blocked (de Wit et al., 2014). This leads to the deposition of eastward momentum and a reversal of the zonal mean wind in the mesosphere as can be seen in Fig. 2a. In addition, there is an accompanying reversal of the meridional circulation and hence a rising motion and cooling in the mesosphere (e.g. Limpasuvan et al., 2012; Chandran et al., 2014, and references within), as can be seen in Fig. 2b. When an SSW is accompanied by an ES event, the stratopause disap-

pears temporarily and than re-forms at higher altitudes (Fig. 2b). The disappearance of the stratopause is related to a complete breakdown of the polar vortex and a nearly isothermal region between the stratosphere and the mesosphere. The stratopause can then reform at higher altitudes (~ 70–80 km) as a so-called elevated stratopause (e.g. Manney et al., 2008).

5 Results

5.1 MLT planetary wave activity during SSW ES events

The Hovmöller diagrams presented in Fig. 1 also show the onset of the stratospheric wind reversal for each of the 7 SSW events that were accompanied by an elevated stratopause, as marked by the horizontal black lines. The wind reversals triggering those events cover maximum magnitudes between −11 and $-30\,\mathrm{m\,s^{-1}}$ and last for 4 to 16 days. However the observations show consistent PW behaviour during SSW events. That is, each event is accompanied by an increase in PW amplitude. The PW activity after the onset of the wind reversal can be observed to propagate with quite stable phase speed for approximately 10 days. The 7 SSW ES events investigated here reveal phase speeds between −45 to 15° longitude per day. In addition many, but not all events show the phase speed after the onset of the wind reversal to be stronger westward than before.

We also observe a coherent PW response during a SSW ES event by forming a composite of PW activity for the 7 SSW ES events. The composite of the PW activity observed by the SuperDARN radar chain is presented in Fig. 3. It shows the PW amplitudes in the MLT (~ 95 km) for the S_1 (a), the S_2 (b) and the sum of both zonal wave components (c). In addition the stratospheric (~ 50 km) polar cap zonal-mean zonal wind is plotted in magenta, and the onset of the stratospheric wind reversal, day zero of the composite, is marked with a vertical green line. A significant increase in PW activity can be seen just after the stratospheric zonal-mean zonal wind reversal in both

Discussion Paper | Discussion Paper | Discussion Paper | Discussion Paper |

wave numbers. The enhancement occurs slightly earlier in the S_1 component but is stronger in the S_2 component.

For comparison with the SuperDARN observations, Fig. 4 shows the composite of the modelled PW activity, derived from the meridional wind of SD-WACCM, from the ground to 10^{-4} hPa (~ 110 km) for the same seven SSW ES events. The zonal wave number 1 component (S_1) is shown in the upper panel, the zonal wave number 2 component (S_2) in the middle panel and the sum of both wave components in the lower panel. The vertical green line marks the onset of the stratospheric wind reversal. The horizontal blue line marks the approximate mean altitude of the SuperDARN wind observations. As expected, strong PW activity can be seen in the stratosphere leading to the wind reversal and the SSW. In the model, the PW activity minimizes at around 80 km due to either strong gravity wave drag (e.g. Smith, 2003) and/or a strong negative wind shear (e.g. Smith, 1983; McDonald et al., 2011). However, similar to the observed PW activity, there is an enhancement in PW activity in the MLT (above 80 km) just after the onset of the stratospheric wind reversal. While stratospheric PW activity seems to be dominated by wave number 1, the amplitudes of the two zonal components (S_1 and S_2) are quite similar in the MLT, with the amplitudes of the S_2 component being slightly stronger. Similar to the PW observed in the MLT, the modelled amplitudes of the S_1 component peak slightly before the S_2 component, although the modelled peaks occur slightly earlier than in the observations.

In summary, the composite of the SSW events that are followed by an elevated stratopause in both the observed (Fig. 3) and the modelled (Fig. 4) cases show a clear increase in PW amplitude above 80 km after the onset of the SSW. In addition a shift of the propagation direction often occurs after the onset of the SSW (Fig. 1). This indicates that SSWs accompanied by an ES event in general have a strong influence on PW activity in the MLT, irrespective of the strength of the reversal.

5.2 MLT planetary wave activity during stratospheric wind reversals

The previous sections showed the typical behaviour of winds, temperatures and PWs during the seven SSWs accompanied by ES events irrespective of the strength of the reversal. In this section the correlation between all stratospheric wind reversals and MLT planetary wave activity is investigated. This includes all 23 SSW events and also 6 additional events where wind reversal is shorter than 4 days. Figure 5 shows the PW amplitudes ($S_1 + S_2$) observed by the SuperDARN radar chain (black) for all winters between 2000/2001–2007/2008 together with the westward component of the polar cap wind at 50 km retrieved from MERRA (magenta). The magnitudes of the reversals vary between −2 and −50 m s^{-1} and last between 1 and 19 days. The SSWs used for the composite study in the previous section are marked with vertical green lines.

A similar composite analysis to that presented in Sect. 5.1 using all stratospheric wind reversals could not be used to investigate the relationship between the wind reversal and PW amplitudes in the MLT because many of them occur shortly after an SSW ES event that has perturbed the background conditions. Therefore, to investigate the general correlation between stratospheric wind reversals of variable strength and the MLT PW amplitudes, polar cap westward winds at 50 km (MERRA) and the observed PW amplitudes (SuperDARN) have been correlated between November and March. Only days for which both the westward polar cap winds and PW measurements exist were correlated. The correlation is shown in Fig. 6. The highest correlation (correlation coefficient = 0.4) occurred with the westward polar cap wind maximum leading the PW activity maximum by 3 days. The correlation between the westward wind and PW bursts is only moderate but more than 99 % significant, and shows that MLT PW enhancements are not just associated with SSWs that are accompanied by ES events but are a general feature attendant with stratospheric polar cap wind reversals of any strength. To make sure that the observed correlation is not being triggered by the SSW ES events but by the bulk of wind reversals, the correlation has been repeated excluding the SSW ES events used in the previous composite study. The correlation coefficient (not shown) becomes slightly smaller (0.3) but still peaks at a 3 days lag (polar cap winds leading) and remains more than 99 % significant.

6 Discussion and conclusion

Limpasuvan et al. (2012) mentioned in a case study using WACCM that the ES event was accompanied by a PW in the MLT region and Chandran et al. (2013a) later established a climatology of SSW events using WACCM. Chandran et al. (2013a) reported that the majority of SSW events studied were accompanied by an increase in PW amplitudes in the MLT. In addition, Chandran et al. (2013b) observed such an increase in PW amplitudes, using SABER data, in a single, strong (polar cap zonal wind reversal at 50 km greater than $-40\,\mathrm{m\,s^{-1}}$ (max westward wind)) SSW ES event in January 2012. Our observations (Fig. 1) indicate the enhancement in PW amplitude approximately 5 days after the wind reversal (Fig. 3) to be a consistent feature of all 7 SSW ES events, irrespective of the magnitude (-11 to $-30\,\mathrm{m\,s^{-1}}$) and duration (4 to 16 days) of the wind reversal. The consistent increase in planetary wave amplitudes near 95 km observed in the SuperDARN wind data that occurs after the onset of the SSW ES events (shown by the horizontal black lines) can be observed in the Hovmöller diagrams of Fig. 1 as well as in the temporal evolution of the PW amplitudes and winds shown in Fig. 3. In addition these observations are consistent with the modelled increases of PW amplitude in the MLT shown in Fig. 4. Furthermore the relation between the observed PW activity and all wind reversals (Fig. 6), including a variety of polar cap zonal wind reversals between -2 and $-50\,\mathrm{m\,s^{-1}}$ that last between 1 and 19 days, is striking. Their moderate but significant correlation indicates PW bursts in the MLT to lag the maximum of the stratospheric wind reversals by 3 days. This 3 day lag between the maximum wind reversal and the maximum PW activity observed in the correlation analysis (Fig. 6) is consistent with the timing observed in the composite analysis (Fig. 3) which shows the maximization of PW activity approximately 5 days after the onset of the reversal and hence approximately 3 days after the maximum of the wind reversal.

Chandran et al. (2013b) observed not only an increase in PW amplitude after the 2012 SSW ES event, but also a change of the PW longitudinal phase speed towards stronger westward propagation and the occurrence of 5–10 day westward propagating waves following the onset of the event. Here we observe an increase in westward propagation in many of the SSW ES events. However, during some SSW ES events no clear phase shift and even eastward wave propagation can be observed after the onset of the SSW.

All these observations together indicate that the enhancement of PW activity in the MLT is a general feature connected to SSWs in the Northern Hemisphere and not just related to strong events, confirming the modelling results of Chandran et al. (2013a). Indications on how the PW in the MLT is related to the SSW can be collected from the modelled background conditions and the modelled PW activity presented in Figs. 2 and 4, respectively. The modelled SD-WACCM PW activity clearly shows that the amplitudes of PWs propagating up from the stratosphere minimize when they reaches altitudes around 80 km before building again in the MLT. This minimum could be related to ducting of PW (Limpasuvan et al., 2012) or indicate that the PW activity in the MLT observed after the onset of the stratospheric wind reversal might be locally generated and is not just a continuation of the stratospheric PW activity. Such in-situ generation of secondary PW activity in the MLT due to zonal asymmetry imposed by gravity wave drag during an SSW has been suggested by e.g. Liu and Roble (2002). Furthermore the model result presented above (Fig. 2) show very strong temperature and wind gradients to develop during all observed SSW events which favor the development of baroclinic and barotropic instabilities (e.g. Matsuno, 1971; Pedlosky, 1979; Nielsen et al., 2010; Limpasuvan et al., 2012; Tomikawa et al., 2012). This suggests that, like in the strong SSW event studied by Chandran et al. (2013b), instabilities associated with those gradients are potentially an additional trigger for the enhanced PW activity seen in the MLT during stratospheric (~ 50 km) polar cap wind reversals.

Acknowledgements. The authors acknowledge the use of SuperDARN data. SuperDARN is a collection of radars funded by the national scientific funding agencies of Australia, Canada, China, France, Japan, South Africa, UK and United States of America. This study was partly supported by the Research Council of Norway/CoE under contract 223252/F50. V. Limpasuvan was supported by the National Science Foundation under grant AGS-1116123 and the Coastal Carolina University Kerns Palmetto Professorship. The authors are grateful for the help of D. E. Kinnison at NCAR for his assistance with SD-WACCM.

References

Chandran, A., Collins, R. L., Garcia, R. R., Marsh, D. R., Harvey, V. L., Yue, J., and de la Torre, L.: A climatology of elevated stratopause events in the whole atmosphere community climate model, J. Geophys. Res., 118, 1234–1246, doi:10.1002/jgrd.50123, 2013a. 395, 397, 403, 404

Chandran, A., Garcia, R. R., Collins, R. L., and Chang, L. C.: Secondary waves in the middle and upper atmosphere following the stratospheric sudden warming event of january 2012, Geophys. Res. Lett., 40, 1–7, doi:10.1002/grl.50373, 2013b. 395, 396, 403, 404

Chandran, A., Collins, R., and Harvey, V.: Stratosphere-mesosphere coupling during stratospheric sudden warming events, Adv. Space Res., 53, 1265–1289, doi:10.1016/j.asr.2014.02.005, 2014. 395, 399

de Wit, R. J., Hibbins, R. E., Espy, P. J., Orsolini, Y. J., Limpasuvan, V., and Kinnison, D. E.: Observations of gravity wave forcing of the mesopause region during the january 2013 major sudden stratospheric warming, Geophys. Res. Lett., 41, 4745–4752, doi:10.1002/2014GL060501, 2014. 399

Eyring, V., Shepherd, T. G., and Waugh, D. W. (eds.): SPARC CCMVal Report on the Evaluation of Chemistry-Climate Models, V., SPARC Report No. 5, WCRP-X, WMO/TD-No.X, available at: http://www.sparc-climate.org/publications/sparc-reports/sparc-report-no5/, 2010. 397

Goncharenko, L. P., Chau, J. L., Liu, H. L., and Coster, A. J.: Unexpected connections between the stratosphere and ionosphere, Geophys. Res. Lett., 37, L10101, doi:10.1029/2010GL043125, 2010. 394

Greenwald, R. A., Baker, K. B., Hutchins, R. A., and Hanuise, C.: An HF phase-array radar for studying small-scale structure in the high-latitude ionosphere, Radio Sci., 20, 63–79, doi:10.1029/RS020i001p00063, 1985. 396

Greenwald, R. A., Baker, K. B., Dudeney, J. R., Pinnock, M., Jones, T. B., Thomas, E. C., Villain, J. P., Cerisier, J. C., Senior, C., Hanuise, C., Hunsucker, R. D., Sofko, G., Koehler, J., Nielsen, E., Pellinen, R., Walker, A. D. M., Sato, N., and Yamagishi, H.: DARN/SUPERDARN – a global view of the dynamics of high-latitude convection, Space Sci. Rev., 71, 761–796, doi:10.1007/BF00751350, 1995. 396

Hall, G. E., MacDougall, J. W., Moorcroft, D. R., StMaurice, J. P., Manson, A. H., and Meek, C. E.: Super dual auroral radar network observations of meteor echoes, J. Geophys. Res., 102, 14603–14614, doi:10.1029/97JA00517, 1997. 396

Hibbins, R. E. and Jarvis, M. J.: A long-term comparison of wind and tide measurements in the upper mesosphere recorded with an imaging Doppler interferometer and SuperDARN radar at Halley, Antarctica, Atmos. Chem. Phys., 8, 1367–1376, doi:10.5194/acp-8-1367-2008, 2008. 396

Kleinknecht, N. H., Espy, P. J., and Hibbins, R. E.: The climatology of zonal wave numbers 1 and 2 planetary wave structure in the MLT using a chain of Northern Hemisphere SuperDARN radars, J. Geophys. Res., 119, 1292–1307, doi:10.1002/2013JD019850, 2014. 396

Limpasuvan, V., Thompson, D. W. J., and Hartmann, D. L.: The life cycle of the Northern Hemisphere sudden stratospheric warmings, J. Climate, 17, 2584–2596, doi:10.1175/1520-0442(2004)017<2584:TLCOTN>2.0.CO;2, 2004. 394

Limpasuvana, V., Richter, J. H., Orsolini, Y. J., Stordal, F., and Kvissel, O.-K.: The roles of planetary and gravity waves during a major stratospheric sudden warming as characterized in WACCM, J. Atmos. Solar-Terr. Phys., 78–79, 84–98, 2012. 395, 399, 403, 404

Liu, H.-L. and Roble, R. G.: A study of a self-generated stratospheric sudden warming and its mesospheric-lower thermospheric impacts using the coupled TIME-GCM/CCM3, J. Geophys. Res., 107, 4695, doi:0.1029/2001JD001533, 2002. 404

Manney, G. L., Krüger, K., Pawson, S., Minschwaner, K., Schwartz, M. J., Daffer, W. H., Livesey, N. J., Mlynczak, M. G., Remsberg, E. E., Russell III, J. M., and Waters, J. W.: The evolution of the stratopause during the 2006 major warming: satellite data and assimilated meteorological analyses, J. Geophys. Res., 113, D11, doi:10.1029/2007JD009097, 2008. 395, 400

Matsuno, T.: A dynamical model of the stratospheric sudden warming, J. Atmos. Sci., 28, 1479–1494, doi:10.1175/1520-0469(1971)028<1479:ADMOTS>2.0.CO;2, 1971. 395, 399, 404

McDonald, A. J., Hibbins, R. E., and Jarvis, M. J.: Properties of the quasi 16 day wave derived from EOS MLS observations, J. Geophys. Res., 116, D06112, doi:10.1029/2010JD014719, 2011. 401

Nielsen, K., Siskind, D. E., Eckermann, S. D., Hoppel, K. W., Coy, L., McCormack, J. P., Benze, S., Randall, C. E., and Hervig, M. E.: Seasonal variation of the quasi 5 day planetary wave: causes and consequences for polar mesospheric cloud variability in 2007, J. Geophys. Res., 115, D18111, doi:10.1029/2009JD012676, 2010. 404

Pancheva, D. and Mukhtarov, P.: Stratospheric warmings: the atmosphere-ionosphere coupling paradigm, J. Atmos. Solar-Terr. Phys., 73, 1697–1702, doi:10.1016/j.jastp.2011.03.006, 2011. 394

Pedlosky, J.: Geophysical Fluid Dynamics, Ch. 7, Spinger Verlag, 1979. 404

Rienecker, M. M., Suarez, M. J., Todling, R., Bacmeister, J., Takacs, L., Liu, H.-C., Gu, W., Sienkiewicz, M., Koster, R., Gelaro, R., Stajner, I., and Nielsen, J.: MERRA: NASA's modern-era retrospective analysis for research and applications, J. Climate, 24, 3624–3648, doi:10.1175/JCLI-D-11-00015.1, 2011. 397

Smith, A. K.: Stationary waves in the winter stratophere – seasonal and interannual varibility, J. Atmos. Sci., 40, 245–261, doi:10.1175/1520-0469(1983)040<0245:SWITWS>2.0.CO;2, 1983. 401

Smith, A. K.: The origin of stationary planetary waves in the upper mesosphere, J. Atmos. Sci., 60, 3033–3041, doi:10.1175/1520-0469(2003)060<3033:TOOSPW>2.0.CO;2, 2003. 401

Tomikawa, Y., Sato, K., Watanabe, S., Kawatani, Y., Miyazaki, K., and Takahashi, M.: Growth of planetary waves and the formation of an elevated stratopause after a major stratospheric sudden warming in a T213L256 GCM, J. Geophys. Res., 117, D16, doi:10.1029/2011JD017243, 2012. 395, 404

Tweedy, O. V., Limpasuvan, V., Orsolini, Y. J., Smith, A. K., Garcia, R. R., Kinnison, D., Randall, C. E., Kvissel, O. K., Stordal, F., Harvey, V. L., and Chandran, A.: Nighttime seconondary ozone layer during major stratospheric sudden warmings in specified-dynamics, J. Geophys. Res., 118, 1–13, doi:10.1002/jgrd.50651, 2013. 397, 398

Yuan, T., Thurairajah, B., She, C.-Y., Chandran, A., Collins, R. L., and Krueger, D. A.: Wind and temperature response of midlatitude mesopause region to the 2009 sudden stratospheric warming, J. Geophys. Res., 117, D09114, doi:10.1029/2011JD017142, 2012. 394

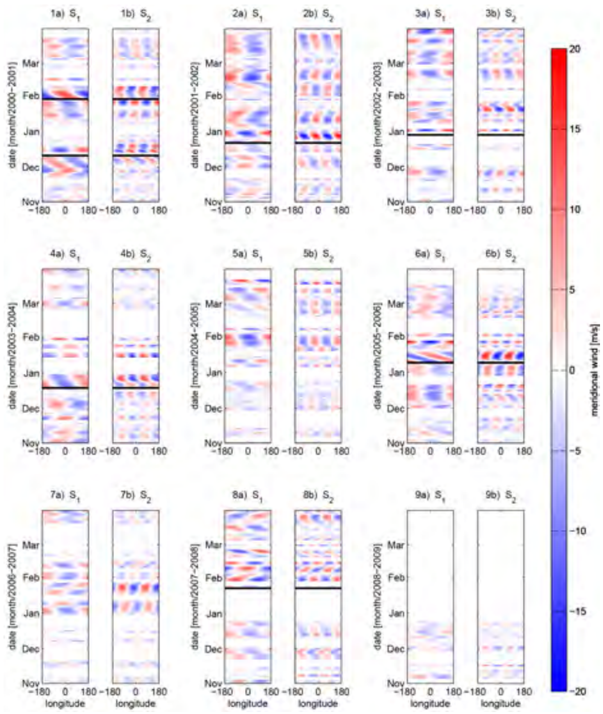

Figure 1. Longitudinal wave components S_1 **(a)** and S_2 **(b)** of the mean meridional wind anomalies for winters, 2000/2001–2008/2009 (1–9). Red and blue colors signify poleward and equatorward wind, respectively. The horizontal black lines indicate the onset of the wind reversal for each of the SSW events that were accompanied by an elevated stratopause (see Sect. 3).

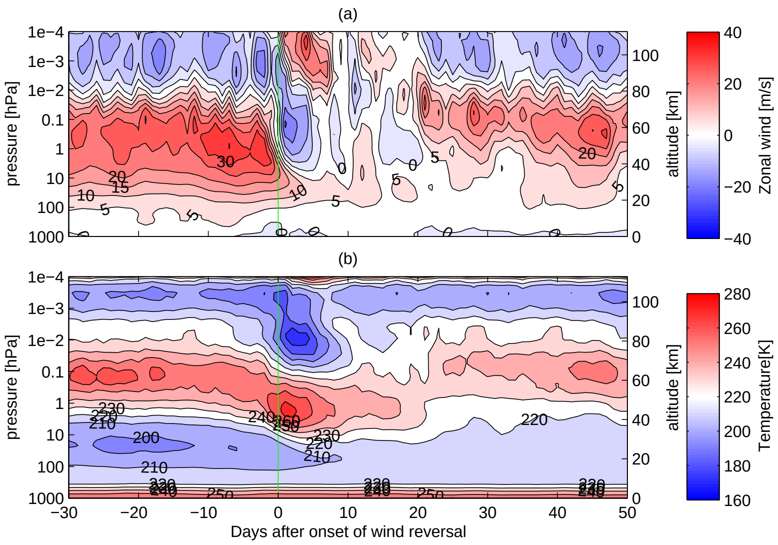

Figure 2. Composite (based on 7 SSW ES events) of polar cap (70–90°) zonal-mean zonal wind (upper panel) and temperature (lower panel) observed by SD-WACCM. Day zero (vertical green line) marks the onset of the polar cap zonal-mean zonal wind reversal at 0.7 hPa (~ 50 km).

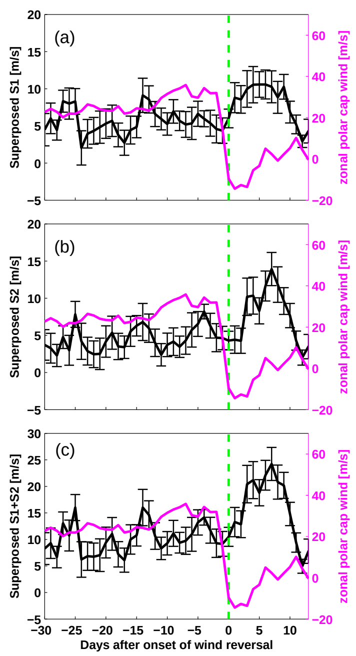

Figure 3. Composites of PW activity observed by SuperDARN around SSW events for the S_1 **(a)**, S_2 **(b)** and $S_1 + S_2$ **(c)** components (black) and the stratospheric (~ 50 km) polar cap zonal-mean zonal wind (magenta). The onset of the wind reversal is marked with a vertical green line at day zero.

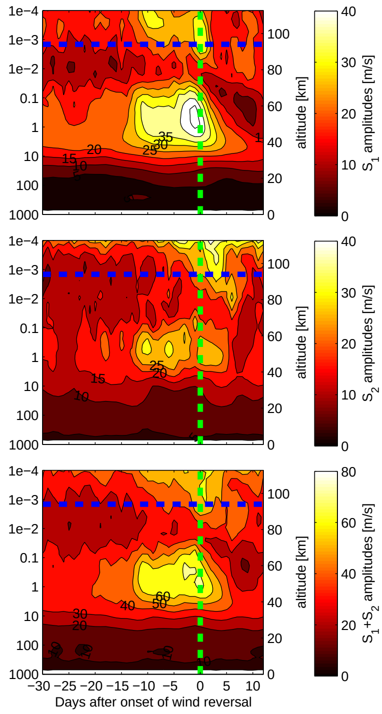

Figure 4. Composites of PW activity observed by SD-WACCM around SSW events for the S_1 (upper panel), the S_2 (middle panel) component and the sum of both components (lower panel) averaged over 48–65° N. The vertical green line marks the onset of the stratospheric wind reversal. The horizontal blue line marks the approximate mean altitude of the SuperDARN wind observations.

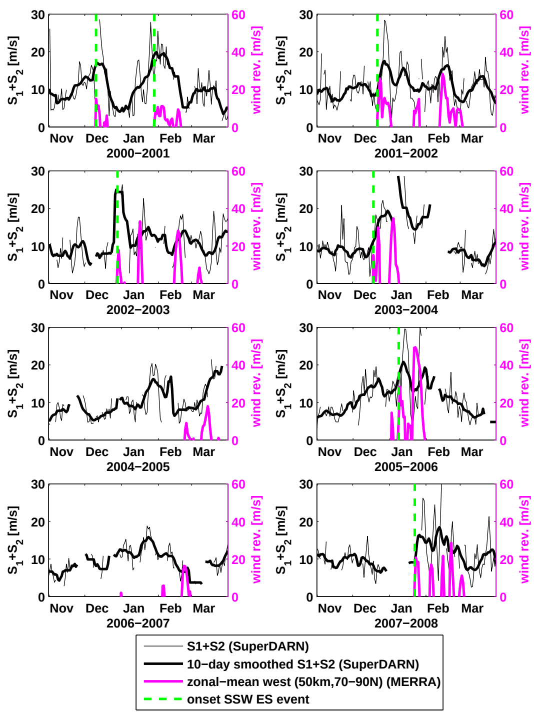

Figure 5. MLT Planetary wave amplitudes from SuperDARN (black) and stratospheric westward polar cap (70–90° N) winds at 0.7 hPa (~ 50 km) from MERRA (magenta) during winters 2000/2001–2007/2008. The PW amplitudes (black) are the sum (thin black line) and the 10 day smoothed sum (thick black line) of the wave number 1 and 2 components ($S_1 + S_2$) retrieved from the SuperDARN data. The vertical green line marks the onset of the stratospheric wind reversal of the composited events.

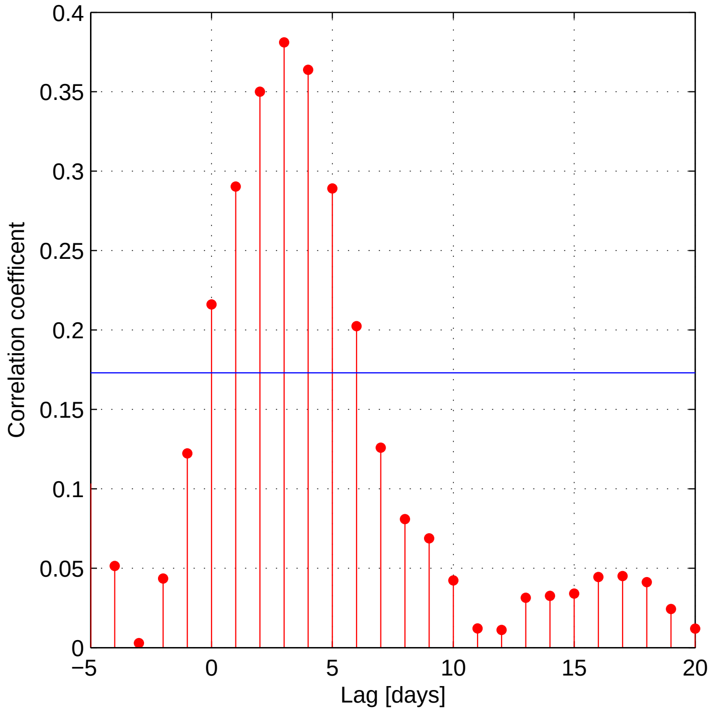

Figure 6. Correlation between westward polar cap stratospheric winds (∼ 50 km) from MERRA and PW amplitudes ($S_1 + S_2$) from MLT meridional SuperDARN winds (∼ 95 km). The stratospheric westward wind leads the PW enhancements in the MLT by approximately 3 days with a moderate correlation coefficient of 0.4. the horizontal blue line represents the 99 % confidence level.

B. Models used

To get information about the state of the surrounding and underlying atmosphere different models have been used. The models were used for validation of the fitting technique and to investigate possible sources of the observed PW activity in the MLT.

B.1 UKMO

The UK Meteorological Office (UKMO) stratospheric assimilated data set [*Swinbank et al.*, 2013; *Swinbank and O'Neill*, 1994] contains temperature, geopotential height and wind components. Model results were obtained through the British Atmospheric Data Centre. The data is available as single daily output at 12 UT and is based on the operational observations. The horizontal resolution is 2.5° x 3.75° (latitude x longitude) before 13 March 2006, and 0.5625° x 0.375° after this date. The vertical coverage presently extends from the ground to 0.1 hPa (65 km). However before 28 October 2003 and from 14 March 2006 to 14 May 2007 the top altitude was at 0.3 hPa and 0.4 hPa, respectively. The zonal wind from UKMO has been used to quantify the tropospheric and stratospheric wind regimes. In addition, the meridional wind from UKMO has been used to validate the method for the extraction of PW zonal wave number components [Section 2.3] and to extract stratospheric PW activity.

B.2 MERRA

Wind components using the Modern-Era Retrospective Analysis for Research and Application (MERRA) of the NASA Global Modelling and Assimilation Office [*Rienecker et al.*, 2011] have been made available by Varavut Limpasuvan from the School of Coastal and Marine Systems Science, Coastal Carolina University, South Carolina, USA. The horizontal resolution of this data product is 0.5° x 3,3° (latitude x longitude) and the vertical resolution contains 72 pressure levels between the ground and 0.015 hPa ($\sim$ 80 km). Up to approximately 50 km the simulations are measurement driven. Above that altitude the model is free running. Outputs have been produced 4 times a day so that the daily average removes the tidal oscillations present. The wind data from MERRA have been used to monitor stratospheric wind conditions and retrieve stratospheric planetary wave activity.

B.3 SD-WACCM

The Whole Atmosphere Community Climate Model (WACCM) is a global circulation model of the National Center of Atmospheric Research (NCAR) with fully coupled chemistry and dynamics that can provide simulations up to $\sim$ 150 km. The dynamics and temperature of the specified dynamics version of WACCM (SD-WACCM) assimilate MERRA [Appendix B.2] up to 0.79 hPa ($\sim$ 50 km). Meteorological fields above this altitude are fully interactive with a linear transition in between. Due to the assimilation, the atmospheric temperature and dynamics for individual dates can be represented by SD-WACCM [*Eyring et al.*, 2010; *Tweedy et al.*, 2013]. The SD-WACCM winds and temperatures used in this thesis have been provided by Yvan J. Orsolini from the Norwegian Institute for Air Research in Kjeller, Norway and Varavut Limpasuvan from the School of Coastal and Marine Systems Science, Coastal Carolina University, South Carolina, USA. The horizontal resolution of this model output is 1.9° x 2.5° (latitude x longitude) and it covers altitudes from the ground to approximately 150 km (88 pressure levels). Here the model has been used to analyse the effect of stratospheric sudden warmings on PW activity in the MLT. Using the model, PW activity throughout the atmosphere (0-150 km) could be simulated.

C. Abbreviations

C.1 General

BAS	British Antarctic Survey
ES	Elevated Stratopause
GW	Gravity Wave
ICON	Ionospheric Connection Explorer
IDI	Imaging Doppler Interferometer
MLT	Mesosphere Lower Thermosphere
NASA	National Aeronautics and Space Administration
MERRA	Modern-Era Retrospective analysis for Research and Application
OH	Hydroxyl
PMC	Polar Mesospheric Cloud
PW	Planetary Wave
QTDW	Quasi-Two-Day Wave
SABER	Sounding of the Atmosphere using Broadband Emission Radiometry
SD-WACCM	Specified Dynamics Whole Atmospheric Community Model
SKiYMET	All-Sky Interferometric
SLT	Solar Local Time
SuperDARN	Super Dual Auroral Radar Network
SSW	Stratospheric Sudden Warming
TIMED	Thermosphere Ionosphere Mesosphere Energetics Dynamics
UKMO	UK Meteorological Office
WMO	World Meteorological Organization

C.2 SuperDARN radars

ade	Adak Island East	adw	Adak Island West
bks	Blackstone	cly	Clyde River
cve	Christmas Valley East	cvw	Christmas Valley West
dce	Dome C	fhe	Fort Hays East
fhw	Fort Hays West	fir	Falkland Islands
gbr	Goose Bay	hal	Halley
han	Hankasalmi	hok	Hokkaido
inv	Inuvik	kap	Kapuskasing
ker	Kerguelen	kod	Kodiak
ksr	King Salmon	mcm	McMurdo
pgr	Prince George	pyk	Pykkvibaer
rnk	Rankin Inlet	san	SANAE
sas	Saskatoon	sch	Schefferville
sps	South Pole Station	sto	Stokkseyri
sye	Syowa East	sys	Syowa South
tig	Tiger	unw	Unwin
wal	Wallops Island	zho	Zhongshan

Table C.1.: Taken from `vt.superdarn.org/tiki-index.php?page=Radar+Overview`.

Acknowledgements

Dear Patrick, thank you for being a perfect supervisor. I learned a lot from you. Your door was always open for scientific discussions and your funny anecdotes made me laugh a lot.

Dear Rob, thanks for inspiring and fruitful discussions, helpful comments and useful suggestions.

Dear Roos, I really enjoyed sharing an office with you for more than 3 years. Talking to you made it much easier to understand the world around us both in terms of science and in terms of every day live. You are a wonderful officemate and very good friend. Travelling to conferences with you was always fun.

Dear Teferi, it was very good having you in the group. With your happy nature you spread joy and harmony every day.

Great thanks also to my other atmospheric physics group colleges Marianne, Amund, Rishi, Corinne and Venkat. You were always very helpful and inspired my work though good scientific discussions.

Thanks to all the people in the D3 corridor for giving my a smile and for refreshing my mind during lunch and coffee breaks and short chats on the corridor.

Thanks to the participants of the Friday cake. I enjoyed your company and all of your cakes.

Thanks to my family!
Danke, dass ihr in mir die Begeisterung für die Physik geweckt und diese gefördert habt. Danke auch für euer Interesse in meine Forschung.
Takk for at dere tok meg hjertelig velkommen i familien og takk for alle de fine opplevelser vi har delt sammen.

Dear Kristian, thanks for supporting me and making me smile every day.